UPPSALA
UNIVERSITET

Digital Comprehensive Summaries of Uppsala Dissertations from the Faculty of Science and Technology 1214

Trends in Magnetism

From Strong Correlations to "-onics" Technology

DMITRY YUDIN

ACTA
UNIVERSITATIS
UPSALIENSIS
UPPSALA
2015

ISSN 1651-6214
ISBN 978-91-554-9130-7
urn:nbn:se:uu:diva-238177

Dissertation presented at Uppsala University to be publicly examined in Hall IX, Main University Building, Biskopsgatan 3, Uppsala, Friday, 13 February 2015 at 09:15 for the degree of Doctor of Philosophy. The examination will be conducted in English. Faculty examiner: Grigori Volovik (Aalto University, School of Science and Technology).

Abstract
Yudin, D. 2015. Trends in Magnetism. From Strong Correlations to "-onics" Technology. *Digital Comprehensive Summaries of Uppsala Dissertations from the Faculty of Science and Technology* 1214. 109 pp. Uppsala: Acta Universitatis Upsaliensis. ISBN 978-91-554-9130-7.

Despite of enormous progress in experimental nanophysics theoretical studies of low-dimensional electron systems still remains a challenging task. Indeed, most of the structures are strongly correlated, so that an effective perturbative treatment is impossible due to the lack of a small parameter. The problem can be partly solved within the dynamical mean-field theory (DMFT) paradigm, nevertheless the correlations in physically relevant high-temperature superconductors are of purely non-local nature. The recently developed dual fermion approximation, combining field-theoretical diagram technique and numerical methods, allows for explicit account of spatial correlations. The approximation was shown to be of fastest convergence compared with standard DMFT extensions, and along with renormalization group is used here to study Fermi condensation on a triangular lattice near van Hove singularities. The still debated phenomenon of Fermi condensation is believed to be a precursor to strongly correlated low-temperature instability and is found in this thesis to be robust even at high temperature, making its experimental verification feasible. Unlike homogeneous ferromagnetic ordering a variety of non-collinear ground state configurations emerge as a result of competition among exchange, anisotropy, and dipole-dipole interaction. These particle-like states, e.g. magnetic soliton, skyrmion, domain wall, form a spatially localized clot of magnetic energy. Consistent study of spin, which essentially is a quantum mechanical entity, led to the emergence of spintronics (spin-based electronics) and magnonics (photonics with spin waves), in the meanwhile topologically protected magnetic solitons and skyrmions might potentially be applied for data processing and information storage in next generation of electronic technology (rapidly advancing solitonics and skyrmionics). An ability to easily create, address, and manipulate such structures is among the prerequisite forming a basis of "-onics" technology. It is shown here that spins on a kagome lattice, interacting via Heisenberg exchange and Dzyaloshinskii-Moriya coupling, allow the formation of topologically protected edge states through which a skyrmion can propagate. Not only can chemical methods be used to design novel functionality, but also geometric structuring. It is demonstrated that for graphene sandwiched between two insulating media external circularly-polarized light serves as an effective magnetic field. The direct practical implication permits to control light polarization and induce spin-waves propagating on the surface of e.g. a topological insulator. The newly discovered Dirac materials, graphene and three-dimensional topological insulators, are not easy to handle. In fact, the quasiparticle band function is gapless preventing them from being used in integrated circuits, nevertheless the problem is shown here to be partially relaxed by placing a vacancy on top of it.

Keywords: Strongly interacting electron systems, Spin dynamics, Topological matter

Dmitry Yudin, Department of Physics and Astronomy, Materials Theory, Box 516, Uppsala University, SE-751 20 Uppsala, Sweden.

ISSN 1651-6214
ISBN 978-91-554-9130-7
urn:nbn:se:uu:diva-238177 (http://urn.kb.se/resolve?urn=urn:nbn:se:uu:diva-238177)

My dear, here we must run as fast as we can, just to stay in place.
And if you wish to go anywhere you must run twice as fast as that.
Lewis Carroll, Alice in Wonderland

List of papers

This thesis is based on the following papers, which are referred to in the text by their Roman numerals.

I **Fermi condensation near van Hove singularities within the Hubbard model on the triangular lattice**
Dmitry Yudin, Daniel Hirschmeier, Hartmut Hafermann, Olle Eriksson, Alexander I. Lichtenstein, and Mikhail I. Katsnelson
Phys. Rev. Lett. 112, 070403 (2014)

II **Topological excitations in a kagome magnet**
Manuel Pereiro, Dmitry Yudin, Jonathan Chico, Corina Etz, Olle Eriksson, and Anders Bergman
Nature Communications 5, 4815 (2014)

III **Spontaneous gap generation on the surface of weakly interacting topological insulators using nonmagnetic impurities**
Annica M. Black-Schaffer and Dmitry Yudin
Phys. Rev. B 90, 161413(R) (2014)

IV **Detecting Zitterbewegung in graphene with surface electromagnetic waves**
Dmitry Yudin, Olle Eriksson, and Mikhail I. Katsnelson
Submitted

Contents

Part I:
Introduction

The triumphant progress of theoretical physics in the last century has been mainly associated with understanding mechanisms underlying the microcosm. General relativity followed by quantum mechanics and quantum field theory revolutionized our views on the world around us. It turned out that a microscopic particle when moving does not have to follow a definite trajectory ascribed to it by Newtonian deterministic mechanics, whereas a quite intuitive and naive band theory due to Bloch appeared indispensable and can be viewed as the dawn of condensed matter era. Today studying of low-dimensional electronic structure remains one of the most exciting and fascinating fields. However, in most of the cases the electrons constituting a solid are what you might call strongly correlated. In general, the correlations are thought as interaction among different components of a solid with each other. However, the paradox today consists in the fact that modern physics can in principle write down equations capable to portray almost any realistic system, but not always is able to solve these equations. Indeed, a solution is possible only when the system under consideration is constituted by a set of particles which do not interact and can be handled separately or interact weakly. In the latter case we say that we can develop a theory that has a small parameter which can be chosen one way or another.

The first successful attempt to address a strongly correlated system was made by Lev Landau (Section 1.1). In accord with Landau Fermi-liquid theory an ensemble of interacting particles needs to be replaced by a set of quasiparticles which are coupled by some effective amplitudes and can be adiabatically connected to a weakly interacting Fermi gas [131, 21, 167, 134, 2]. A proper many-body description can not be addressed within a linear the-

ory, though small anharmonic perturbations do not change qualitatively the quasiparticle picture and can be treated as scattering processes between them, leading thus to multiple harmonic generation, quasiparticle dressing, etc. The study of low-dimensional lattice models can potentially unveil the nature of exotic materials like unconventional superconductors and quantum spin liquids. After their almost simultaneous discovery, high-temperature superconductivity in cuprates and the fractional quantum Hall effect posed some awkward questions to Landau Fermi liquid theory. For both systems, the Coulomb interaction is sufficiently strong to cause the breakdown of perturbative expansions. In such cases, the concept of quasiparticles providing a basis for understanding most of the condensed-matter phenomena is questionable, and new physics can arise. At sufficiently large coupling one can rely on numerical implementation only, unless a problem can be solved exactly, e.g. at quite large on-site Coulomb repulsion (the interaction strength is of the order of band-width) a metal-insulator transition takes place. This effect is essentially of non-perturbative nature and can be captured within the dynamical mean-field theory approach, in which an interacting lattice model is mapped onto a local impurity problem [79]. However, being of purely local nature DMFT is not capable to probe the effects due to spatial correlations. To get over the difficulty a fast converging dual fermion method have been recently developed (Section 1.2). In this method non-local effects are treated perturbatively around DMFT. Making use of a set of exact transformations to dual variables allows to consider vertices of a local impurity problem as small parameters and correctly reproduce the weak- and strong-coupling limit. The antiferromagnetic pseudogap, Fermi-arc formations, and non-Fermi-liquid effects due to the van Hove singularity have been captured by the lowest-order diagrams.

Soon after high-temperature superconductivity was detected in cuprates, it was pointed out that for the optimal doping the Fermi level lies in the vicinity of van Hove singularities (VHSs) with divergent density of states (DOS), and that in this case the Fermi liquid picture can be violated even for a weak interaction, due to singularities of the electron-electron vertex [61]. The concept of the so-called van Hove scenario has been pushed forward to explain a variety of phases associated with the presence of VHSs, e.g., superconductivity, itinerant ferromagnetism, and density waves. If the VHS is near the Fermi level, both antiferromagnetism and d-wave superconductivity can be produced even at small on-site Coulomb repulsion, as can be shown from a renormalization group analysis or the parquet approximation [232, 84, 89, 95]. The nature of exotic ground states is determined by the delicate interplay of these fluctuations, which therefore remain controversial. However, a precursor of a strongly correlated low-temperature instability, exists at sufficiently high temperatures and can be probed in the paramagnetic phase of fermionic cold atoms on a triangular lattice. The effect can be understood in terms of Fermi condensation. As long as the group velocity is positive, all variations δF of Landau functional are positive and the Fermi distribution corresponds

to the minimum. If the group velocity of the quasiparticles becomes negative, there exist variations for which $\delta F < 0$. This leads to a restructuring of the distribution function in a certain interval of momenta $k_0 < k < k_1$, where the resulting occupation fraction differs from the Fermi distribution, but still minimizes the functional (section 1.3). In the limit $T \to 0$, the dispersion becomes entirely flat in this interval. In analogy to the Bose-Einstein condensate, this highly degenerate state has been termed Fermi condensation. If it exists, a Fermi condensate is a new state of matter which is topologically different from both the Fermi liquid and the Luttinger liquid. Because of the formation of flat bands, there is a pinning of the Fermi energy to the VHS point for a whole range of electron concentrations. Otherwise, below a critical temperature, the highly degenerate state may give way to another fermionic instability associated with a non-Fermi liquid ground state. We address this effect for the Hubbard model for a triangular lattice from both weak-coupling and strong-coupling limits, by means of field-theoretical renormalization group and dual-fermion approaches, respectively. Our analysis clearly indicates that the phenomenon is robust and can be observed in experiments with ultracold Fermi gases at sufficiently high temperatures.

In addition, the ground state configuration of magnetic structures can be understood by studying corresponding magnetization dynamics, which is based on the solution of phenomenologically derived Landau-Lifshitz equation expressing magnetization precession about effective field (Section 2.1). This equation does not take account of dissipation which is physically meaningful and needs to be supplied with the Gilbert term responsible for relaxation [36]. When passing through a magnetic system spin-polarized current produces an extra torque on system's magnetization, this term known as spin-transfer torque due to Slonczewski has to be handled. Both Gilbert damping and spin-transfer torque have to be treated on equal footing and can be microscopically derived [57]. The spin waves are known to be quantized thus leading to the notion of magnons, that can be excited in magnetic materials. In most of spin-wave phenomena a number of magnons is a macroscopic quantity and can be well described by the Landau-Lifshitz equation. As a result, the concept of coherent magnon states analogous to that of quantum optics can be pushed forward; we review the concept of coherent magnon states and show that they are the quantum states generated in a linear microwave pumping process. We also overview the recently observed Bose-Einstein condensation of magnons in magnetic films under strong microwave pumping (Section 2.2).

In low-dimensional magnetic structures depending on the distance between neighboring spins, crystalline symmetry, and hybridization with substrate, a wide range of magnetic configurations ranging from collinear ferromagnetic, antiferromagnetic, and non-collinear helimagnetic configurations to more complicated textures can be observed. If in addition, inversion symmetry is broken the spins alignment gains a certain chirality due to spin-orbit driven antisymmetric Dzyaloshinskii-Moriya interaction (DM) [60]. A certain class of non-

linear equations allow particle-like solution, solitary waves or solitons, which preserve their shape in the duration of their motion and collision processes. There also exists a class of topological solitons whose ground state can not be connected to their excited states and is characterized by some topological number. Magnetic skyrmions are chiral spin structures with a whirling configurations so that the plane on which the spins are specified is topologically equivalent to a sphere. Because of that, a certain topological invariant, namely degree of mapping can be ascribed to the structure. It can be thought of as skyrmion number. A kagome ferromagnet characterized by a structure with lack of inversion symmetry in the presence of considerably large DM interaction mimics the band structure of a topological insulator, as is shown in this thesis. In such a system the magnon dispersion is gapped in the bulk allowing the traveling gapless edge states, making thus this structure perfect for creating and manipulating magnetic skyrmions (Section 2.3). The nucleation and manipulation of individual skyrmions in magnetic nanostructures will be essential in any future skyrmionic device.

Progress in storage technology demands new mechanisms allowing high-speed data manipulations. Typically, performance of up-to-date devices is determined by the duration of electric or magnetic field pulse resulting in demagnetization of magnetic domains. The laser might be used instead as its characteristic time is up to a few femtoseconds. The only limitation one can encounter on a way to all-optical technologies is related to the transformation of optical energy into electrical. Recently, it has been demonstrated that in magneto-crystalline structures a strong magnetic field up to a few Tesla of magnitude might be set up through instantaneous pulses due to the Inverse Faraday effect, the generation of magnetic field by non-resonant circularly polarized light. Dysprosium orthoferrite ($DyFeO_3$), irradiated by 200 fs circularly polarized laser pulse, set up an induce magnetic field of the same order. In case of elliptically polarized electromagnetic wave, orientations of spin polarization in forward and backward directions are not equally probable. As a consequence, in addition to energy and momentum light transfers angular momentum. The implication of photonic structures consisting a magnetic layer allows to enhance magnetooptical effects dramatically, leading to magnetoplasmonics (Section 3.1).

Graphene, a two-dimensional sheet of graphite, has recently attracted a lot of attention owing to potential application in novel devices [108, 47, 146, 78, 160, 42, 1, 128]. Quite remarkable progress has been achieved on a way to study its behavior in intense external fields. In a circularly polarized electric field quite a few novel phenomena such as photovoltaic Hall effect, metal-insulator transition in graphene, valley-polarized currents in both monolayer and bilayer graphene, and photo-induced Hall effect in the absence of magnetic fields have been predicted (Section 3.2). One of the most intriguing features of a system irradiated by circularly polarized light is the redistribution of electrons in the band structure. Thus, presence of external field results

in some of the electrons from the valence band being moved to the conduction band (photon-assisted doping). As it was already discussed if one of the bands is completely filled topological properties might appear, these properties are extremely robust for the system driven out of equilibrium by light.

Strong nonmagnetic impurities on the surface of three-dimensional topological insulators (TIs) generate localized resonance peaks close to the Dirac point. We show that this results in a strongly reduced critical Coulomb interaction strength to reach a magnetic surface state, following a Stoner-like criterion. Thus even weakly interacting TIs host a finite (local) magnetization around strong nonmagnetic impurities. The local magnetization gives rise to a global energy gap, linearly dependent on the maximum value of the magnetization but decreasing with reduced impurity concentration (Section 3.3).

The title of this thesis "Trends in Magnetism: From Strong Correlations to -onics Technology" should not be confusing: In fact, subsequent progress towards the new techno-economic paradigm seems illusory without proper understanding of mechanisms ruling the world of nano. Nanotechnology, along with IT, biotech, and harmonious exploitation, have been accepted as the mainstream which is believed to change the social landscape. Typically, nanotechnology is thought of as the manipulation of matter on a characteristic length-scale (approximately 100 nm). In contrast to that, we assume any system governed by the laws of quantum mechanics has to be treated as nano. An example is low-dimensional electron system where the correlations effects among constituents become prominent. In this thesis we make a theoretical attempt to describe underlying physics and possible engineering applications on equal footing from both analytical and numerical perspective without opposing them to each other: Indeed, the dual fermion method at strong coupling complemented with field-theoretical renormalization group at weak- and intermediate-coupling enables us to inspect the Hubbard model on a triangular lattice and discover effects, like Fermi-condensation, which can be probed with ultracold quantum gases. In the meanwhile, a numerical solution of the Landau-Lifshitz equation within atomistic spin dynamics confirms theoretical findings and suggests a technique how to create and manipulate a skyrmion on a kagome lattice, making thus the concept of skyrmionics viable. Furthermore, magnetic engineering with the recently discovered Dirac materials in the presence of certain non-lineariaty also deserves attention. Thus, the thesis is devoted to systematic studies of spatial correlations and non-linear effects in electron models. We believe that our results will contribute to the solution of puzzles of Nature.

1. On the nature of magnetism

1.1 Fermi-liquid Theory: A gentle reminder

It is known that in most of the cases the solution to strongly correlated electronic problem can not be found in closed analytical form. Instead of solving a complicated many-body problem it is easy to operate in the spirit of Landau Fermi-liquid theory [131, 134, 2, 167, 21, 150]: One can develop a low-energy theory where high-energy degrees of freedom are eliminated by defining a number of amplitudes, characterizing interaction among a set of quasiparticles at low temperatures. Stability of the ground state configuration is determined in full agreement with Pomeranchuk's criterion [170]: The system under consideration is stable as long as the amplitudes in question are positive and finite. Within Landau formalism the quasiparticles can be adiabatically connected to weakly excited states of a normal Fermi gas. The ground state, the corresponding free energy and entropy are supposed to be the functionals of the quasiparticle distribution $n_{\mathbf{k}}(T)$ which can be determined by minimizing the grand canonical potential $\Omega[n_{\mathbf{k}}(T)] = F[n_{\mathbf{k}}(T)] - \mu N$, while the quasiparticle energy in the vicinity of the Fermi surface can be calculated according to

$$\varepsilon[n_{\mathbf{k}}(T)] = \mu + v_F\,(k - k_F) + \int \frac{d^3\mathbf{p}}{(2\pi)^3} f_{\mathbf{k},\mathbf{p}}\,\delta n_{\mathbf{p}}(T), \tag{1.1}$$

and the entropy of an ideal gas obeying the Fermi-statistics:

$$S[n_{\mathbf{k}}(T)] = -2\int \frac{d^3\mathbf{k}}{(2\pi)^3}\Big[n_{\mathbf{k}}(T)\log n_{\mathbf{k}}(T) + \big(1 - n_{\mathbf{k}}(T)\big)\log\big(1 - n_{\mathbf{k}}(T)\big)\Big], \tag{1.2}$$

here a factor of 2 stands for spin projections. Linearization of quasiparticle dispersion relation in the vicinity of the Fermi level (1.1) allows one to identify the parameter of a theory, an effective mass,

$$\frac{1}{m^*} = \frac{1}{k}\frac{d\varepsilon_k}{dk}\bigg|_{k=k_F,\,T=0}, \tag{1.3}$$

provided m^* is finite and positive at the Fermi-surface. The effective mass of a quasiparticle can be linked to that of bare fermion m by requiring Galilean invariance. At $T \to 0$, keeping the notion m^* for the Landau effective mass (1.3), the quasiparticle dispersion in close vicinity to the Fermi level can be

represented by $\varepsilon_{\mathbf{k}} - \mu = k_F (k - k_F)/m^*$. In general, the relation between the physical mass m and the Landau effective mass m^* can be seen from invariance to Galilean boost: The momentum per unit volume transported by the quasiparticles must be equal to the mass density of the real particles, namely is

$$\int \frac{d^3\mathbf{k}}{(2\pi)^3}\, k_i n_{\mathbf{k}} = \int \frac{d^3\mathbf{k}}{(2\pi)^3}\, m n_{\mathbf{k}} \nabla_{k_i} \varepsilon_{\mathbf{k}}. \tag{1.4}$$

By varying the identity (1.4) with respect to distribution function $n_{\mathbf{k}}$ and restricting to Fermi momentum we finally derive

$$\frac{1}{m^*} = \frac{1}{m} + \int \frac{d^3\mathbf{k}}{(2\pi)^3} \frac{(\mathbf{k}_F \cdot \mathbf{k})}{k_F^3} f_{\mathbf{k}_F,\mathbf{k}} \frac{\partial n_{\mathbf{k}}(T)}{\partial k} \tag{1.5}$$

To proceed we obtain the distribution $n_{\mathbf{k}}(T)$ by minimizing the grand canonical potential $\Omega[n_{\mathbf{k}}(T)]$, provided the free energy $F[n_{\mathbf{k}}(T)] = E[n_{\mathbf{k}}(T)] - TS[n_{\mathbf{k}}(T)]$; as a result, the quasiparticle energy

$$\varepsilon_{\mathbf{k}}(T) = \frac{\delta E[n_{\mathbf{k}}(T)]}{\delta n_{\mathbf{k}}(T)} = \mu(T) + T \log\left(\frac{1 - n_{\mathbf{k}}(T)}{n_{\mathbf{k}}(T)}\right). \tag{1.6}$$

In general, the chemical potential $\mu(T)$ depends on temperature, and the variation of quasiparticle energy according to (1.1) has to be of the form

$$\delta\varepsilon_{\mathbf{k}}(T) = \int \frac{d^3\mathbf{p}}{(2\pi)^3}\, f_{\mathbf{k},\mathbf{p}}\, \delta n_{\mathbf{p}}(T). \tag{1.7}$$

Therefore, as it was pointed out in the beginning, the interaction among the quasiparticles is replaced by a set of Landau amplitudes $f_{\mathbf{k},\mathbf{p}}$, so that for a non-interacting Fermi-gas $f_{\mathbf{k},\mathbf{p}} = 0$. Basically,

$$f_{\mathbf{k},\mathbf{p}} = \frac{\delta^2 E[n_{\mathbf{k}}(T)]}{\delta n_{\mathbf{k}}(T) \delta n_{\mathbf{p}}(T)}. \tag{1.8}$$

The amplitude defined in such a way is symmetric with respect to permutation of indices (for clarity, we omit the spin indices). Low-lying excitations are well fit by the quasiparticles in the vicinity of the Fermi-level with the band function (1.1). Typically, $\delta n_{\mathbf{p}}(T)$ is non-zero in the tiny region around the Fermi-surface, so that $\mathbf{k} = \mathbf{p} \approx \mathbf{k}_F$. Rewriting the expression (1.6) in a more convenient form we arrive at the celebrated Fermi-Dirac distribution function

$$n_{\mathbf{k}}(T) = \left(1 + \exp\left[\frac{\varepsilon_{\mathbf{k}}(T) - \mu}{T}\right]\right)^{-1}. \tag{1.9}$$

Close inspection of the formula (1.5) at $T = 0$ suggests $m/m^* = 1 - N_0 f^1(x)/3$, where the density of states at the Fermi level is N_0, while the p – wave component of Landau amplitude is written as $f^1(x)$ (the latter is possible

since the quasiparticle density $x = k_F^3/(3\pi^2)$ in Landau Fermi-liquid picture is uniquely determined by Fermi-momentum , therefore $f^1(k_F, k_F) = f(x)$). Interestingly, in the vicinity of some x_{FC} the expression $\left(1 - N_0 f^1(x)/3\right) \sim (x - x_{FC}) + a\,(x - x_{FC})^2 + \ldots \to 0$, as a result

$$\frac{m^*}{m} \propto A + \frac{B}{x - x_{FC}} \sim \frac{1}{r}, \tag{1.10}$$

here A and B are some constants, while $r = (x - x_{FC})/x_{FC}$ is in common use in the literature. In agreement with the general criterion [170] the expression (1.10) makes sense as long as $x > x_{FC}$ (i.e., $r > 0$), e.g. in narrow band heavy-fermion metals [113, 9]. Thus, on approaching x_{FC} the formation of a new state of matter that does not satisfy Pomeranchuk criterion can be observed: At $T = 0$ and $r = (x - x_{FC})/x_{FC} \to 0$ the effective mass diverges and becomes negative at $x < x_{FC}$, therefore a phase transition at $x = x_{FC}$ occurs. It is worthy to note that the ground state energy of such a state is mainly determined by the potential forces since the kinetic contribution approaches zero in the vicinity of the Fermi-surface. The quasiparticles with momenta $k_0 \leq k \leq k_1$ possess at $T = 0$ the same single particle energy $\varepsilon_{\mathbf{k}} = \mu$ [as it seen from (1.6)], this state in analogy to the Bose condensate is referred to as Fermi condensate. The density of states in this region is peaked and highly degenerate as a result.

To summarize, Fermi-liquid theory developed by Landau [131] to explain the rich physics of normal metal and Fermi-liquid like ^{3}He basically implies that low energy excitations are nothing but quasiparticles with some effective mass m^* which is independent of external field, pressure, and temperature. However, for the recently discovered class of high-temperature superconductors, heavy-fermion compounds, and quasi-two-dimensional Fermi-liquids [202, 222, 142, 22, 217] the direct application of Landau theory is questionable [184, 182, 186, 185, 46, 45]. In fact, for strongly correlated heavy-fermion compounds the effective mass can not be considered like a parameter in the theory and functional dependence on external field and temperature is assumed to take place. Thermodynamic properties and correlation functions are typically characterized by power-law dependence on temperature. The latter could be interpreted to destroy the quasiparticle picture in strongly correlated systems, while the possible explanation of anomalous behavior in a variety of observed phenomena in high-temperature superconductors and heavy-fermion metals is relevant to quantum phase transitions happening at $T = 0$. In this case the behavior of a system is governed by macroscopic parameters, e.g. electron density, pressure, external magnetic field [142].

Keen interest to studying low-dimensional electronic structures is mainly motivated today by experimental progress in fabrication and characterization of thin ferromagnet films and multilayers, copper- and iron-based superconductors, and organic compounds. Main efforts to gain theoretical insight are made by the use of advanced numerical algorithms , e.g. various combinations

of renormalization group or quantum Monte Carlo simulations. However the detailed analytical considerations which go beyond well established perturbation schemes are of great interest as well. For instance, the standard perturbation theory breaks down on an attempt to explain weak itinerant magnetism in the vicinity of VHSs. VHSs mostly present in two-dimensional systems are still to be found in three-dimensional models [96] depending on the geometry of underlying lattice. In the presence of VHSs the perturbation series are logarithmically divergent enforcing thus to sum up an infinite number of diagrams. Interestingly, the divergence in question does not show up in a certain channel exclusively and is ubiquitous for both particle-particle and particle-hole channels. In this case, to clear up ambiguity one has either to accomplish well-known parquet summation or proceed with renormalization group (RG) analysis similar to the technique developed for quasi-one-dimensional systems [201] (despite of being square-log divergent in two-dimensional systems).

Capability to sustain a superconducting state is among the peculiarities of itinerant electronic systems. Contrary to conventional superconductors where the formation of a gapped state is attributed to the electron-phonon coupling and only a limited fraction of electrons around the Fermi surface are paired in an s – wave state, forming a rather uniform superconducting gap around the Fermi-level, magnetic fluctuations present in the model in question can potentially lead to unconventional type of pairing (e.g., p – or d – wave state), in which low-lying excitations result in gapless points or lines on the Fermi surface. In addition, it was recently discovered that antiferromagnetism is closely connected to d – wave superconductivity, in particular the formation of high-temperature superconductors in copper-based compounds is believed to be closely associated with antiferromagnetic correlations, while most of the properties inherent to these systems can be explained by the competition between antiferromagnetic and superconducting correlations [234]. Triplet, or p – wave, pairing (e.g., in layered ruthenates Sr_2RuO_4 [149]) is driven by ferromagnet fluctuations [151, 158], which however are indistinguishable in the experiments with inelastic neutron scattering [195], but were to be found by measuring susceptibility in electron doped $Sr_{2-x}La_xRuO_4$ [115]. Thus, the detailed investigation of a competition between instabilities of both types (either magnetic or superconducting) has to be based on careful account of Fermi surface topology and quasiparticle band dispersion.

One of the most interesting models which is rather simple from one side but permits to keep track of all relevant effects from the other is the $t - t'$ Hubbard model on a square lattice. Quite intuitive mean-field and quantum Monte Carlo analysis show that different types of instabilities, depending on t'/t ratio and filling fraction, exist [138]. At small t'/t around half-filling the Fermi surface is nested giving rise to the formation of an antiferromagnetic state. For non-nested Fermi-surface (when t' is large enough) the effect of frustration relevant to hopping appears and leads to superconducting instability [56]. However,

the system becomes ferromagnetic at $t'/t \approx 1/2$ as a result of band flattening [207, 70, 88, 87].

In the vicinity of VHSs the tendency towards magnetism or superconductivity can be also observed. In fact, near van Hove filling both particle-particle and particle-hole contributions are divergent, making mean field or T – matrix methods, which keep track of particle-hole or particle-particle instability respectively, inapplicable. Formally the problem can be resolved by applying parquet summation [41, 62, 61, 63], allowing to sum up leading logarithmic singularities stemming from different channels, or functional RG [232, 84, 89, 90] (in this case the standard field-theoretical RG is a special case as shown below). In principle, the use of functional RG is more preferable since the full momentum dependence of electron-electron vertices as well as both regular and singular contributions to their renormalization are treated in a more delicate way.

Furthermore, the formation of non-Fermi liquid state is another option for two-dimensional itinerant systems. Typically non-Fermi liquid behavior results from the failure of Landau approach for certain energies in the vicinity of Fermi surface. The formation of pseudogap phase is likely to be considered as the most paradigmatic example that might be used to illustrate a violation of Landau theory, e.g., the appearance of hole pockets in this regime in weakly doped high-temperature superconductors near the nodal points on the Brillouin zone diagonals can be detected [103] (formally, it corresponds to the case $m^* < 0$). Meanwhile, pseudogap phase takes place on Fermi surface sheets connected by antiferromagnetic ordering wave vector, therefore these are antiferromagnetic fluctuations which are responsible for its formation. However, different numerical methods, e.g., FLEX [49, 7] or two-particle self-consistent approximation [221, 155], turn out to be not satisfactory enough to pursue a systematic study of two-dimensional Hubbard model as they are limited by a certain class of skeleton diagrams. Nevertheless, FLEX demonstrate the formation of non-Fermi liquid state at half-filling at low temperatures, while the behavior of a spectral function at strong coupling can be addressed within quantum Monte Carlo implemented for finite-sized clusters [219], remaining however regimes of weak and intermediate interaction unsolved.

1.2 Dual Fermion Method: A step beyond DMFT

When interaction in a many-body system is strong enough, so that collective effects come into play, the standard paradigm of elementary excitations can not be directly applied. In particular, at low temperatures physical properties are purely determined by the trade-off between quantum-mechanical extended state of electrons on a lattice and Coulomb repulsion of local nature. The latter could happen in transition metals or rare-earth compounds with partially filled $3d$ – and $4f$ – shells which are the systems with strong electron correla-

tions. A radial wave-function in these systems is non zero everywhere, making electronic density higher in the proximity to nuclei. The matrix element of Coulomb repulsion U is comparable to that of exchange interaction t requiring the use of atomic and itinerant approaches simultaneously. The simplest theoretical model which treats both on equal footing is the Hubbard model, while the relevant dimensionless parameter is the ratio U/t or U/W, where W is band width. The Hubbard model is believed to be well suited for studying strongly correlated electronic systems and is capable to keep track of a number of relevant phenomena from metal-insulator transition and magnetic ordering to non-Fermi liquid behavior. However, the absence of a small parameter in the most interesting regime $U/W \sim 1$ does not permit to develop a reliable perturbative treatment, stimulating thus practical implementation of different numerical algorithms smoothly interpolating between analytically accessible regimes. With the discovery of high-temperature superconductivity the interest to the Hubbard model has been revived since it captures the basic features characteristic of copper-based materials.

In general one can suggest the classification of numerical routines used for model Hamiltonians by belonging to one of the following groups:

1. *Quantum Monte Carlo algorithms*: The basic idea behind this method is to approximate a physical quantity with the sum of a number of terms (e.g., one can sum up over diagrams, configurations, etc.). However, the number of summands increases exponentially with the number of degrees of freedom though it can be relaxed by means of Markov random walks on the set of all summands. The probability of transition from one state to another is basically determined in accord with Metropolis-Hastings criterion [152] and is relevant to its weight in the sum. Employing Quantum Monte Carlo algorithms, in principle, allows to compute the correlation functions with prescribed accuracy, being however limited by the sign-problem [141]: For fermions averaging is represented by sign-alternating series that can not satisfy the Metropolis criterion. The latter results from antisymmetry of corresponding wave-functions and leads to exponential growth of computational time when lowering the temperature. Thus, the most interesting low temperature regime is hardly to be addressed with Quantum Monte Carlo. Inability to work out thermodynamic quantities on real axis is another disadvantage of the algorithm in question, making the use of analytical continuation from Matsubara frequency domain unavoidable. Thus, the direct implication of this method becomes highly undesirable when dealing with dynamic quantities (susceptibility and Green's function on real axis) and requires to perform poorly-defined analytical continuation, which is very sensitive to numerical noise.
2. There exists a set of methods developed specifically for studying a particular problem or phenomenon, giving rise to quite informative and intuitively clear data. Among them are *Exact Diagonalization*, *Density*

Matrix Renormalization Group [183], and *Numerical Renormalization Group* [37].

3. The methods which suffer from pathological disadvantage (sum rule violation or casuality), e.g. *Non-Crossing Approximation*, *Large – N expansion* [29].

The Coulomb interaction couples indirectly an infinite number of frequencies and spatial modes, making reliable application of the methods like exact diagonalization or quantum Monte Carlo quite illusive due to their exponential complexity and sign-problem respectively. To get over this difficulty the formalism analogous to mean-field approximation has been developed: A standard model of correlated electrons on a lattice is substituted for an impurity interacting with effective medium, which it is embedded into, that needs to be determined self-consistently. Unlike the rest of mean-filed methods, e.g. the one elaborated for Ising model, thus defined substitution known as *Dynamical Mean-Field Theory* (DMFT) takes account of many-body interaction (this indeed takes pace because the effective field acting on each site of a lattice depends on energy). However, by construction DMFT totally disregards the non-local correlations and smoothly interpolates between two exact solutions, namely atomic limit for extremely strong correlation and Landau Fermi-liquid in weakly-coupled system, while the self-energy is purely constructed by solving corresponding Anderson impurity model [11].

Despite of local nature DMFT turns out to be quite successful, e.g., a number of experimental facts are known to be solvable within LDA-DMFT approximation when the lattice dispersion is replaced by that obtained from Density Functional Theory: One is able to reproduce Mott transition in V_2O_3 doped by Cr, or the metal-insulator transition in $La_{1-x}Sr_xTiO_{3-\delta}$. Nevertheless, the effects of non-locality must be treated carefully in an attempt to explain the formation of Luttinger liquid in low-dimensional systems, establish the nature of insulating phase in V_2O_3, address systems with strong quantum fluctuations and VHSs, elucidate experiments with copper-based high-temperature superconductors, and basically deal with the systems where self-energy part is characterized by non-trivial dispersion.

To subdue the limitations inherent to DMFT and expand the scope of its applicability the *Dual Fermion Method* has been recently proposed [180, 83]. In fact, within DMFT decoupling of frequencies and lattice degrees of freedom is formally achieved by splitting the problem into two independent pieces: The impurity problem is accomplished on frequency domain, while the lattice part is solved by self-consistency. Dual Fermion Method [180] suggests to apply Hubbard-Stratonovich transformation to the original lattice model and define a control parameter to develop perturbative expansion on top of DMFT. The zero-order approximation in this case would exactly correspond to DMFT, while the higher-order contributions account for non-local corrections to DMFT.

We assume a many-body problem is determined by its action on Matsubara-frequency domain

$$S\left[\bar{c},c\right]=S_{\mathrm{ex}}\left[\bar{c},c\right]+\sum_{\omega_n}\sum_{\alpha\beta}\bar{c}_{\alpha\omega}D_{\alpha\beta}(\omega_n)c_{\beta\omega}. \tag{1.11}$$

The philosophy of dual fermion method is to split the action (1.11) into two parts: An exactly solvable one $S_{\mathrm{ex}}\left[\bar{c},c\right]$ (e.g., by exactly diagonalizing the corresponding Hamiltonian), so that any correlation function can be estimated with prescribed accuracy, and some quadratic part with the matrix $D_{\alpha\beta}(\omega_n)$. Applying the Hubbard-Stratonovich transformation, which for Fermi-fields reads [235]

$$\begin{aligned}\int\mathscr{D}\left[\bar{f},f\right]\exp\left\{-\sum_{ab}\left[\bar{f}_a\left(ADA\right)^{-1}_{ab}f_b+\bar{c}_aA^{-1}_{ab}f_b+\bar{f}_aA^{-1}_{ab}c_b\right]\right\}\\ =\frac{1}{\det\left(ADA\right)}\exp\left[\sum_{ab}\bar{c}_aD_{ab}c_b\right],\end{aligned} \tag{1.12}$$

where the subscripts label a spin and a frequency $a=\{\alpha,\omega\}$. We defined a collection of Fermi-fields $\bar{f}$, f which are referred to as dual fermions in the following, while the matrix A is to be specified (we choose it in a way to preserve normalization of dual Green's function). With the help of (1.12) the partition function corresponding to the action (1.11) can be rewritten as the integral over the original Fermi fields $\bar{c}$, c as well as dual ones $\bar{f}$, f

$$\mathscr{Z}=\det\left(ADA\right)\int\mathscr{D}\left[\bar{c},c;\bar{f},f\right]\exp\left(-S\left[\bar{c},c;\bar{f},f\right]\right), \tag{1.13}$$

here the newly defined action

$$\begin{aligned}S\left[\bar{c},c;\bar{f},f\right]=S_{\mathrm{ex}}\left[\bar{c},c\right]\\ +\sum_{\omega_n}\sum_{\alpha\beta}\left[\bar{f}_{\alpha\omega}\left(ADA\right)^{-1}_{\alpha\beta}f_{\beta\omega}+\bar{c}_{\alpha\omega}A^{-1}_{\alpha\beta}f_{\beta\omega}+\bar{f}_{\alpha\omega}A^{-1}_{\alpha\beta}c_{\beta\omega}\right].\end{aligned} \tag{1.14}$$

The next step is to integrate the original fields, that leads to so called dual action

$$\frac{\mathscr{Z}}{\mathscr{Z}_{\mathrm{ex}}}=\det\left(ADA\right)\int\mathscr{D}\left[\bar{f},f\right]exp\left(-S^d\left[\bar{f},f\right]\right), \tag{1.15}$$

in general the integration in (1.15) can not be done exactly as the action $S_{\mathrm{ex}}\left[\bar{c},c\right]$ is an arbitrary function of $\bar{c}$, c. However, we can expand the exponential in powers of mixed term $\bar{c}_{\alpha\omega}A^{-1}_{\alpha\beta}f_{\beta\omega}+\bar{f}_{\alpha\omega}A^{-1}_{\alpha\beta}c_{\beta\omega}$ and move back to the exponential taking account of correlation function of the exactly solvable

model. Choosing A to be equal to the exact Green's function of a reference problem $g_{\alpha\beta}(\omega_n)$ we eventually derive the dual action which is the function of dual fields $\bar{f}$, f only

$$S^d\left[\bar{f},f\right] = -\sum_{\omega_n}\sum_{\alpha\beta}\bar{f}_{\alpha\omega}\left[\mathscr{G}_0^d(\omega_n)\right]^{-1}_{\alpha\beta}f_{\beta\omega}$$
$$-\frac{1}{4}\sum_{\omega_1\ldots\omega_4}\sum_{\alpha\beta\gamma\delta}\gamma^{(4)}_{\alpha\beta\gamma\delta}(\omega_1,\omega_2,\omega_3,\omega_4)\,\bar{f}_{\alpha\omega_1}\bar{f}_{\beta\omega_2}f_{\gamma\omega_3}f_{\delta\omega_4}$$
$$-\frac{1}{36}\sum_{\omega_1\ldots\omega_6}\sum_{\alpha\beta\gamma\delta\mu\nu}\gamma^{(6)}_{\alpha\beta\gamma\delta\mu\nu}(\omega_1,\ldots,\omega_6)\bar{f}_{\alpha\omega_1}\bar{f}_{\beta\omega_2}\bar{f}_{\gamma\omega_3}f_{\delta\omega_4}f_{\mu\omega_5}f_{\nu\omega_6}, \quad (1.16)$$

the bare dual Green's function is determined by

$$\mathscr{G}_0^d(\omega_n) = -g(\omega_n)\left[g(\omega_n)+D^{-1}(\omega_n)\right]g(\omega_n). \quad (1.17)$$

We can see that the dual action $S^d\left[\bar{f},f\right]$ is more complicated than the original one and comprises the non-linear terms to all orders in fields, while the coefficients $\gamma^{(4)}$ and $\gamma^{(6)}$ in the formula (1.16) are the irreducible vertices of the reference problem. Developing perturbation theory with respect to the quadratic part of the dual action basically provides more reliable results compared to the bare perturbation expansion, the reason for that is in the fact that the correlation functions g, $\gamma^{(4)}$, $\gamma^{(6)}$ already contain information on the dynamics of the system. It is easy to show the direct relation between the dual Green's function $\mathscr{G}^d(\omega_n)$ with that of original fermions $G(\omega_n)$

$$G(\omega_n) = D^{-1}(\omega_n) + \left(G(\omega_n)D(\omega_n)\right)^{-1}\mathscr{G}^d(\omega_n)\left(D(\omega_n)G(\omega_n)\right)^{-1}, \quad (1.18)$$

here we defined $\mathscr{G}^d_{\alpha\beta}(\omega_n) = -\langle f_{\alpha\omega}\bar{f}_{\beta\omega}\rangle_{S^d}$. Based on the expression (1.18) we can argue the equivalence of the dual picture to the original problem.

Numerical computation of higher-order correlation function from QMC or ED in general is very sophisticated task, therefore typically one restricts oneself to the lowest vertex $\gamma^{(4)}$. The realization of dual fermion method in practice can be done by performing the following steps:

1. For a randomly chosen hybridization the corresponding Green's function $g(\omega_n)$ and vertex part $\gamma^{(4)}$ are determined, e.g. by means of quantum Monte Carlo.
2. The bare dual Green's function $\mathscr{G}_0^d(\omega_n)$ determined by (1.17) needs to be computed.
3. The dual self-energy $\Sigma^d(\omega_n)$ is constructed from perturbative expansion (typically one estimates the lowest diagrams).
4. Knowing both the Green's functions $\mathscr{G}_0^d(\omega_n)$ and the self energy part $\Sigma^d(\omega_n)$ allows to estimate the dual Green's function $\mathscr{G}^d(\omega_n)$ from the

Dyson equation:

$$\mathscr{G}^d(\omega_n) = \mathscr{G}_0^d(\omega_n) + \mathscr{G}_0^d(\omega)\Sigma^d(\omega_n)\mathscr{G}^d(\omega_n). \tag{1.19}$$

Calculation of skeleton diagrams can be done iteratively by computing $\Sigma^d(\omega_n)$ and $\mathscr{G}^d(\omega_n)$ unless convergence.

5. To obtain the new hybridization function and meet the self-consistency condition.
6. Repeat the steps unless convergence of $\mathscr{G}^d(\omega_n)$ and the hybridization. The last step is to calculate the Green's function of an original problem (1.18).

1.3 Fermi Condensate: A new approach to the old problems

It was shown recently that Pomeranchuk criterion is not exhaustive and does not include at least one kind of instability [112]. In fact, under certain conditions the effective mass (1.10) of a quasiparticle can be large enough, reducing thus kinetic energy dramatically and making the potential part dominant. The latter results in a new state of matter, namely the fermion condensate [113, 112, 223], which is separated from a normal Fermi liquid by a quantum phase transition. At $T = 0$ when $(x - x_{FC}) \to 0$ the effective mass m^* diverges, and in this case the ground state is purely determined by potential energy and the phase transition [10, 189], reducing the total energy, must rebuild the distribution function (1.6) according to

$$\frac{\delta E\left[n_{\mathbf{k}}\right]}{\delta n_{\mathbf{k}}} = \varepsilon_{\mathbf{k}} = \mu \tag{1.20}$$

for certain momenta $k_0 \leq k \leq k_1$. Consequently, within this interval the occupation fraction does not coincide with the Fermi-Dirac distribution (1.9). In fact, at $T = 0$ the step-like distribution function $n_{\mathbf{k}} = \theta(k_F - k)$ is not unique, there exists anomalous solution (1.20) if the logarithm on the right-hand side of (1.6) is finite, which is possible as long as $0 < n_{\mathbf{k}} < 1$ for momenta $k_0 < k < k_1$.

The distribution function obtained by solving the variational problem corresponds to a new class of solutions of Landau functional and is characterized by high degree of degeneracy, while the entropy (1.2) goes to some finite value $S(T \to 0) \to S_0$. On approaching the critical density $x \to x_{FC}$, when the Fermi condensate appears, the momenta $k_0 \to k_1 \to k_F$ and deviation $\delta n_{\mathbf{k}} = n_{\mathbf{k}} - \theta\left(k_F - k\right)$ becomes small enough. The energy functional (1.1) can be expanded in powers of $\delta n_{\mathbf{k}}$, keeping the lowest order we derive

$$\mu = \varepsilon_{\mathbf{k}} = \varepsilon_{\mathbf{k}}^{(0)} + \int \frac{d^3\mathbf{p}}{(2\pi)^3} f_{\mathbf{k},\mathbf{p}} \delta n_{\mathbf{p}} \tag{1.21}$$

for $k_0 \leq k \leq k_1$, provided the single-particle quasiparticle energy is equal to $\varepsilon_{\mathbf{k}}^{(0)} = \delta E[n_{\mathbf{k}}]/\delta n_{\mathbf{k}}$ as well as Landau amplitude $f_{\mathbf{k},\mathbf{p}}$ are calculated for step-like distribution function. The equation (1.21) allows non-trivial solution for $x \leq x_{FC}$ if the corresponding Landau amplitude is positive and large enough to guarantee the kinetic energy is much smaller than the potential one. Consequently, by means of (1.21) the usual Fermi-Dirac distribution transforms into a continuous function which defines the Fermi condensate quantum phase transition.

Summarizing, the Fermi condensate can be thought of as strongly correlated Fermi-liquid at $x < x_{FC}$, where quasiparticles form a collective state, governed by a macroscopic number of quasiparticles with momenta $k_0 < k < k_1$. The shape of the quasiparticle band-function is universal and independent of Landau amplitudes, characterizing the system taken in its entirety, and determines only the width of the interval $(k_1 - k_0)$ occupied by the Fermi condensate, making the notion of quantum protection viable. In particular, quantum protection [135, 12] means that thermodynamic and transport properties are determined by the Fermi condensate exclusively.

It is worth studying the topological properties of a Fermi condensate. Well known normal and marginal Fermi liquids as well as Luttinger liquid belong to the same topological class: Green's functions correspondent to the states in question are characterized by a vortex-like state in the reciprocal space, whereas in Fermi condensate this vortex is split into two half-quantum vortices connected by a vortex sheet. The Green's function of normal Fermi-liquid is given by

$$G_{\mathbf{k}}(\omega) = \frac{Z}{\omega - v_F(k - k_F) + i\Gamma_{\mathbf{k}}\mathrm{sgn}(k - k_F)}, \tag{1.22}$$

where Z is the quasiparticle residue. To understand the topological nature of the Fermi condensate we consider a single particle Green's function $G_{\mathbf{k}}(\Omega)$ given on Matsubara frequency domain $\omega = i\Omega$, which is singular at $\Omega = 0$ [2]. For a normal Fermi-liquid the singular points are distributed along the Fermi surface and characterized by the following invariant [223]

$$N = \oint \frac{d\lambda}{2\pi i} \mathrm{Tr}\left[G_{\mathbf{k}}(i\omega)\partial_\lambda G_{\mathbf{k}}^{-1}(i\omega)\right], \tag{1.23}$$

where the trace stands for the summation over spin and momentum degrees of freedom and the integration has to be done over an arbitrary contour enclosing the singularity of Green's function. If a singularity allows analytical treatment, e.g., a pole, N coincides with its multiplicity. In case of a normal Fermi-liquid the Green's function (1.22) is characterized by a simple pole, so that $N = 1$ per spin. The index N remains integer even for non-analytic singularities and can not be changed in a continuous way, making it insensitive to smooth variation of the corresponding Green's function. Physically N is analogous to topologically stable singularities of the phase of a superfluid

condensate. The invariant in question preserves its value even for non-pole systems (marginal Fermi and Luttinger liquids), making them topologically equivalent to a normal Fermi liquid. However, that does not hold for the Fermi condensate: In this case a topological defect with $N = 1$ can not disappear due to topological stability and transforms into a vortex sheet, where the discontinuity of the phase of the Green's function happens. For $\varepsilon_{\mathbf{k}} = \mu$ the Green's function $G(\Omega) = (i\Omega)^{-1}$ picks up π, meaning that the boundaries form the half-quanta vortices, i.e. $N = 1/2$. Thus, contrary to the well-known marginal Fermi and Luttinger liquids a system with Fermi condensate belongs to this class of Fermi liquids, while the transition to a new class can be ascribed as a Lifshitz topological phase transition that happens at $T = 0$ [223, 225, 226]. Interestingly, the Fermi condensation can appear in superconducting states as well, provided the interaction is strong enough.

It is noticeable to see how robust Fermi condensation is in an external magnetic field B. In the presence of two-body interaction, which however is assumed to be very small, the superconducting order parameter $\kappa_{\mathbf{k}}$ is finite in the region occupied by the Fermi condensate, but the gap being proportional to the coupling is small, so that even weak magnetic field destroys both $\kappa_{\mathbf{k}}$ and the Fermi condensate: In fact, on destroying the Fermi condensate the magnetic field lowers the energy of a system by $\Delta E_B \propto B^2$ (so that the Fermi condensate restores when $B \to 0$). Nevertheless, the new distribution function $n_{\mathbf{k}}$ in the region $(k_1 - k_0)$, occupied by the Fermi condensate, has to lead to a finite energy gain compared with a normal Fermi-liquid. Therefore, for weak magnetic fields a new state with no Fermi condensate has to be of the same energy as that with Fermi condensate. The latter can be achieved by assuming multiply connected Fermi-spheres (see Fig. 1.1), where the smooth distribution function $n_{\mathbf{k}}$ in $k_0 \le k \le k_1$ is replaced by [17, 169, 48, 236]

$$\nu_{\mathbf{k}} = \sum_{m=1}^{n} \theta\left(k - k_{2m-1}\right) \theta\left(k_{2m} - k\right) \tag{1.24}$$

with $k_0 \le k_1 < k_2 < \ldots < k_{2m} \le k_1$, such that

$$\int_{k_{2m-1}}^{k_{2m+3}} \nu_{\mathbf{k}} \frac{d^3\mathbf{k}}{(2\pi)^3} = \int_{k_{2m-1}}^{k_{2m+3}} n_{\mathbf{k}}^{(0)} \frac{d^3\mathbf{k}}{(2\pi)^3} \tag{1.25}$$

and the width of each block of the Fermi sphere $\delta k = k_{2m+1} - k_{2m} \propto \sqrt{B}$. Thus, at $T = 0$ and $B \to 0$ the width $\delta k \to 0$, while the behaviour of a Fermi liquid with Fermi condensate is replaced by that of a normal Fermi liquid with Fermi momentum $k_1 > k_F$ and constant electron density.

Despite of being quite promising and attractive, the concept of Fermi condensation can not be developed purely on theoretical grounds. However, a number of exactly solvable models and experimental facts, which are hard to

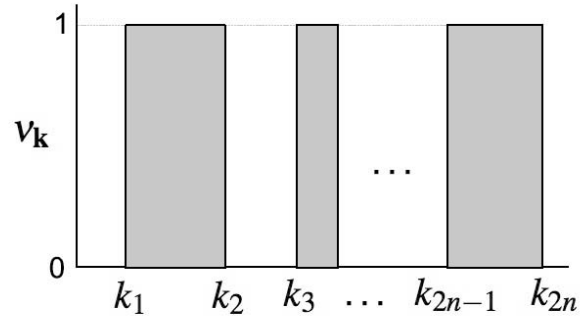

Figure 1.1. The picture illustrates the expression (1.24). The region occupied by the Fermi condensate $k_0 < k_F < k_1$, whenever $k \approx k_{2n} \approx k_1$ the distribution is nothing but the step-wise function and the system is in a Fermi-liquid state.

be explained without addressing the model in question, mimics Fermi condensation behavior. In this section we briefly consider a variety of exactly solvable models which definitely manifest the formation of Fermi condensation [113, 114, 64, 136, 95].

1. Detailed investigation of Fermi condensation has been initiated by Khodel and Shaginyan [113]. We start from a model Landau functional comprising two-body interaction only

$$E[n_{\mathbf{k}}] = \int \frac{d^3\mathbf{k}}{(2\pi)^3}\frac{k^2}{2m} + \frac{1}{2}\int \frac{d^3\mathbf{k}}{(2\pi)^3}\frac{d^3\mathbf{p}}{(2\pi)^3} U(\mathbf{k}-\mathbf{p})\, n_{\mathbf{k}} n_{\mathbf{p}}. \qquad (1.26)$$

Basically, on working out the functional (1.26) one is restricted to particle-hole channel only with no possibility to deal with superconducting correlations. In the simplest model a finite long-range interaction in coordinate space is considered: $U(\mathbf{k}-\mathbf{p}) = U(2\pi)^3\delta(\mathbf{k}-\mathbf{p})$ [113, 161], which leads to the chemical potential

$$\mu = \frac{k_F^2}{2m} + \frac{U}{2}, \qquad (1.27)$$

whereas the quasiparticle energy $\varepsilon_k = k^2/(2m) + Un_{\mathbf{k}}$. This model is stable as long as $U > 0$, and there are two critical values $U_1 = 0$ (when Fermi condensation appears) and $U_2 = \varepsilon_F (5/2)^{2/3}$ (when $k_0 \to 0$). For $U > U_2$ all particles are in Fermi condensed phase, and the distribution function can be written as

$$n_{\mathbf{k}} = \begin{cases} 1, & k < k_0, \\ \frac{k_1^2 - k^2}{k_1^2 - k_0^2}, & k_0 < k < k_1, \\ 0, & k > k_1. \end{cases} \tag{1.28}$$

2. Another model that describes particles subjected to a harmonic potential $V(\mathbf{r}) = \mathbf{r}^2/(2m)$ and interacting via Coulomb forces corresponds to $U(\mathbf{k}-\mathbf{p}) = g/|\mathbf{k}-\mathbf{p}|$. In agreement with Pauli exclusion principle $n_{\mathbf{k}} < 1/(2\pi)^3$ and the Fermi-Dirac step function coincides with the distribution function of the problem in question as long as $\xi = 1 - m/m^* \leq \xi_c = gm/(6\pi^2)$ (harmonic potential dominates over Coulomb interaction). The chemical potential reads $\mu = k_F^2 (1+2\xi)/(2m)$, while

$$\varepsilon_{\mathbf{k}} = \begin{cases} \frac{k^2(1-\xi)}{2m} + \frac{3k_F^2\xi}{2m}, & k < k_F, \\ \frac{k^2}{2m} + \frac{k_F^3\xi}{km}, & k > k_F. \end{cases} \tag{1.29}$$

The effective mass m^* diverges when $\xi \to 1$, at $\xi > 1$ Coulomb repulsion exceeds quasi-elastic forces, and the distribution function needs to be reshaped as follows $n_{\mathbf{k}} = \theta(k-k_1)/\xi$, whereas $k_1 = k_F \xi^{1/3}$ and $\mu_1 = 3k_1^2/(2m)$, while

$$\varepsilon_{\mathbf{k}} = \begin{cases} \mu_1, & k < k_1, \\ \mu_1 + A(k-k_1)^2, & k > k_1, \end{cases} \tag{1.30}$$

here A is a constant.

3. One more interesting toy system can be developed based on an extended two-dimensional Khatsugai-Komoto model [136] which to some degree is equivalent to the Hubbard problem, provided the latter allows the hopping to an arbitrary site. The Hamiltonian is written as

$$H = \sum_{\mathbf{k}} \varepsilon_{\mathbf{k}} n_{\mathbf{k}} + \frac{1}{2V} \sum_{\mathbf{k},\mathbf{p}} f_{\mathbf{k},\mathbf{p}} n_{\mathbf{k}} n_{\mathbf{p}}, \tag{1.31}$$

here we put $n_{\mathbf{k}} = \bar{c}_{\mathbf{k}} c_{\mathbf{k}}$ and $f_{\mathbf{k},\mathbf{p}}$ is the operator responsible for interaction among the particles. In thermodynamical limit $V \to \infty$, and

$$f_{\mathbf{k},\mathbf{p}} = U_k (2\pi)^2 \delta(\mathbf{k}-\mathbf{p}) \frac{g(\varphi)}{k}. \tag{1.32}$$

Here φ is the angle between $\mathbf{k}$ and $\mathbf{p}$, while the functions U_k and $g(\varphi)$ are chosen randomly, provided the function $g(\varphi)$ has even 2π – periodic. In addition, we assume $g(\varphi)$ takes the maximum value at $\varphi = \pi$ and monotonically decreases when $\varphi \to 0$. By doing so we are able to estimate the ground state energy as well as distribution function continuous in k (non-Fermi liquid behavior typical to Fermi condensate) in closed analytical form. The distribution function is determined by $n_{\mathbf{k}} = \varphi_k/(2\pi)$, where φ_k is the solution to

$$\varepsilon_k + U_k \int_0^{\varphi_k} g(\varphi) d\varphi = \mu. \tag{1.33}$$

In the formula we assume that $\varepsilon_{\mathbf{k}}$ is independent of φ. To illustrate our speculations we try

$$g(\varphi) = \begin{cases} \left(\pi^2 - \varphi^2\right)^{-1/2}, & 0 < \varphi < \pi, \\ \left(\pi^2 - (2\pi - \varphi)^2\right)^{-1/2}, & \pi < \varphi < 2\pi. \end{cases} \tag{1.34}$$

We can identify an artificial singularity at $\varphi = \pi$, where the tangential to $n_{\mathbf{k}}$ is horizontal at $n_{\mathbf{k}} = 1/2$. The function is non-analytical at k_a and k_b

$$n_{\mathbf{k}} = \begin{cases} 1 - \frac{1}{2}\sin\left(\frac{\mu - \varepsilon_k}{U}\right), & k_a < k < k_*, \\ \frac{1}{2}\sin\left(\frac{\mu - \varepsilon_k}{U}\right), & k_* < k < k_b. \end{cases} \tag{1.35}$$

4. One can also work out analytically two-dimensional Fermi systems with the ground state given by the energy functional [114]

$$E\left[n_{\mathbf{k}}\right] = \int \varepsilon_{\mathbf{k}} n_{\mathbf{k}} d^2\mathbf{k} + \frac{1}{2V} \int f_{\mathbf{k},\mathbf{p}} n_{\mathbf{k}} n_{\mathbf{p}} d^2\mathbf{k} d^2\mathbf{p} \tag{1.36}$$

(the notation used in the formula are in full agreement with those of Landau Fermi-liquid theory). Taking account of the constraint $0 < n_{\mathbf{k}} < 1$ one can try to reformulate the interaction among the electrons in terms of magnetic (Ampere) forces which act between currents. If this is the case the Landau amplitude can be replaced by a screened vertex function

$$f_{\mathbf{k},\mathbf{p}} = -\Gamma\left(\mathbf{k},\mathbf{p};\mathbf{q}\right) = -g\frac{\left(\mathbf{k}\cdot\mathbf{q}\right)\left(\mathbf{p}\cdot\mathbf{q}\right) - q^2\left(\mathbf{k}\cdot\mathbf{p}\right)}{kpq^2}, \tag{1.37}$$

here $\mathbf{q} = \mathbf{k} - \mathbf{p}$. There exists a critical value $g_c = 6/\pi$, so that for $g > g_c$

$$n_{\mathbf{k}} = \begin{cases} 1, & k < k_1, \\ \frac{1}{2\pi g}\frac{k_0^2 + 3k^2}{k^2}, & k_1 < k < k_2, \\ 0, & k > k_2, \end{cases} \tag{1.38}$$

where $k_0 = k_F\sqrt{\frac{2\pi g}{4 + \log\left(\frac{2\pi g - 3}{g}\right)}}$, $k_1 = k_0\left(2\pi g/3 - 1\right)^{-1/2}$, and $k_2 = k_0/\sqrt{3}$.

We describe as the fifth example the Hubbard model on a triangular lattice. The results from this consideration constitute the main parts of Paper I, in the list of publications of this thesis, and for that reason we describe this model in more detail than the previous four examples of Fermi condensation. We start with the Hamiltonian

$$H = \sum_{\mathbf{k}\sigma} \varepsilon_{\mathbf{k}} d^{\dagger}_{\mathbf{k}\sigma} d_{\mathbf{k}\sigma} + U \sum_i n_{i\uparrow} n_{i\downarrow} \tag{1.39}$$

with local Coulomb repulsion $U > 0$ and dispersion relation

$$\varepsilon_{\mathbf{k}} = -2t\left[\cos(k_x a) + 2\cos(k_x a/2)\cos(k_y a\sqrt{3}/2)\right] - \mu, \tag{1.40}$$

where $t > 0$ is the hopping amplitude, μ the chemical potential, and a is the lattice spacing. We take $a = 1$ in the following. The reciprocal lattice is spanned by the vectors $\mathbf{G}_1 = 2\pi\left(\mathbf{e}_x\sqrt{3} - \mathbf{e}_y\right)/\sqrt{3}$ and $\mathbf{G}_2 = 4\pi\mathbf{e}_y/\sqrt{3}$, while the first Brillouin zone is hexagon shaped. At $3/4$ filling, logarithmic VHSs (kinks in the DOS) appear in three inequivalent saddle points $M_1 = (0, 2\pi/\sqrt{3})$, $M_{2,3} = (\pi, \pm\pi/\sqrt{3})$, and the hexagon-shaped Fermi surface becomes highly nested (Fig. 1.2). It is well known that in the weak coupling limit $U/t \ll 1$, the dominant instability for a non-nested Fermi surface away from VHSs is related to superconductivity. Contrary to this, at saddle points ($\nabla_{\mathbf{k}}\varepsilon_{\mathbf{k}} = 0$) the Fermi surface has flat sides and is nested as a result. The vector $\mathbf{Q}_{\alpha\beta}$ connecting different points M_α and M_β is such that $2\mathbf{Q}_{\alpha\beta} = 0$ modulo a reciprocal lattice vector. In what follows we will focus on the model doped exactly to the VHS ($\mu = 2t$) and perfect nesting.

As it was mentioned the random phase approximation is not sufficient even at weak coupling, excluding the case when divergence appears in one particular channel only. We deal with two-dimensional system doped to van Hove filling, in this case the susceptibilities diverge in both channels it is important to account of the mutual dependence. At weak and intermediate coupling the field-theoretical RG approach might be an optimal option (we refer to that as Wilsonian which operates with successive mass shell integration, $\Lambda - d\Lambda < \varepsilon_{\mathbf{k}} < \Lambda$) [192]. However, in the vicinity of VHSs the direct application of this method becomes problematic: In fact, being doped to van Hove level the Fermi surface is characterized by a number of saddle points, $\nabla_{\mathbf{k}}\varepsilon_{\mathbf{k}} = 0$ (e.g. these are M_1, M_2, and M_3 points on triangular lattice). In this case the states with the same energy become inequivalent: The states with momenta close to the saddle points result in leading divergence in electron-electron vertices. Thus, besides the standard division into fast ($\varepsilon_{\mathbf{k}} > \Lambda$) and slow ($\varepsilon_{\mathbf{k}} < \Lambda$) an extra patching must be done [74]. To provide an analytical estimate for the Hubbard model in question three-patch scheme is to be realized, i.e., the most singular contributions from the close neighbourhood (patch) of saddle points are considered. The momentum-dependence of electron-electron vertices is assumed to be the same all around the patch.

At van Hove filling the density of states on the Fermi surface as well as electron-electron interaction contain logarithmic divergencies stemming from integration near the saddle points. These terms provide the leading contribution to the RG analysis, while the rest are subleading and do not change the physics qualitatively. Thus, the integration area can be defined by a set of

$$\text{area}\,(M_i) = \{\mathbf{k} :\ |\mathbf{k} - \mathbf{k}_i| < \Lambda\} \cap \{\mathbf{k} :\ |\varepsilon_{\mathbf{k}}|/t > e^{-\Lambda/|\mathbf{k}-\mathbf{k}_i|}\}, \tag{1.41}$$

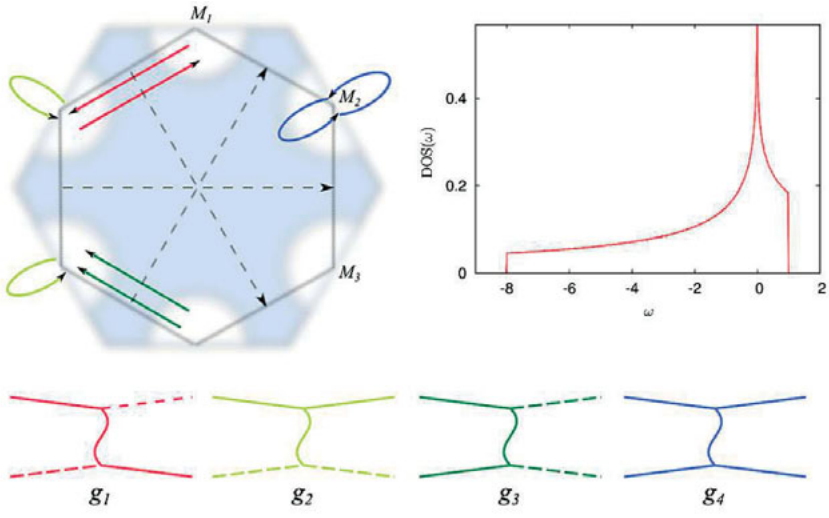

Figure 1.2. Hexagon-shaped Brillouin zone and DOS of the system doped to the VHS. From momenta and spin conservation the following two-particle processes are allowed: exchange scattering (g_1), forward scattering (g_2), umklapp scattering (g_3), and intra-patch scattering (g_4).

where Λ is the cut-off parameter, and $i = 1,2,3$. To develop RG we define a set of quasiparticles operators that act on each patch $a_{i\sigma}(\mathbf{k}-\mathbf{k}_i)$ for $\mathbf{k} \in \text{area}(M_i)$.

The number of patches for the triangular lattice agrees with the number of inequivalent saddle points, in which the DOS diverges logarithmically: $N = N_0 \log[\Lambda/\max(2t,T)]$ (here Λ is a high-energy cutoff). The problem in question can be reduced to a quasi-one-dimensional one if we introduce those two-particle scattering processes between different patches, which are allowed by momentum conservation. One-dimensional systems are known to be unstable to the formation of pair instabilities in both Cooper (particle-particle) and Peierls (particle-hole) channels, and result in logarithmic singularities for pair susceptibilities. Extending the quasi-one-dimensional analysis we define four different interactions associated with two-particle scattering between different patches: exchange (or backward) scattering (g_1), forward scattering (g_2), umklapp scattering (g_3), which conserves momentum modulo a reciprocal lattice vector, and intrapatch scattering (g_4). All four interactions are marginal at tree level, but acquire logarithmic corrections from the integration near the VHS, thus justifying the use of logarithmic RG. These logarithmic corrections come from energy scales $E < \Lambda \approx t$, the energy scale at which higher order corrections to the dispersion become important.

The susceptibilities in the particle-particle $\chi_{pp}(\mathbf{q}=\mathbf{0}) = N_0 \log(\Lambda/T)/2\times$ $\log[\Lambda/\max(2t,T)]$ and particle-hole $\chi_{ph}(\mathbf{q}=\mathbf{Q}_{\alpha\beta}) = \frac{N_0}{2}\log^2[\Lambda/\max(2t,T)]$ channels, evaluated at momentum transfers zero and $\mathbf{Q}_{\alpha\beta}$ between points M_α and M_β, are log-square divergent. One logarithm stems from the DOS,

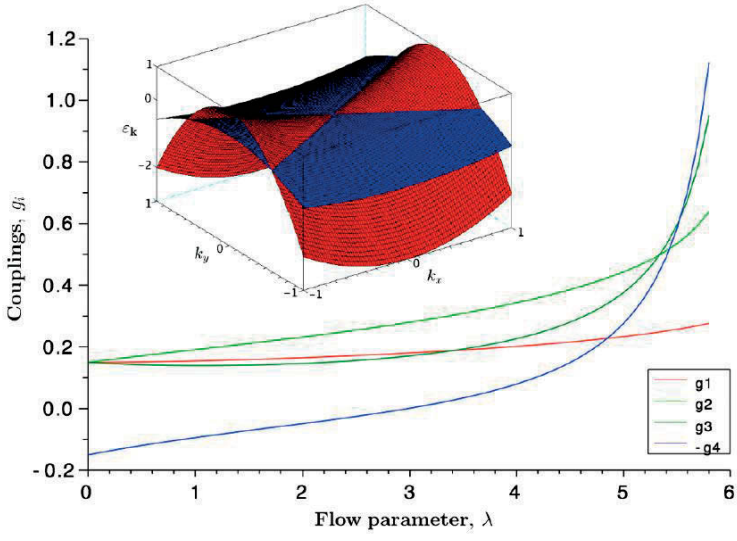

Figure 1.3. Main panel: Renormalization group flow of the couplings g_i. Inset: Dispersion relation in the vicinity of the saddle point corresponding to the bare (red) and renormalized (blue) action. The flattening of the band is clearly visible. The plotting region is determined by the cutoff parameter $\Lambda/t \sim 1$.

whereas the second is inherent to the divergence in the Cooper channel for χ_{pp} and appears in $\chi_{ph}(\mathbf{Q})$ due to perfect nesting of the Fermi surface. For the analysis of the low-energy properties we neglect the logarithmically divergent contributions $\chi_{ph}(\mathbf{0})$ and $\chi_{pp}(\mathbf{Q})$, which are parametrically smaller. Restricting the integration region to the patches and placing external momenta at the critical points, we derive one-loop RG equations using momentum-shell integration [192] with respect to the flow parameter $\lambda = \chi_{pp}(\mathbf{q} = \mathbf{0}, E)$. It is noteworthy that to leading order the solution to a set of RG equations is defined by the relative weight between the Peierls and Cooper channels only. Because of nesting the flow of the coupling constants is strongly modified and the effect of interactions is dramatically enhanced. An inspection of RG flow in Fig. 1.3 reveals that the couplings diverge when approaching instability region λ_c with $|g_4| > g_3 > g_2 > g_1$; i.e., intrapatch scattering prevails. Thus, the local repulsive coupling can favor the formation of instabilities towards magnetic or superconducting states at relatively high temperatures $\lambda_c = \chi_{pp}(E = T_c)$, e.g., for the initial values of running couplings g_0,

$$T_c \sim t \exp\left(-1/\sqrt{g_0 N_0}\right) \tag{1.42}$$

even if the interaction strength is weak compared to the fermionic bandwidth W.

In order to obtain the renormalized band function we proceed by estimating the second-order correction to the self-energy $\Sigma_\omega(\mathbf{k})$ for $\mathbf{k}$ near M_1. We make a distinction among three contributions stemming from intermediate integration with quasimomentum corresponding to the same point and the two other VHSs: $\Sigma_\omega(\mathbf{k}) = \sum_{i=1,2,3} \Sigma^i_\omega(\mathbf{k})$. The band function is determined by the pole of the cutoff-independent Green's function that can be obtained by solving the corresponding Dyson equation, whereas the effects of spectrum renormalization, which describe the flattening, can be absorbed into mass renormalization factors. The remaining divergencies are to be associated with the quasiparticle residue. The resulting quasiparticle spectrum in the vicinity of the M point (with initial $g_1 = g_2 = g_3 = g_4 = 0.15$) is shown in the inset of Fig. 1.3: The spectrum is almost flat in a rather wide range of $\mathbf{k}$ resulting from mass renormalization. The quasiparticle weight is also renormalized under the RG flow (not shown). We find that the pinning of the Fermi level to the VHS remains robust under the RG flow. Thus, we conclude that the effects of renormalization drastically affect the Fermi surface topology, leading to the formation of an extended VHS (EVHS).

In order to demonstrate the robustness and experimental accessibility of the phenomenon, it is necessary to show that the effect persists at finite temperatures and strong interaction. This is a challenging task: While DMFT captures non-perturbative phenomena such as the Mott transition, it neglects spatial correlations. Because of the important role of susceptibilities, the problem cannot be treated in DMFT. Cluster extensions of DMFT lack sufficient momentum resolution. Both criteria are met only in novel approaches combining DMFT with analytical methods. Here we employ the dual fermion technique [180] (see [83] for a comprehensive overview). The resulting spectral function $-(1/\pi)\mathrm{Im}G_\omega(\mathbf{k})$ for $U/t = 8$ is shown in Fig. 1.4. We observe a broadening and flattening of the spectrum at the M point. While flattening of the spectrum is partly present in DMFT due to band renormalization, including spatial correlations leads to the formation of an EVHS. Apart from the incoherent high-energy excitations we observe a well-defined and only slightly dispersive band at low energies, which spans a large region of the Brillouin zone between the M and K points.We have marked the local maxima with a white line. We find that this band agrees perfectly well with the prediction $\varepsilon_\mathbf{k} - \mu = T \log[(1-n_\mathbf{k})/n_\mathbf{k}]$ from Eq. (1.6) (black line) everywhere in the vicinity of the Fermi level. While the results are described by the Landau functional, the self-energy clearly exhibits a power law and hence non-Fermi liquid behavior. For $T \to 0$ this leads to a flat band and Fermi condensation, or the system becomes unstable due to the degeneracy. We therefore interpret the effect as a precursor to a correlated magnetic or superconducting ground state. The formation of this band is correlation driven, as it disappears when the interaction is lowered.

In order to further elucidate the origin of this effect, we note that because of the large DOS at the M point due to the proximity of the VHS, the dom-

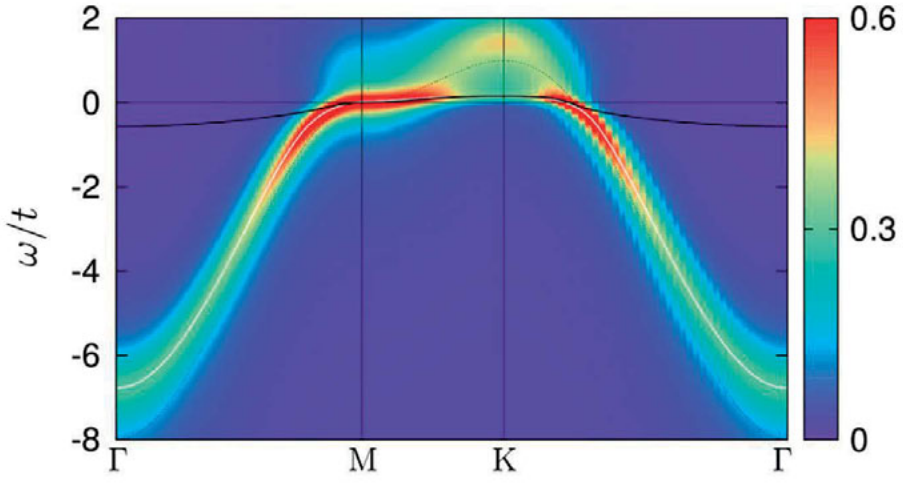

Figure 1.4. Spectral function in dual fermion approach at $U/t = 8$ and $T/t = 0.05$. Local maxima corresponding to the lower band are indicated by a white line. In the vicinity of the Fermi level, this lower band perfectly matches the prediction $\varepsilon_{\mathbf{k}} - \mu = T \log\left[\left(1 - n_{\mathbf{k}}\right)/n_{\mathbf{k}}\right]$ following from the Fermi condensate hypothesis (thick black line). The bare dispersion is shown for comparison (blue, dashed).

inating contribution to the convolution in the self-energy in the vicinity of the M point is expected to stem from the vicinity of the Γ point. An analysis of the leading eigenvalues of the Bethe-Salpeter equation reveals that the spin channel dominates in the vicinity of Γ in agreement with our RG analysis, where intrapatch scattering is found to give the dominant contribution. Hence the effect results from the combination of a large DOS and coupling to strong ferromagnetic spin fluctuations. Indeed, our calculations unambiguously determine this effect to originate from collective excitations in the spin channel. The large self-energy in the vicinity of the M point leads to both a broadening of the spectrum and a strong reduction of spectral weight at the M point, also in agreement with the RG. The flattening is considerably stronger in non-selfconsistent calculations, where attenuation of the fluctuations due to damping of quasiparticles at the M point is not taken into account. The absence of the low-energy band in second-order approximation to the dual self-energy underlines the importance of the feedback of collective excitations onto the electronic degrees of freedom. In the top panel of Fig. 1.5 we plot the so-called broadened Fermi surface within ± 0.1 electrons from the value 0.5 corresponding to the interacting Fermi surface for given temperature. This quantity is directly related to the occupation function for different momenta, which is experimentally measurable. The comparison with the noninteracting case shows that the effect of flattening is substantial. Increasing the interaction strength U strongly enhances the flattening while lowering the temperature mitigates it. The correlation-driven effect can, nevertheless, clearly be

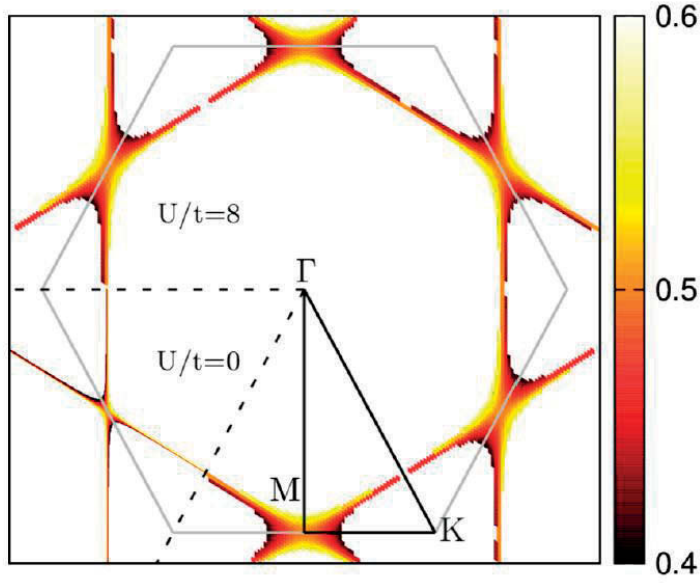

Figure 1.5. Broadened Fermi surface within ± 0.1 electrons for $U/t = 8$ and $T/t = 0.1$. The lower left sextant shows the noninteracting result.

separated from this purely thermal effect even at the highest temperatures. We find that the effect persists up to shifts in chemical potential of at least $0.5t$, showing that it is robust to the presence of a trapping potential

We end this chapter of Fermi condensation with a general analysis of thermodynamic and conducting properties that are expected to emerge from such a state. In the vicinity of Fermi condensate quantum phase transition from the disordered state (Landau Fermi-liquid) the entropy is known to be determined by $S(T) \sim \sqrt{T}$ [188], while the entropy in the Fermi condensed state has to be modified. We know the distribution function $n_{\mathbf{k}}$ is to be rearranged in accord with (1.20), and the entropy contains temperature-independent contribution $S_0 \sim (k_1 - k_0)/k_F \sim |r|$ [here $r = (x - x_{FC})/x_{FC}$]. The quasiparticle spectrum $\varepsilon_{\mathbf{k}} \propto (k - k_1)^2 \sim (k_0 - k)^2$ which links dispersionless phase, occupied by Fermi condensate, and Landau quasiparticles at $k < k_0$ and $k > k_1$ (and can be easily confirmed by toy-model systems), while the entropy at $T \to 0$ [112]

$$S(T) = S_0 + a\sqrt{T} + bT, \tag{1.43}$$

here a and b are constants. The first term on the right-hand side is temperature independent and is responsible for universal thermodynamic and transport properties of heavy electron liquid, whereas the rest terms are purely defined by the quasiparticle spectrum.

The direct consequence of (1.43) is: At Fermi condensate quantum phase transition finite discontinuity of the Hall coefficient $R_H(B)$ as a function of

external magnetic field at $T \to 0$ when the applied field exceeds some critical value $B > B_c$ (observed in $YbRh_2Si_2$ [163]) shows up. In principle, the applied field suppresses the antiferromagnetic phase with Fermi momentum k_F and restore a normal Landau Fermi liquid with the Fermi momentum $k_1 > k_F$. It is quite clear that at $B < B_c$ the ground state of antiferromagnetic phase is well below that of paramagnetic Landau Fermi liquid, and vice versa at $B > B_c$. We already established the state correspondent to Fermi condensate quantum phase transition is highly degenerate, so that in this case the ground state energies of antiferromagnetic state and Landau Fermi liquid coincide. Thus, one can show

$$\frac{R_H(B_c-\delta)}{R_H(B_c+\delta)} \approx 1+\frac{3}{k_F}\left(k_1-k_F\right) \sim 1+\frac{S_0}{x_{FC}}, \tag{1.44}$$

the entropy per a heavy electron is S_0/x_{FC}. Hence, the discontinuity is directly associated with anomalous behavior of entropy and the presence of S_0.

The unusual expression (1.43) also results in a non-Fermi liquid thermal expansion coefficient [8]

$$\alpha(T) = \frac{1}{3V}\left(\frac{\partial V}{\partial T}\right)_p = -\frac{1}{3V}\left(\frac{\partial\left(S/x\right)}{\partial p}\right)_T, \tag{1.45}$$

here p and V are pressure and volume respectively. It is worthy to note the compressibility $K = d\mu/d(Vx)$ is non-sensitive to Fermi condensate quantum phase transition, while

$$\alpha_{FC}(T) \sim \frac{\partial S_0}{\partial p} = a_0 \sim \frac{m^* T}{k_F^2 K}. \tag{1.46}$$

Well-known thermodynamic relation for heat capacity reads

$$C(T) = T\frac{\partial S(T)}{\partial T} \sim \frac{a}{2}\sqrt{T} \tag{1.47}$$

and apparently demonstrates that the Grüneisen ratio

$$\Gamma(T) = \frac{\alpha(T)}{C(T)} \sim \frac{2a_0}{a\sqrt{T}} \tag{1.48}$$

diverges and the Grüneisen law does not hold for Fermi condensed phase.

Typically, in experiments with heavy-fermion compounds the thermodynamic quantities are investigated. However, it would be interesting to observe the fingerprints of distribution function $n_{\mathbf{k}}$ [187, 190] and not only the density of states or effective mass. The latter is possible in transport measurements, scanning tunneling microscopy, contact spectroscopy [54] (closely related with Andreev reflection [13] and is sensitive to the tunneling density of states and the distribution function, as a result). In the following we restrict

our discussion to the normal metals (calculations for superconducting states can performed in the same fashion).

The tunneling current through a point contact between two normal metals is proportional to a gate voltage and the squared transition amplitude $|t|^2$. Within WKB approximation the tunneling current is independent of the density of states, as a consequence at $T \to 0$ the differential conductivity $\sigma_d(V) = dI/dV$ of a normal Landau Fermi-liquid is symmetric and even with respect to the bias V. Formally, the shape of $\sigma_d(V)$ is preserved as long as particle-hole symmetry takes place (that is present in a normal Fermi liquid).

In general, at low temperatures (using atomic units $e = m = \hbar = 1$) $I(V) = a_1 V$, provided $|t|^2 = 1$ differential conductivity $\sigma_d(V) = a_1 = \text{const}$ is a symmetric function of V. The asymmetric part inherent to Fermi condensate can be viewed from the general formula

$$\sigma_d(V) = \frac{1}{T} \int dz n\left[\varepsilon(z) - V, T\right] \left(1 - n\left[\varepsilon(x) - V, T\right]\right) \frac{\partial \varepsilon}{\partial z}, \tag{1.49}$$

where $z = k/k_F$ stands for dimensionless momentum. It is worthy to mention that in the interval $(k_1 - k_0)$ the integration variable ε equals the chemical potential. After some straightforward algebra $\Delta\sigma_d(V) = \left[\sigma_d(V) - \sigma_d(-V)\right]/2$ is given by

$$\Delta\sigma_d(V) = \int \frac{dz}{2} \frac{\alpha\left(1 - \alpha^2\right)\left(1 - 2n(z,T)\right)}{\left[n(z,T)\left(1 - \alpha\right)^2\left(1 - n(z,T)\right) + \alpha\right]^2} \frac{\partial n(z,T)}{\partial z}, \tag{1.50}$$

where $\alpha = \exp\left(-V/T\right)$. Asymmetric tunneling conductivity can be verified in the Fermi-condensed systems, for instance in high-temperature superconductors or heavy-fermion compounds, e.g. $YbRh_2(Si_{0.95}Ge_{0.05})_2$, $CeCoIn_5$, or $YbRh_2Si_2$, when they are in either normal metallic or superconducting phase.

Recent experiments on $CeCoIn_5$ in point-contact spectroscopy explicitly demonstrate asymmetric differential conductivity in both superconducting ($T_c = 2.3$ K) and normal states: $\sigma_d(V)$ is almost constant when the heavy-fermion compound is in a superconducting phase, does not change qualitatively around T_c, and monotonically decreases with temperature away from T_c [162].

To qualitatively estimate $\Delta_d\sigma(V)$ we make use of the fact that $\Delta\sigma_d(V) \propto V$ at low voltage. Being asymmetric with respect to V the differential conductivity switches sign when $V \to -V$. We expect the asymmetric part to be proportional to $\left(k_1 - k_0\right)/k_F$, in the region occupied by the Fermi condensate:

$$\Delta\sigma_d(V) \approx \frac{cV}{2T} \frac{k_1 - k_0}{k_F} \approx \frac{cV}{2T} \frac{S_0}{x_{FC}} \tag{1.51}$$

since $\left(k_1 - k_0\right)/k_F \sim S_0/x_{FC}$, where S_0 is the entropy peculiar to Fermi condensed phase, whereas c is the constant of the order of one (can be estimated from exactly solvable toy models).

Thus, based on the concept of Fermi condensation a variety of systems from high-temperature superconductors and heavy-fermion compounds to quasi-two-dimensional strongly correlated systems can be studied and characterized by a universal behavior which can be developed within the formalism in question.

2. On the exploration of magnetization dynamics

2.1 Landau-Lifshitz equation: More than spin dynamics

In recent years the focus in solid-state electronics has shifted towards the use of ferromagnet materials. In fact, electronic circuits are known to exploit the charge degree of freedom which can be controlled by applying external electric or magnetic fields and totally disregard the spin degree of freedom. For practical applications the use of normal metals with high electron mobility, which effectively screen an external field, are undesirable due to the lack of their ability to be manipulated by this field. In ferromagnet materials exchange interaction among d – electrons leads to spontaneous magnetization, this interaction is known to be of non-relativistic electrostatic nature (contrary to the standard Lorentz force), therefore being of the order of $0.1 - 1$ eV per an electron, it quantitatively changes the electron dynamics. Interestingly, to achieve spin splitting commensurate with that due to exchange coupling a normal paramagnet has to be placed in external field of the magnitude 10^3 T. However, even a weak magnetic field ($10^{-3} - 1$ T) can influence the electron dynamics in ferromagnet materials profoundly: The exchange interaction is in general isotropic, so that it does not affect the magnetization direction which is determined by magneto-crystalline anisotropy present in real magnetic materials, making thus the use of external field quite effective to tune the magnetization direction. The exchange interaction is of short range ~ 10 nm or less.

Experimental studies of spin-dependent phenomena have been initiated a few decades ago by pioneering works of Aronov and Pikus [16] on spin injection into semiconductors, Dyakonov and Perel [59] on current-induced spin orientation of electrons in semiconductors, and Jullière on tunneling magnetoresistance [102]. Nevertheless, the groundbreaking experiment, demonstrated that electron current in ferromagnet materials is spin-polarized, is believed to be the dawn of the era of spintronics [18]. The spin valve made of two ferromagnetic layers separated by a spacer from non-magnetic metal or insulator today is a workhorse in the field. Depending on the nature of a spacer one can basically outline two mechanisms of spin transport in such a structure: Ballistic regime, when the electron current passes through a normal metal spacer, and tunneling regime that occurs for an insulating layer. In its simplest realization a spin valve is constituted by two ferromagnetic layers that are typically referred to as free layer, characterizing by rather small anisotropy, so that its magnetization direction can be easily tuned by an applied magnetic

field or an external current, and a pinned layer with much stronger magnetocrystalline anisotropy. The phenomenon known as *giant magnetoresistance* could happen depending on relative alignment of magnetization in the layers: Electrical resistance takes the largest value for antiparallel orientation, being extremely sensitive to an external magnetic field. Not only is magnetization controlled by the current, but also the inverse magnetoresistance exists: When the magnitude of the electric current passing to a free layer exceeds a certain critical value its magnetization becomes aligned with that of a pinned layer. This paradox has been successfully resolved by Berger and Slonczewski [23, 197]: The electric current is known also to transport spin current transferring the finite momentum to the second one fitting its magnetization.

Phenomenological theory of ferromagnetism at low temperatures is based on the assumption that the state of magnetic material can be described in terms of magnetization. The magnetization direction is supposed to be a smooth function of the spacial coordinates on the scale of the lattice constant, while the absolute value of the magnetization vector remains unchanged. In this picture the energy of a magnetic material is defined as a functional of the magnetization vector. The minimization of the functional results in the celebrated Landau-Lifshitz equation. The dissipation terms, which are typically present in any physical system, are taken into account phenomenologically via the Gilbert damping. The damping is characterized by a single parameter, which makes this equation inapplicable for studying phenomena related to non-equilibrium spin-dynamics. The discovery of domain wall motion as well as current-driven phenomena in magnetic systems has led to the conclusion that the Landau-Lifshitz equation must be supplemented with the term responsible for such non-equilibrium processes, the so called spin-transfer torque. Contributions of that kind have been first introduced by Slonczewski purely on the grounds of the symmetry consideration and are described by some dissipative coefficients. Dissipative nature of spin-transfer torque is related to the fact that being proportional to the current it breaks inversion symmetry, i.e. couple terms which are odd under time-reversal symmetry with those which are even. This brings a distinction between adiabatic and non-adiabatic spin-transfers torques. Non-adiabatic torques contain information about all processes which violate spin conservation in the systems with no Galilean-invariance.

It has to be said that magnons are collective excitations of localized spins in the crystal lattice which can be viewed as elementary particles, spin-wave quanta. Unlike spin currents, which are carried by electrons in a conductor, the spin-wave currents carry spin but not charge and are immune to dissipation from Joule heating. The main damping mechanism for the spin-wave current is the so-called Gilbert damping, which enters the Landau-Lifshitz-Gilbert-Slonczewski phenomenological equation for magnetization dynamics (Fig. 2.1). In usual ferromagnets this equation takes the form

$$\frac{\partial \mathbf{m}}{\partial t} = -\gamma \mathbf{m} \times \mathbf{H}_{\text{eff}} + \alpha \mathbf{m} \times \frac{\partial \mathbf{m}}{\partial t} + \tau, \tag{2.1}$$

where $\mathbf{m}$ is the magnetization direction, $\gamma = g\mu_B/\hbar$ is the gyromagnetic ratio (expressed through the Bohr magneton, μ_B, and the Lande g – factor), α is the Gilbert damping constant, and τ represents the current-induced torques, which are discussed below. In the following we provide microscopic derivation of the Landau-Lifshitz equation using non-equilibrium Keldysh technique.

Spin-transfer torque lays in the heart of rapidly advancing field of current-induced magnetization dynamics [36]. The interaction of a conduction electron spin with the magnetization of a thin ferromagnetic layer results in a reorientation of the electron spin after transmission. At the same time the change in the direction of an electron spin leads to a torque on the magnetization of the ferromagnet. Thus, the spin-transfer torque provides the coupling between magnetization and electric current. Extraction and detection of spin-wave currents can be realized by the reciprocal effects: Spin pumping from dynamic magnetic insulator emits spin current in the metal [209], while the inverse spin-Hall effect converts the spin current into an electrical signal [212]. These and other experiments demonstrate the possibility to realize spin circuits in insulators, which have low dissipation loss and provide novel forms of signal transmission. This development establishes the field of pure spintronics. The possibility to convert spin-waves, which carry no charge, to electric currents stays behind novel high-performance and power-saving logic schemes such as spin-MOS transistors [206], magnetologic gates [53], and spin-wave logic [126], which have been proposed to meet the challenge of the CMOS scaling coming to an end using current technology. The main contribution to the spin-transfer torque, τ, in the Landau-Lifshitz equation is usually described by the Slonczewski term $\tau \propto \mathbf{m} \times (\mathbf{m} \times \mathbf{I}_s)$, where $\mathbf{I}_s$ is the spin current.

Transport properties of magnetic multilayers and nanostructures made of ferromagnets have been recently attracted considerable attention. Conducting ferromagnets are known to be characterized by spin-polarized current carriers: In this case the energy spectrum is split into two sub-bands, in one of which the electrons align their spins parallel and, in the other, antiparallel to the sample magnetization. The resulting spin splitting is of the order of the Curie temperature, while the giant exchange field present in the ferromagnet can be estimated as $H \sim k_B T_c/\mu_B \sim 10^6 - 10^7$ Oe, where k_B and μ_B are the Boltzmann constant the Bohr magneton respectively. The presence of this field makes the spin-dependent phenomena to be of great interest for practical applications. Newly developed methods of nanostructures formation greatly facilitate control and manipulation of magnetic state in ferromagnets and permit to tune magnetization distribution. The trade-off among magneto-crystalline anisotropy, exchange coupling, and magnetostatic interaction basically determines the magnetization distribution in a specific ferromagnet sample [132]. The resulting magnetic domain structure is not universal and varies from sam-

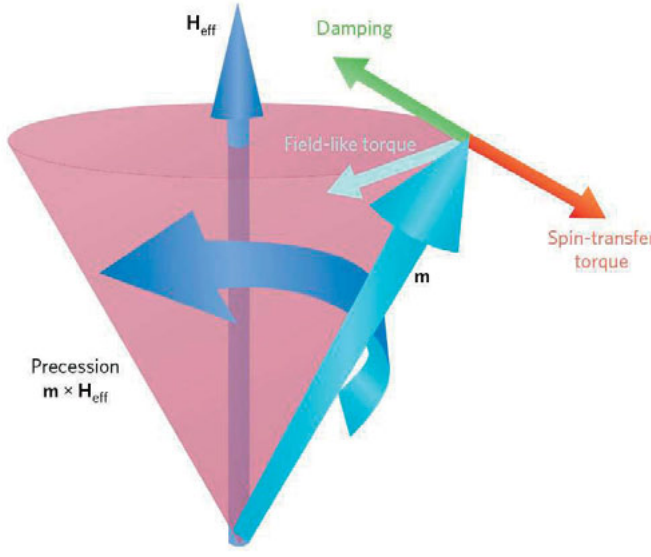

Figure 2.1. The magnetization (**m**) precesses about the effective field direction ($\mathbf{H}_{\text{eff}}$). The green arrow illustrates the dissipative (damping) torque that tends to move the magnetization toward the effective field direction. The red arrow is the spin-transfer torque and the light-blue arrow is the effective field torque with an electron spin polarization collinear with the effective field (the illustration is taken from [36]).

ple to sample and is susceptible to its shape and geometry. On nanometer scale there exist two characteristic lengthscales: The domain wall thickness and the exchange length which are of the order of 10 nm for a transition metal ferromagnet. In the following we briefly review the unique properties inherent to a conducting ferromagnet:

- *Diode and topological Hall effects:* The presence of exchange interaction in inhomogeneous conducting magnetic media can potentially modify the transport properties. Indeed, the current density in spatially uniform electric field **E** is well approximated by

$$j_i = \sigma_{ik} E_k + \gamma_{ikl} E_k E_l + \ldots, \tag{2.2}$$

where we have restricted the description to the linear and quadratic contributions only. Explicit form of the conductivity tensors σ_{ik} and γ_{ikl} strongly depends on the sample magnetization and its spatial derivatives. If a ferromagnet owns a center of inversion symmetry and the passing current does not lead to energy dissipation γ_{ikl} is an odd function of magnetization and its spatial derivatives, while σ_{ik} is an odd function of magnetization and even relative to its spatial derivatives. Requiring the current to be invariant under coherent rotation of a sample magnetization [132], i.e. both linear and non-linear parts of the conductivity tensors do not contain convolution of spatial indices with magnetic ones, and be at-

tributed to exchange effects exclusively the expression of electric current through inhomogeneously magnetized ferromagnet is [72]

$$j_i = \sigma\left(\mathbf{m}\cdot\left[\frac{\partial\mathbf{m}}{\partial x_i}\times\frac{\partial\mathbf{m}}{\partial x_j}\right]\right)E_j + \gamma\left(\mathbf{m}\cdot\left[\frac{\partial\mathbf{m}}{\partial x_i}\times\frac{\partial^2\mathbf{m}}{\partial x_j\partial x_k}\right]\right)E_jE_k, \tag{2.3}$$

here σ and γ are constants (which takes place in isotropic or cubic crystalline structure). The linear conductivity tensor is antisymmetric, contributing thus to the exchange-induced Hall effect, while the non-linear term is responsible for rectification by ferromagnets. We can see the expression (2.3) makes sense and formally is non-zero for magnet with non-coplanar magnetization distribution. One of the paradigmatic examples is a vortex-like configuration with magnetization defined by

$$\mathbf{m} = \left(\sin\theta(\rho)\cos\left(n\varphi+\varphi_0\right), \sin\theta(\rho)\sin\left(\nu\varphi+\varphi_0\right), \cos\theta(\rho)\right), \tag{2.4}$$

where the variables φ and ρ are the corresponding cylindrical coordinates, there is a phase shift φ_0, and ν is an integer number. Thus, for (2.4) the expression (2.3) gives rise to $\mathbf{j} = \mathbf{E}\times\mathbf{B}_{\text{eff}}$ with the effective magnetic field

$$\mathbf{B}_{\text{eff}} = \sigma\left(\mathbf{m}\left[\frac{\partial\mathbf{m}}{\partial x}\times\frac{\partial\mathbf{m}}{\partial y}\right]\right) = \frac{\nu\sigma}{\rho}\frac{d\cos\theta(\rho)}{d\rho}, \tag{2.5}$$

implying a vortex ($\nu = 1, \varphi_0 = \pm\pi/2$) or an anti-vortex ($\nu = -1, \varphi = 0, \pi$) non-coplanar magnetization distribution contributes to the Hall effect. Another example is a conical spin-spiral with magnetic moment

$$\mathbf{m}(z) = (m\cos(qz), m\sin(qz), m_z) \tag{2.6}$$

provided $\mathbf{m}^2 = m^2 + m_z^2$. This type of magnetization manifests that a spin-spiral state permits diode-like properties $j_z = \gamma q^3 m_z\left(1-m_z^2\right)E_z^2$ to be present in the system. We showed the existence of non-trivial effects from simple phenomenological considerations, however a more thorough microscopic picture can be developed.

- *Optical effects:* The basic properties of conduction electrons in ferromagnets can be established from the solution of Schrödinger equation with $s-d$ – exchange potential $(-J\mathbf{m}(\mathbf{r})\cdot\sigma)$, with exchange interaction constant J between localized magnetic texture $\mathbf{m}(\mathbf{r})$ and conduction electrons. In particular, one can show that quasiparticle spectrum in a conical phase ($m_z \neq 0$) is not even with respect to quasimomentum, implying the difference in group velocities between the ensembles of electrons traveling in opposite directions. In a macroscopic system, this difference does not produce any electric current because it is

exactly compensated for by the difference in the number of opposite-moving equilibrium electrons. In mesoscopic systems, however such as small ferromagnetic rings with a non-coplanar distribution of the magnetic moment the removal of Kramers degeneracy and the quantization of quasimomentum can lead to the appearance of predicted [143, 208] persistent electric currents.

In a conical magnetic spiral, spectral asymmetry is responsible for the occurrence of the diode effect, with "easy" current flow direction being determined by the sign of the spiral wave number (left-right spiral) and by where the perpendicular magnetic moment component m_z is directed. The important point is that the wave function components, and hence the expectation value of the electron's intrinsic magnetic moment, depend on the quasimomentum component along the spiral axis. This results in electron scattering by nonmagnetic impurities becoming asymmetric, thus adding to the diode effect [72]. Similar effects (asymmetry in both the group velocity and the scattering rate by nonmagnetic impurities) are responsible for the peculiarities in the spatial dispersion of the permittivity. For a conical magnetic spiral, the expansion of the permittivity tensor may contain an additional term of the form [105]

$$\varepsilon_{\alpha\alpha} = K_{\alpha\alpha}\left(\mathbf{m}\left[\frac{\partial \mathbf{m}}{\partial z} \times \frac{\partial^2 \mathbf{m}}{\partial z^2}\right]\right)k_z \tag{2.7}$$

with k_z being the wave-vector component projected onto the spiral axis. Interestingly, the electric component of the external electromagnetic field can induce sub-bands transitions with probability determined by [73]

$$w_{\mathbf{kp}} = \frac{2\pi}{\hbar}\left(\frac{eqJE_z}{2m\omega^2}\right)\left(1-m_z^2\right)\delta\left(\mathbf{k}-\mathbf{p}\right)\delta\left(\Delta-\hbar\omega\right), \tag{2.8}$$

where ω is the electromagnetic wave frequency, Δ is the spin splitting. In non-complanar magnetic systems the dipole transitions determined by (2.8) lead to a constant electric current, i.e. the photovoltaic effect.

There exists a technical possibility to realize non-collinear helical states in multilayered structures (Fig. 2.2). Indeed, instead of searching for a specific class of materials one can form a multilayered ferromagnetic structure due to the magnetostatic interaction between the layers, the stability of the state being determined by the shape of the particle [218]. Let us consider three homogeneous magnetized magnetic discs with dielectric interlayers between them. The magnetostatic interaction between the layers is antiferromagnetic in character, resulting, as shown theoretically [71, 157], in the ground state of the system being spiral (provided that the interaction energy between the discs is much higher than the energy of anisotropy due to, for example, the disc shape). The magnetic state of a multilayered structure can be analysed experimentally by examining the dependence of its electrical resistance on

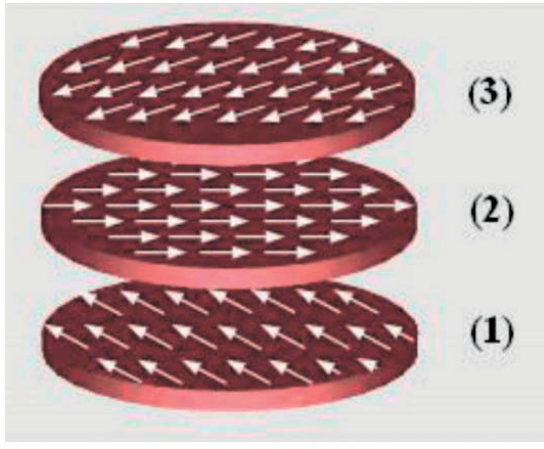

Figure 2.2. Non-collinear helical magnet state in three single-domain discs system (the illustration is taken from [71]).

the external magnetic field. Alternatively, the magnetic states can be investigated by magnetic-force microscopy, but the fact that the signal to measure is dominated by the contribution from the upper magnetic layer [71] makes this approach difficult to apply.

The ballistic regime discussed earlier consists in elastic scattering of spin-polarized electrons at the interface of two magnetic layers and results from the transverse spin component being absorbed by one-two atomic layers of a magnet in the vicinity of the interface, whereas the spin-torque is directed towards the localized magnetic moments of a ferromagnet. To establish the simplest quantitative picture one has to solve the Schrödinger equation [197, 203] provided the wave functions for spin-up and spin-down electrons are not equivalent. The quantum-mechanical expressions for charge- and spin-currents are determined by

$$\mathscr{Q}_e = -\frac{ie\hbar}{2m}\sum_{\mathbf{k}\sigma}\left\langle \bar{\psi}_{\mathbf{k}\sigma}\nabla\psi_{\mathbf{k}\sigma} - (\nabla\bar{\psi}_{\mathbf{k}\sigma}\psi_{\mathbf{k}\sigma})\right\rangle, \tag{2.9}$$

and

$$\mathscr{Q}_s^i = -\frac{i\hbar^2}{4m}\sum_{\mathbf{k}\sigma\sigma'}\left\langle \bar{\psi}_{\mathbf{k}\sigma}\sigma^i_{\sigma\sigma'}\nabla\psi_{\mathbf{k}\sigma} - (\nabla\bar{\psi}_{\mathbf{k}\sigma})\,\sigma^i_{\sigma\sigma'}\psi_{\mathbf{k}\sigma'}\right\rangle, \tag{2.10}$$

here σ^i stands for a set of Pauli matrices, $\psi_{\mathbf{k}\sigma}$ is the correspondent spin-dependent wave-function and $\langle\ldots\rangle$ means the quantum-mechanical averaging. Detailed studies demonstrate that the longitudinal spin component (i.e., spin projection onto magnetization direction of a ferromagnet) remains constant, whereas the transverse component oscillates around an effective field in the layer. Electrons incoming from a metal side are not well correlated, so that

the total coherence is destroyed rather fast on the length scale of the order of spin-spin relaxation, which more or less corresponds to a lattice period. Thus, spin-torque is only present in the close proximity to the interface. Being averaged over the size of a magnetic layer (of the width d) the spin-current leads to a quasi-dissipative term in Landau-Lifshitz equation in full agreement with continuity equation

$$\frac{\partial S^i}{\partial t} + \frac{\mathscr{Q}_s^i}{d} = 0. \tag{2.11}$$

The expression $\mathscr{Q}_s^i$ in the ballistic regime is constituted by two contributions: One of them is aligned with magnetization in the layers and is defined by the celebrated Slonczewski relation [197]

$$\left(\frac{\partial \mathbf{m}}{\partial t}\right)_{\parallel} = J\eta_{\parallel}\frac{\gamma\hbar}{2edm_s^2}\mathbf{m}\times(\mathbf{n}\times\mathbf{m}), \tag{2.12}$$

where $\mathbf{n} = \mathbf{m}/m_s$ is the direction of magnetization (m_s is known to be saturation magnetization) and $\eta_{\parallel}$ spin-polarized Slonczewski factor, whereas the second contribution, or quasi-field, is perpendicular to the layers' magnetization

$$\left(\frac{\partial \mathbf{m}}{\partial t}\right)_{\perp} = J\eta_{\perp}\frac{\gamma\hbar}{2edm_s^2}\mathbf{m}\times\mathbf{n}, \tag{2.13}$$

analogously, $\eta_{\perp}$ is the second Slonczewski factor. In metallic structures the contribution due to (2.13) is typically much smaller than (2.12), being comparable however in tunneling systems. Therefore, in the most general form the Landau-Lifshitz equation in ballistic regime needs to be modified according to the following prescription [238]:

$$\frac{\partial \mathbf{m}}{\partial t} = -\gamma\mathbf{m}\times\mathbf{H}_{\text{eff}} + \frac{\alpha}{m}\mathbf{m}\times\frac{\partial \mathbf{m}}{\partial t} + \frac{\gamma\hbar J}{2edm_s^2}\Big(\eta_{\parallel}\mathbf{m}\times(\mathbf{n}\times\mathbf{m}) + \eta_{\perp}\mathbf{m}\times\mathbf{n}\Big). \tag{2.14}$$

When the typical size of a magnetic heterostructure exceeds a few atomic layers spin-transport becomes diffusive. In equilibrium both spin sub-bands are populated in accord with the Fermi-Dirac distribution and the interband transitions are compensated. However, in the presence of spin-polarized current the equilibrium is disturbed and the time needed for the system to relax to a new quasi-equilibrium is determined by spin-lattice relaxation. Due to diffusive nature of electron motion there always exists a region [118, 82] with non-compensated magnetization. This phenomenon is known as spin accumulation and has been observed in both metallic and semiconductor structures. Thus, spin accumulation consists in the appearance of non-equilibrium spin-density in the vicinity of the interface between two magnetic media and contributes to magnetoresistance [210, 101, 100, 215, 213, 177].

Summarizing, the generalized Landau-Lifshitz equation, including both adiabatic and non-adiabatic spin-transfer torques which are proportional to the current and perpendicular to the magnetization direction (Figure 5), can be rewritten as follows [57]

$$\left(\frac{\partial}{\partial t}+\mathbf{v}\cdot\nabla\right)\mathbf{m}=-\gamma\mathbf{m}\times\mathbf{H}_{\text{eff}}-\alpha\mathbf{m}\times\left(\frac{\partial}{\partial t}+\frac{\beta}{\alpha}\mathbf{v}\cdot\nabla\right)\mathbf{m}, \tag{2.15}$$

here $\mathbf{v}$ is a velocity which can be determined from the current. The effective magnetic field $\mathbf{H}_{\text{eff}}=-\delta W[\mathbf{m}]/\delta\mathbf{m}$ represents variation of the free energy with respect to magnetization, and the Gilbert damping constant is labeled by α. It is easy to establish from (2.15) that $\beta=\alpha$ as long as Galilean invariance is ensured, while in most of realistic materials $\beta\neq\alpha$. The coefficient β, corresponding to non-adiabatic spin-transfer torque, collects all the terms which are non-invariant with respect to spin rotation.

It turns out that the coefficients can be estimated based on a simple microscopic model: An ensemble of electrons that couple via short-ranged repulsive interaction are placed in external electromagnetic field. The Hamiltonian reads

$$\begin{aligned}H[\bar{\psi},\psi]=\int d\mathbf{r}\Big[&\bar{\psi}(\mathbf{r},t)\hat{H}_0\psi(\mathbf{r},t)\\&+g\bar{\psi}_\uparrow(\mathbf{r},t)\bar{\psi}_\downarrow(\mathbf{r},t)\psi_\downarrow(\mathbf{r},t)\psi_\uparrow(\mathbf{r},t)+\frac{1}{c}\hat{\mathbf{j}}(\mathbf{r},t)\cdot\mathbf{A}(\mathbf{r},t)\Big],\end{aligned} \tag{2.16}$$

the coupling strength is g, while the current $\mathbf{j}(\mathbf{r},t)$ and for homogeneous external field one can choose $\mathbf{A}(t)=-ic\mathbf{E}e^{-i\Omega t}/\Omega$. The single-particle Hamiltonian $\hat{H}_0$ can be identified for a specific problem. We will turn to the Keldysh contour to study magnetization dynamics and decouple the Hubbard term into a sum of charge- and spin-densities according to

$$\bar{\psi}_\uparrow\bar{\psi}_\downarrow\psi_\downarrow\psi_\uparrow=\left(\frac{1}{2}\sum_\sigma\bar{\psi}_\sigma\psi_\sigma\right)^2-\left(\frac{1}{2}\sum_{\sigma\sigma'}\bar{\psi}_\sigma\left(\mathbf{n}\cdot\tau\right)_{\sigma\sigma'}\psi_{\sigma'}\right)^2, \tag{2.17}$$

here a unit vector $\mathbf{n}(\mathbf{r},t)$ points in the direction of a quantization axis. With the help of Hubbard-Stratonovich transformation one can define a density field $\langle\rho(\mathbf{r},t)\rangle=\langle\bar{\psi}(\mathbf{r},t)\psi(\mathbf{r},t)\rangle$ and a spin-density field $\langle\Delta(\mathbf{r},t)\mathbf{n}(\mathbf{r},t)\rangle=g\langle\bar{\psi}\tau\psi\rangle/2$ as dynamical variables into the path integral. The density and spin-density are known to be gapped, so that they can be approximated by their saddle-point values.

Performing perturbative expansion around the collinear state, i.e.

$$\mathbf{n}(\mathbf{r},t)=\begin{pmatrix}\delta n_x(\mathbf{r},t)\\ \delta n_y(\mathbf{r},t)\\ 1-\left(\delta n_x(\mathbf{r},t)\right)^2/2-\left(\delta n_y(\mathbf{r},t)\right)^2/2\end{pmatrix}, \tag{2.18}$$

integrating over fermionic fields and keeping the quadratic contribution only the effective action on Keldysh contour reads

$$S_{\text{eff}}[\delta\mathbf{n}] = \int\limits_{\mathscr{C}} dt_1 \int d\mathbf{r}_1 \int\limits_{\mathscr{C}} dt_2 \int d\mathbf{r}_2 \delta n_a(\mathbf{r}_1,t_1)\Pi_{ab}(\mathbf{r}_1,t_1;\mathbf{r}_2,t_2)\delta n_b(\mathbf{r}_2,t_2) + \int\limits_{\mathscr{C}} dt_1 \int d\mathbf{r}_1 \int\limits_{\mathscr{C}} dt_2 \int d\mathbf{r}_2 \delta n_a(\mathbf{r}_1,t_1)K_{ab}(\mathbf{r}_1,t_1;\mathbf{r}_2,t_2)\delta n_b(\mathbf{r}_2,t_2), \tag{2.19}$$

the indices a and b run over x, y. Thus, one can see that magnon propagator $\Pi_{ab}(\mathbf{r}_1,t_1;\mathbf{r}_2,t_2)$ (spin-density spin-density correlation function) determines the Gilbert damping, whereas the photon two-magnon term $K_{ab}(\mathbf{r}_1,t_1;\mathbf{r}_2,t_2)$ contributes to both adiabatic and non-adiabatic spin-transfer torque. To proceed the magnetization $\delta n_a(\mathbf{r},t_\pm) = \delta m_a(\mathbf{r},t) \pm \xi(\mathbf{r},t)/2$, where the $\pm$ stands for the forward and backward branches of the Keldysh contour. The quasiclassical magnetization is determined by $\delta m_a(\mathbf{r},t)$, while the field $\xi_a(\mathbf{r},t)$ is of fluctuating nature. Decomposing the integrals one can immediately identify the saddle point

$$-\Big[\Pi^R_{ab}\left(-i\nabla, i\frac{\partial}{\partial t}\right) + \Pi^A_{ba}\left(i\nabla, -i\frac{\partial}{\partial t}\right) + K^R_{ab}\left(-i\nabla, i\frac{\partial}{\partial t}\right) + K^A_{ba}\left(i\nabla, -i\frac{\partial}{\partial t}\right)\Big] m_b(\mathbf{r},t) = \eta_a(\mathbf{r},t) \tag{2.20}$$

which, in principle, is nothing but generalized Landau-Lifshitz equation, whose more convenient form can be established by expanding the correlation functions in the brackets. The correlation function of the stochastic magnetic field satisfy

$$\langle \eta_a(\mathbf{r}_1,t_1)\eta_b(\mathbf{r}_2,t_2)\rangle = -i\hbar\Big(\Pi^K_{ab}(\mathbf{r}_1-\mathbf{r}_2,t_1-t_2) + K^K_{ab}(\mathbf{r}_1-\mathbf{r}_2,t_1-t_2)\Big) \tag{2.21}$$

here the components with superscripts R, A, and K stand for retarded, advanced, and Keldysh correlations functions respectively. For the sake of simplicity, we provide the expressions which do not take account of vertex corrections (due to scattering off impurities). The casual magnon-magnon response function

$$\Pi_{ab}(\mathbf{q};t_1,t_2) = \frac{i\Delta^2}{8\hbar}\int \frac{d^3\mathbf{p}}{(2\pi)^3}\mathrm{Tr}\big[\tau_a G(\mathbf{p}+\mathbf{q},t_1,t_2)\tau_b G(\mathbf{p};t_2,t_1)\big], \tag{2.22}$$

the photon two-magnon correlation function is determined by a more complicated identity

$$K_{ab}(\mathbf{q};t_1,t_2) = \frac{e\Delta^2}{4m\hbar}\int dt_3 \int \frac{d^3\mathbf{p}}{(2\pi)^3}\frac{e^{-i\Omega t_3}}{\Omega}(\mathbf{p}\cdot\mathbf{E})\times$$
$$\times \mathrm{Tr}\big[\tau_a G(\mathbf{p}+\mathbf{q};t_1,t_2)\tau_b G(\mathbf{p};t_2,t_3)G(\mathbf{p};t_3,t_1)\big]. \qquad (2.23)$$

2.2 BEC of magnons: Quantum coherence at room temperature

The quntum-mechanical exchange interaction is the key concept in the modern theory of ferromagnetism: Indeed, the interaction of this type is known to orient the spin of localized atoms parallel to each other, while the fluctuations above the ground state magnons represent the spin-wave quanta and are known to be the low-energy excitations in magnetically ordered media. In thermal equilibrium the ground state configuration does not impact on transverse spin component which remains uncorrelated even in a ferromagnet state at $T \neq 0$ making coherence of a magnon gas to be quite illusive. For coherent magnon states in full analogy with their photon counterparts [80] an adequate formalism can be developed [178]. One of the most striking quantum phenomena leading to spontaneous quantum coherence on a macroscopic scale is Bose-Einstein condensation (BEC). BEC is a condensation of particles with integer spin, i.e. bosons, which must occupy the lowest available energy state at zero temperature [133]. As the temperature T of the boson gas decreases at a given density n or, vice versa, the number of particles increases at a given temperature, the chemical potential μ describing the gas increases as well. On the other hand, μ cannot be larger than the minimum energy of the bosons, $\varepsilon_{\min}$. The condition $\mu(n,T) = \varepsilon_{\min}$ defines a critical density $N_c(T)$. If the density of the particles in the system is larger than N_c, BEC takes place: The gas is spontaneously divided into two fractions, namely incoherent particles with the density N_c distributed over the entire spectrum of possible boson states, and a coherent ensemble of particles accumulated in the lowest state with $\varepsilon_{\min}$ [133]. Even though the phenomenon was predicted as early as in 1920s it remained experimentally unaccessible for a long time because its observation usually requires extremely low temperatures. This obstacle has been overcome with the invention of laser cooling technique. Currently the BEC of cold atoms in optical traps is well established and a dynamic field [205].

The notion of BEC can be extended to quasiparticles which yield Bose statistics such as polaritons and magnons. At temperatures far below the temperature T_c of magnetic ordering, magnons can be considered as weakly interacting bosons: The Bloch law for the temperature dependence of static magnetization, which nicely describes a bulk amount of experimental data, has been

obtained based on this assumption. Since magnons are bosons one can expect that they undergo the BEC transition. Several groups have reported observation of the magnetic field-induced BEC of magnetic excitations in the quantum antiferromagnetics $TlCuCl_3$ [159, 181], Cs_2CuCl_4 [44, 174], and $BaCuSi_2O_6$ [99]. In these materials, a phase transition from a non-magnetic singlet state to an ordered triplet state, accompanied by magnetic mode softening, occurs if the applied magnetic field is strong enough to overcome the antiferromagnetic exchange coupling. Such a transition can be treated as BEC in an ensemble of magnetic excitations. However, these excitations can hardly be considered as magnons - quanta of spin precession waves propagating in a magnetically ordered system.

The BEC of magnons predicted more than 20 years ago has been recently observed by the group of Demokritov [52]. The experiments were carried out in epitaxially grown films of yttrium iron garnet (YIG) magnetized by an in-plane field at room temperature. Magnetic interactions in such a system are usually characterized by the Heisenberg exchange and dipolar interactions between the spins. The trade-off between these two coupling mechanisms results in the dispersion relation which has a minimum at a certain non-zero value of the wave vector. As a result, the BEC of magnons can hardly be detected unless their chemical potential approaches the threshold energy. Thus the key problem in observing the BEC of magnons was to attain the desired threshold value because equilibrium magnons are normally characterized by zero chemical potential. It was shown that magnons continuously driven by microwave parametric pumping can enormously overpopulate the lowest energy level, even at room temperature [52]. This observation has been associated with the BEC of magnons. At the same time, the possibility of the BEC of quasiparticles in the thermodynamic sense is not evident [199], since quasiparticles are characterized by a finite lifetime which is often comparable to the time a system needs to reach thermal equilibrium. Moreover, an observation of the spontaneous coherence is an important proof of the existence of BEC [51]. Therefore, the study of the thermalization processes for a gas of magnons and the experimental observation of the spontaneous coherence of the magnons overpopulating the lowest state are of special importance for a clear understanding of the phase transition observed in the earlier works [52]. Experiments on the room-temperature BEC of magnons were performed on monocrystalline films of yttrium iron garnet (YIG) with a thickness of 5 mm. YIG ($Y_3Fe_2(FeO_4)_3$) is one of the most studied magnetic substances. YIG films are characterized by very small magnetic losses providing a long magnon lifetime in this substance: It appears to be much longer than the characteristic time of magnon-magnon interaction [50, 51]. This relation is a necessary precondition for Bose-Einstein condensation in a gas of quasiparticles whose number is not exactly conserved [199]. Samples with lateral sizes of several millimeters were cut from the films and were placed into a static uniform magnetic field of $H = 700 - 1000$ Oe oriented in the plane of the film.

The injection of the magnons was performed by means of parallel parametric pumping with a frequency of $8.0 - 8.1$ GHz. The pumping field was created using a microstrip resonator with a width of 25 mm attached to the surface of the sample. The peak pumping power was varied from 0.1 to 6 W. Details on the pumping process can be found in Refs [52, 51, 65]. The redistribution of magnons over the spectrum was studied with a temporal resolution of 10 ns using time-resolved BLS spectroscopy in the quasi-backward scattering geometry [200].

Under the laser pumping certain magnonic modes absorb energy, which is subsequently redistributed over the spectrum via magnon-magnon coupling and eventually transferred to the lattice by means of magnon-phonon interaction. Due to the intense magnon-magnon interaction, the primary magnons are rapidly redistributed over the phase space. The main mechanisms responsible for the energy redistribution within the magnon system are the two-magnon and the four-magnon scattering processes [50]. Four-magnon scattering dominates in high quality epitaxial YIG films. It can be considered as an inelastic scattering mechanism, since it changes the energies of the scattered magnons. As a consequence, four-magnon scattering leads to the spreading of the magnons over the spectrum, keeping, however, the number of magnons in the system constant. Note here that the three-magnon scattering process which does not conserve the number of magnons does not play an important role in the described experiments [65]. In parallel, an energy transfer out of the magnon system due to the spin-lattice (magnon-phonon) interaction takes place. Moreover, the magnon-magnon scattering mechanisms preserving the number of magnons are much faster than spin-lattice relaxation. Under these conditions, a stepwise pumping should create a magnon gas characterized by a steady, quasi-equilibrium distribution of magnons over the phase space after a certain transition period characterized by a thermalization time. After the magnon population at the bottom of the spectrum saturates, the entire magnon gas reaches a steady state. Comparison of the measured distribution with the Bose-Einstein one confirms that this steady state corresponds to a quasi-equilibrium thermodynamic state. After the thermal quasi-equilibrium is reached, further pumping increases the density of magnons as a function of time. As a result, the value of the chemical potential μ increases as well. For the values of the pumping powers used in the experiments, this growth in μ happens much more slowly than the thermalization process; therefore, it can be considered adiabatic.

The magnon-magnon relaxation time in YIG is of the order of few nanoseconds, while that of magnon-phonon interaction is longer than 1μs. Thus, the process of thermalization contains two well-separated time scales. As both mechanisms keep the number of magnons constant, a quasi-equilibrium state for the magnon gas can be realized with a non-zero chemical potential. The ultimate confirmation of coherence of the observed collective quantum state might be interference of two condensates with each other. In the sys-

tem studied, such an experiment can be performed in a direct way. Indeed, the magnon spectrum exhibits two degenerate minima, therefore two condensates with different wave vectors are created simultaneously. The interference between them should result in a standing wave of the condensate density in real space. Since each pumping pulse creates a condensate with an arbitrary phase, the phase difference between the two condensates should vary from event to event. Therefore, to detect the interference between two condensates, the pumping was applied continuously. For this purpose, a resonator allowing continuous pumping without significant overheating was designed [51].

A two-slab magnetic system can be designed to support BEC. The magnons in the slabs can be weakly coupled through both exchange and dipolar tunnelling. In fact, one can demonstrate that such a system forms a prototype of a Cooper-pair box at room temperature. Magnon qubit is an entirely new concept which has been recently proposed [14]. The concept exploits an analogy with the Josephson qubit, which is based upon the mechanism of superconductivity in order to avoid dissipation and ensure the phase coherence. Depending on the realization of the Josephson qubit one can have phase or charge as a good quantum number. The charge-based Josephson qubit, which is also called the Cooper-pair box, was proposed by Büttiker [40] and first realized by the Saclay group [34]. The phase qubits, which appear to have longer decoherence times, were subsequently designed and characterized. A qubit is essentially a two-level quantum system, which is well decoupled from the outside world, so that its quantum dynamics is unperturbed for a long time. Still, the coupling mechanism must exist to prepare the qubit in a given state and to read out its state when necessary. Many other proposals to implement a quantum computer were based on qubits constructed from microscopic degrees of freedom: spin of electrons or nuclei, transition dipoles of atoms or ions, etc. These degrees of freedom are naturally very well decoupled from their environment, and hence decohere very slowly. The main challenge for such implementations is to enhance the inter-qubit coupling to the level required for fast gate operations without introducing decoherence from parasitic environmental modes and noise. The Josephson qubit is the only one which seems to allow such operations but its realization still require liquid-helium temperatures. It is well-known that superconductivity can be viewed as a Bose-Einstein condensation of Cooper pairs in a conductor. We can also turn to a similar effect for magnonic system, the Bose-Einstein condensation of magnons discussed earlier, to realize the magnon qubit which will be fully functional at room temperature. In a magnonic analog of the Cooper-pair box the role of charge is played by the magnon concentration and the operations are performed by an external magnetic field.

2.3 Skyrmions: Tying spins in a knot

According to Landau: The ordered phases arising from the second order phase transitions are homogeneous, however this statement has to be made more accurate. In fact, spatially inhomogeneous phases occur if the free energy contains spatial derivatives of the order parameter. In metals with lack of inversion symmetry, when the underlying lattice is not invariant under reflections in the origin, a number of extra terms in free energy functional shows up. The celebrated DM interaction $\mathbf{D}_{ij}(\mathbf{S}_i \times \mathbf{S}_j)$ acting between two neighboring spins is among them; DM constructed from Lifshitz-invariants originates from relativistic spin-orbit coupling and in its simplest form for a cubic lattice $\sim \mathbf{m} \cdot (\nabla \times \mathbf{m})$, where $\mathbf{m}$ is the magnetization. In some magnetic structures a modulation of the spin arrangements over periods, which are long compared to the size of the lattice cell and usually not commensurate with it, can be observed. The existence of such magnetic structures is due to competition between exchange interactions and relativistic effects like spin-orbit coupling. The direction of the DM vector $\mathbf{D}_{ij}$ is determined by the bond symmetry, whereas the strength of spin-orbit coupling gives its intensity. Among the macroscopic manifestations of DM interaction are:

1. DM stabilizes long-periodic spatially modulated structures with a fixed sense of rotation.
2. DM favors arrangements of the magnetic moments in antiferromagnetic materials (weak ferromagnetism).

An interesting playground to try the formulas (2.22) and (2.23) are the helical magnets, a special class of magnetic structures where a magnetic periodicity is incommensurate with crystalline lattice. A number of reasons cause the formation of incommensurate magnets. For cubic crystals the exchange interaction exclusively would force collinear orientation of magnetic moments. The macroscopic robustness of the magnetic structure is determined by its stability with respect to perturbation violating spatial uniformity. Meanwhile, the relativistic effects of non-exchange nature can be permitted by crystalline structure contributing to the total energy with the terms linear in spatial derivatives (i.e. lack of inversion symmetry). In helical magnets the formation of ground state energy results from the competition between the Heisenberg exchange and DM couplings. In two-dimensional structures this competition leads to a spin-spiral ground state configuration which becomes unstable with magnetic field having the tendency towards skyrmionic crystal. For three-dimensional structures the phase diagram is even richer allowing the formation of conical state [179].

Microscopically when passing through the lattice an electron feels the magnetic field associated with its motion relative to the lattice, coupling thus this magnetic field with electron spin via the Zeeman term. The spin-orbit coupling of the Rashba-type is $H_{\mathrm{so}} = \alpha_{\mathrm{so}} \boldsymbol{\sigma} \cdot \mathbf{k}$, where α_{so} is spin-orbit constant, while a set of Pauli matrices $\boldsymbol{\sigma}$ acts on spin space. Thus, the bare Hamiltonian

of a helical magnet can be chosen to be the sum of that of a non-interacting two-dimensional electron gas in the presence of spin-orbit coupling. According to Moriya the DM interaction stems from spin-orbit coupling, so one has to keep track of the terms proportional to α_{so}, e.g. in the first order in α_{so} the Gilbert damping [216] [by doing integral (2.22), expanding it in ω and plugging into (2.15)]

$$\alpha = \frac{2}{\pi} \log^{-1} \left(\frac{\alpha_{so}\sqrt{8\mu m} - \Delta}{\alpha_{so}\sqrt{8\mu m} + \Delta} \right), \tag{2.24}$$

where Δ is spin-splitting constant and μ is the corresponding chemical potential. Almost the only theoretical approach that can be applied for studying the dynamics of magnetic structures is the Landau-Lifshitz equation. However, the validity of Landau-Lifshitz equation is limited to low temperatures when the magnitude of magnetization is fixed. The interplay between DM and exchange interaction, as described above, provides a microscopic explanation for many observed spin-spiral structures, and as we will discuss below, are essential ingredients when discussing the newly discovered magnetic phases with non-trivial topology, like the skyrmions [179, 31].

The model due to Skyrme treats a nucleon as a vortex-state of pion-matter, which existence is guaranteed by topological reasons and analogous to a vector field on sphere. Thus the obtained chiral soliton turns out to be stable with respect to smooth perturbations. Its stability is preserved by a generalized Hobart – Derrick criterion, but the price one has to pay for that consists in stability with respect to a certain class of perturbation only (i.e. to some degree conditional stability). However, this theorem is satisfied for chiral solitons that are characterized by a topological charge Q. Skyrme's model results in the Lagrangian with terms containing antisymmetric spatial derivatives of field components. There exists a condensed matter analog of field-theoretical skyrmions, namely two-dimensional cylindrically-symmetric soliton stabilized by DM interaction (proportional to Lifshitz invariants and thus similar to Skyrme term). The existence of skyrmions in antiferromagnets and magnetic metals have been shown theoretically. In the last case the Hamiltonian comprises the terms capable to change magnetization direction, leading thus to spontaneous crystallization. Besides crystals with lack of inversion symmetry, skyrmions can be observed on the interface of two magnetic materials thanks to the boundary effects which violate the symmetry in question. For example, in case of nanodisc, the magnetization direction is forced to align along tangent line to minimize demagnetization fields on the lateral area and being combined with exchange field gives rise to a vortex-like structure singular in the origin. Topological charge characterizing the skyrmion can be defined by

$$Q = \frac{1}{4\pi} \int dxdy \left(\mathbf{n} \cdot \left[\frac{\partial \mathbf{n}}{\partial x} \times \frac{\partial \mathbf{n}}{\partial y} \right] \right), \tag{2.25}$$

where $\mathbf{n} = \mathbf{m}/|\mathbf{m}|$ points in the direction of magnetization. The skyrmions are believed to be applied in the rapidly developing field of storage devices. The formal Boolean logic can be implemented by the presence of a skyrmion in a specific region, which might be controlled and easily manipulated with external spin-polarized current or an STM tip, and in contrast to domain walls the motion of skyrmions can be achieved by applying a lower field. These topological objects were first observed in bulk MnSi belonging to the class of helical magnets. Well below the Curie temperature a spin-helix or conical state is present at low external magnetic field along [100] direction.

In Dzyaloshinskii's seminal work [60] on non-centrosymmetric magnets and their inhomogeneous magnetic states, only one-dimensional magnetic spiral states had been identified. Bogdanov's major achievement [31] is the recognition that the field equations of Dzyaloshinskii's theory allows true solitonic solutions that destroy the homogeneity of magnetic states. Helices as one-dimensional modulations in Dzyaloshinskii's theory are also only successions of localized domain-walls, i.e., helical kinks. Existence of such localized states, and the mechanism of phase transformations by their nucleation as fixed (infinite size) mesoscale objects are ruling principles of all continuum systems described by an energy including Lifshitz invariants [179]. Therefore, and more impressively, the magnetic state built up from skyrmions decomposes into an assembly of molecular units. Depending on small energy differences owing to additional effects, different extended textures with variable arrangements of the skyrmion cores may arise, just as in a molecular crystal. In three-dimensional magnets, hence, in any magnetic crystal with Lifshitz invariants in the magnetic free energy, the skyrmions form tubular string-like solitonic objects with a fixed diameter and a stable core structure.

Chiral magnets have recently attracted the interest of the spintronics community since they present novel opportunities to control the electron spin. Heterostructures consisting of thin layers of helical magnets and traditional ferromagnet would enable injection and control of spin-polarized currents into helical magnets. A spin-polarized current flowing in a helical magnetic system is predicted to induce a torque that would produce new kinds of magnetic excitations. The wave vector of the spin spiral in bulk MnSi is oriented along [111] in the absence of magnetic field, forming four domains at $T < T_c$ in four equivalent directions. At low temperatures the magnetic structure tends towards a conical mono-domain structure at $B \approx 0.1$ T and turns to become a ferromagnet at higher fields, $B \approx 0.6$ T. The behavior is qualitatively different close to the critical temperature $T_c \approx 27$ K in the fields $B \approx 0.120 - 0.2$ T allowing the formation of the so called A – phase, whose spin structure is still under debate. The idea that the A – phase is of paramagnet nature had been rejected when neutron scattering experiments confirmed the existence of magnetic order. Recent experiments revealed the formation of a skyrmion crystalline structure, which can be visualized as a set of three spin spirals allocated at $2\pi/3$ relative to each other on the plane perpendicular to the exter-

nal field. A set of subsequent measurements with $Mn_{1-x}Fe_xSi$, $Mn_{1-x}Co_xSi$, $Fe_{1-x}Co_xSi$ which crystallize similar to MnSi in the B20 structure verified the early studies. Thermodynamic stability of skyrmionic condensed phases relative to helices can become favourable in cubic chiral helimagnets near the magnetic ordering transitions where the magnitude of the order parameter (the local magnetization) becomes inhomogeneous [204]. Here, spin-structures twisted into the localized configuration have simultaneously strongly varying magnetization density. This picture is now rendered more precisely by a confinement effect of solitons. Near the magnetic ordering transition, when directional and longitudinal degrees of freedom start to couple, localized chiral modulations begin to interact in an attractive manner. This confinement is in contrast to the major part of the $H-T-$ phase diagram in chiral magnets where kink modulations and skyrmions have repulsive soliton-soliton interactions. In this temperature range the condensed phases like helicoids or skymion lattices are stable due to the negative formation energy of the chiral solitonic units overcoming the repulsion. A transformation of these condensed phases takes place by setting free these units as in a crystal-gas resublimation. Hence, the radius of the isolated skyrmion diverges at such nucleation transitions. This process has been seen in recent direct microscopic observations of skyrmions and skyrmion lattices at low temperatures in nanolayers of B20 metals. Above a definite temperature which is called confinement temperature, below the magnetic ordering temperature $T_c < T_N$, the soliton-soliton interactions become oscillatory and attractive for certain separations between solitons. Magnetic states in that temperature region, therefore, display strong longitudinal modulations, clustering behavior of localized states, frustration effects, and the ability to form mesophases. The puzzling magnetic anomalies in chiral helimagnets, like MnSi and other B20 metals (Fig. 2.3) near the magnetic ordering transition, must be rooted in this mechanism as it is generic to non-centrosymmetric magnets.

Vortex states in magnetic nanodisks provide the simplest example of a magnetic structure, where effects of the chiral couplings may become noticeable. Within the usual micromagnetic description the shape and size of the vortices are determined by the competition between the exchange and stray-field energy. In particular, the vortices with different chirality are degenerate: The four possible vortex ground states differentiated by their handedness and polarity all have the same energy. However, these studies did not take into account the induced DM interactions, which should generically exist in these systems due to broken mirror symmetry by the surface. As the vortex states are chiral themselves, the effect of the chiral DM interactions is subtle: In the presence of DM couplings the chiral degeneracy of the left- and right-handed vortices is lifted. The different chiral versions of the vortex states are shown to display strong dependencies on the materials properties of such nanodisks. Within a micromagnetic model for these effects, numerical calculations of the shape, size, and stability of the vortices in equilibrium as functions of magnetic

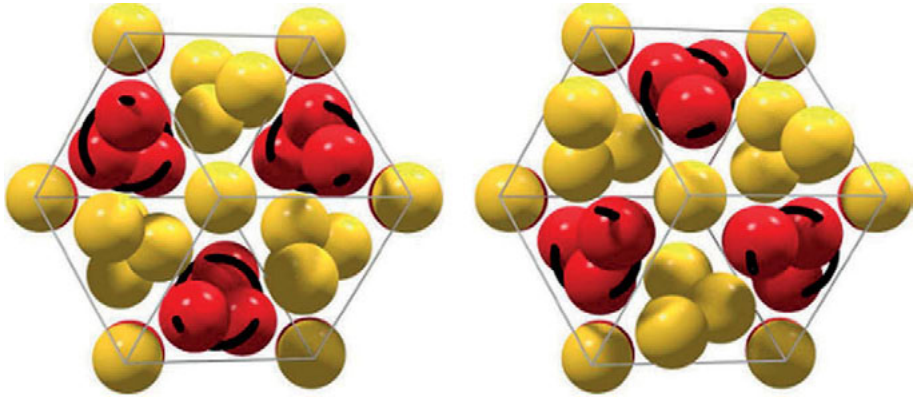

Figure 2.3. Crystallographic structure of MnSi, a cubic magnet of B20 structure with lack of inversion symmetry, belongs to $P2_13$ and is characterized by a certain chirality. In the right structure Mn atoms (red spheres) move clockwise (left panel), and counterclockwise otherwise (right panel). The illustration is from www.nsp.phys.spbu.ru.

field and the material and geometrical parameters provide a general analysis of the influence of the broken mirror symmetry caused by the surface/interfaces on their properties [38, 39]. The DM interactions impose differences in the energies and sizes of vortices with different chirality: These couplings can considerably increase sizes of vortices with one sense of rotation and suppress vortices with opposite sense of rotation. Numerical calculations show that vortices with different chirality have not only different energies and sizes, but also their magnetic structures differ. In case of chirality that is unfavourable with respect to the chiral DM couplings, the vortex core consists of a narrow internal part and an adjacent ring with a reverse magnetization rotation. Measured sizes and total perpendicular magnetization for vortices with opposite chirality may be used for experimental determination of strength of surface/interfaces-induced DM interactions in ultrathin magnetic films/film elements.

DM interactions are also an important ingredient of the complex magnetic behavior observed in magnetic insulators, such as transition-metal oxides. Ternary and quaternary oxides are natural hosts for the DM couplings because of the complex crystal structures that often have low crystallographic symmetry and polar atomic arrangement. Unfortunately, even a qualitative assessment of these couplings is generally impossible, which makes the DM interactions one of the most enigmatic aspects of real materials. One of the main problems in spintronics is a controllable motion of magnetic textures. There are two ways of to drive the motion, i.e. incoherent and coherent methods. The first one is typically realized by injecting a spin-polarized current into a sample. On the other hand, the coherent method is realized in a magnetically ordered state by twisting the phase angle of the magnetic order parameter which directly couples to a magnetic field. For example, one can use a

rotating magnetic field, which is applied to one end of the sample and is strong enough to orient the magnetization parallel to it. Because of the stiffness of the spin system, the spin rotation at one end is transmitted to the other end of the sample, which is not subject to the direct effect of the rotating magnetic field. Transmission of the torque through the sample presents a spin current. The incoherent current injection method to drive the sliding dynamics has already been proposed in Ref.[120]. Meanwhile, chiral helimagnets are promising candidates to realize the coherent method [119]. In particular, it was demonstrated that the chiral soliton lattice in a chiral helimagnet exhibits a sliding motion when a time-dependent magnetic field is applied parallel to the helical axis, in addition to a static field perpendicular to the helical axis. As it has been pointed out in Ref. [33, 32], once the sliding is triggered, the soliton lattice maintains its persistent motion assisted by a generation of inertial mass. Another observable consequence of the coherent motion is an appearance of the spin motive force (SMF) [19], when the time dependence of the longitudinal magnetic field manifests itself in the temporal regime of the SMF. Remarkably, the chiral soliton lattice is a macroscopically ordered object, which contains macroscopic amounts of magnetic solitons (kinks). Due to this very large number of the solitons, the SMF is expected to be strongly amplified as compared with the SMF caused by a single magnetic domain wall in a ferromagnet. Numerical estimations [33, 32] show that the SMF reaches the order of millivolts that makes chiral magnetic crystals to be extremely promising for spintronic applications.

Topological magnon insulators have so far completely avoided attention despite their potential importance for spin-wave logic and memory devices. The main focus is, therefore, to extend the physical understanding developed for topological insulators and graphene to these magnonic systems. At the moment there exists a number of works [193, 194, 233, 139] which exploit the idea of topological protection for spin waves. One is due to Shindou, Matsumoto, and Murakami [193] who demonstrate that a suitably designed 2D magnonic crystal can support topologically protected magnonic edge modes. A magnonic crystal, proposed in [193], is a periodic array of iron islands in yttrium iron garnet (YIG). The latter provides the highest coherence length for magnons, which is of the order of centimeters. It has to be noted that magnons are bosons, hence magnonic crystal has much in common with photonic or phononic ones. It is, therefore, no wonder that the idea of magnonic edge modes roots in the seminal work by Raghu and Haldane [176] who recently discussed the chiral edge states in photonics crystals and introduced the boson Chern numbers and Berry curvature for photonic bands. The proposed edge modes were subsequently realized in actual photonic crystals (metamaterials) by Wang et al. [228]. Unidirectional propagation of electromagnetic waves was indeed experimentally observed and lead to new applications of the metamaterials. This shows that the idea of designing magnonic insulators with helical (chiral) edge modes is more than viable. In analogy to the spin Hall ef-

fect, which arises due to strong spin-orbit interaction, the magnon Hall effect may be induced in actual materials by strong DM interaction. This paves the way for the existence of topological magnon insulators (topological magnets) which are ferromagnetic insulators in the bulk but posses topologically protected spin-wave surface states. Another work [233] proposes that thin films of some insulating ferromagnets, such as $Lu_2V_20_7$, may become topological magnon insulators where the topologically protected edge modes exist due to DM interaction.

It is known that spin Hall effect is associated with spin-orbit interaction which breaks the underlying symmetry. The observation of a magnon Hall effect due to DM interaction may be addressed within the same paradigm. In fact, DM interaction acts as an effective magnetic field resulting in that non-trivial topological properties show up. This enables the existence of topological magnon insulators (topological magnets) which are ferromagnetic insulators in the bulk but posses topologically protected spin-wave excitations. In Paper II in the list of publications of the thesis, this was worked out in some detail, and is discussed further here. We start by considering spins on a Kagome lattice which interact via exchange and DM couplings. The Hamiltonian reads

$$H = \sum_{i,j} \Big(J_{ij} \mathbf{S}_i \cdot \mathbf{S}_j + \mathbf{D}_{ij} [\mathbf{S}_i \times \mathbf{S}_j] \Big). \tag{2.26}$$

We keep exchange interaction for both nearest (NN) J_1 and next-nearest neighbors (NNN) J_2, whereas DM acts between NN only $\mathbf{D} = D\mathbf{e}_z$. In what follows, we show that real-valued J_2 can drive topological phase transitions in the system. Thus, the Hamiltonian can be written

$$H = \frac{1}{2} \sum_{\langle i,j \rangle} \left(\sqrt{J_1^2 + D^2} \left[e^{i\phi} S_i^+ S_j^- + e^{-i\phi} S_i^- S_j^+ \right] + J_1 S_i^z S_j^z \right) + \sum_{\langle\langle i,j \rangle\rangle} J_2 \mathbf{S}_i \cdot \mathbf{S}_j, \tag{2.27}$$

where $\tan\phi = D/J_1$. Kagome-like structures possess three inequivalent lattice cites in a unit cell, on employing Holstein-Primakoff transformation $S_i^+ = a_i\sqrt{2S}$, $S_z^i = S - a_i^\dagger a_i$ we reduce (2.27) to

$$h_{\mathbf{k}} = \begin{pmatrix} 0 & \varepsilon_1(\mathbf{k}) & \varepsilon_3^*(\mathbf{k}) \\ \varepsilon_1^*(\mathbf{k}) & 0 & \varepsilon_2^*(\mathbf{k}) \\ \varepsilon_3(\mathbf{k}) & \varepsilon_2^*(\mathbf{k}) & 0 \end{pmatrix}, \tag{2.28}$$

where we have defined $\varepsilon_n(\mathbf{k}) = \alpha e^{-i\phi} \cos(\mathbf{k} \cdot \mathbf{e}_n) + \beta \cos(\mathbf{k} \cdot \mathbf{g}_n)$. We have chosen the following parametrization for the basis vectors $\mathbf{e}_1 = (1,0)$, $\mathbf{e}_2 = (-1,\sqrt{3})/2$, and $\mathbf{e}_3 = (-1,-\sqrt{3})/2$, while $\mathbf{g}_1 = \mathbf{e}_2 - \mathbf{e}_3$, $\mathbf{g}_2 = \mathbf{e}_3 - \mathbf{e}_1$, and $\mathbf{g}_3 = \mathbf{e}_1 - \mathbf{e}_2$. We have also defined $\alpha = 2S\sqrt{J_1^2 + D^2}$, and $\beta = 2SJ_2$. It is well known that for NN couplings exclusively the band structure contains a flat region while the rest touch each other in the corners of hexagon $(\pm 2\pi/3, 0)$,

$(\pm\pi/3, \pm\pi/\sqrt{3})$ provided $\phi = 0, \pi/6, \pi/3$. Thus, for certain values of DM interaction the system becomes gapless, while any small deviation results in the gap being opened up. The latter signals that the Kagome lattice allows appearance of an edge mode. We now show that inclusion of J_2 does not violate this picture for certain J_2. Indeed, the energy spectrum of the Hamiltonian is determined by three independent roots of a secular equation and is given by

$$E_n = 2\sqrt{\frac{A}{3}}\cos\left(\frac{\theta + 2\pi n}{3}\right), \quad \tan\theta = \sqrt{\frac{4A^3}{27B^2} - 1}, \tag{2.29}$$

where $n = 0, \pm 1$ and we put

$$A = \alpha^2(f+1) + 2\alpha\beta(2f-1)\cos\phi + \beta^2(h+1) \tag{2.30}$$

and

$$B = \alpha^3 f\cos(3\phi) + \alpha^2\beta(2f+h)\cos(2\phi) + \alpha\beta^2(3f+g-2)\cos\phi + \beta^3 h, \tag{2.31}$$

provided the functions $f = 2\cos(\mathbf{k}\cdot\mathbf{e}_1)\cos(\mathbf{k}\cdot\mathbf{e}_2)\cos(\mathbf{k}\cdot\mathbf{e}_3)$, $g = 2\cos(2\mathbf{k}\cdot\mathbf{e}_1)\cos(2\mathbf{k}\cdot\mathbf{e}_2)\cos(2\mathbf{k}\cdot\mathbf{e}_3)$, and $h = 2\cos(\mathbf{k}\cdot\mathbf{g}_1)\cos(\mathbf{k}\cdot\mathbf{g}_2)\cos(\mathbf{k}\cdot\mathbf{g}_3)$. In the most general case

$$\tan\theta = \left|\frac{3\sqrt{3}\alpha\beta(\alpha-2\beta)}{(\alpha+2\beta)(\alpha-\beta)(\alpha-4\beta)}\right|, \tag{2.32}$$

which is zero whenever $\beta = 0$ or $\alpha/\beta = 2$. Thus, two bands touch each other when $J_2 = 0$, that which was expected, and when $J_2 = \sqrt{J_1^2 + D^2}/2$, or which is equivalent $J_1 = J_2 = D/\sqrt{3}$. To identify a topological invariant for the two-dimensional Hamiltonian (2.26) which is translationally invariant, thus, its eigenstates are of the Bloch-type signaling Berry curvature and corresponding Chern number can be defined in the usual manner

$$\mathscr{C}_n = \frac{1}{2\pi}\int_{BZ} d^2\mathbf{k}\Omega_n(\mathbf{k}) \tag{2.33}$$

with $\Omega_n(\mathbf{k}) = \nabla_{\mathbf{k}} \times \langle u_n(\mathbf{k})|i\nabla_{\mathbf{k}}|u_n(\mathbf{k})\rangle$. To proceed and estimate the Chern numbers we linearize the Hamiltonian by placing the quasimomentum in the vicinity of $(\pm 2\pi/3, 0)$ and tuning $\beta = \alpha/2 + \Delta$ (we choose $\phi = \pi/3$)

$$h_{\mathbf{k}} = \begin{pmatrix} E_0 & a(\tilde{k}_x + i\tilde{k}_y) & b(\tilde{k}_x - i\tilde{k}_y) \\ a(\tilde{k}_x - i\tilde{k}_y) & E_{-1} & c(\tilde{k}_x + i\tilde{k}_y) \\ b(\tilde{k}_x + i\tilde{k}_y) & c(\tilde{k}_x - i\tilde{k}_y) & E_1 \end{pmatrix}, \tag{2.34}$$

here $\tilde{k}_x = k_x - k_{0x}$, $\tilde{k}_y = k_y - k_{0y}$, whereas $E_1 = \alpha/2 - \Delta$, $E_0 = -\alpha - \Delta$, $E_1 = \alpha/2 + 2\Delta$ ($a = c = \alpha\sqrt{3}/4$, $b = \alpha\sqrt{3}/2$). The upper band is isolated from

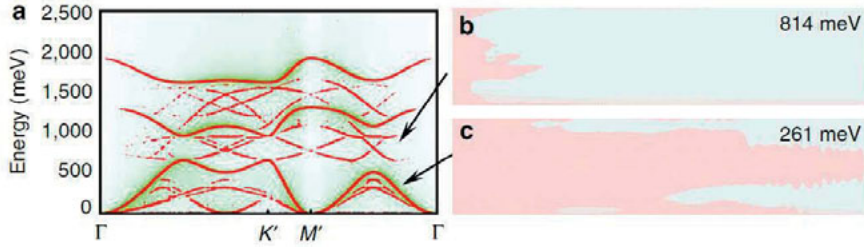

Figure 2.4. (a) The dynamic structure factor is shown along the high symmetry points $\Gamma \to K' \to M' \to \Gamma$, where $K' = 2K$ and $M' = 2M$. K' and M' are referred to as points in the extended Brillouin zone. (b,c) Berry curvature shown in real spin-space averaged over a time interval of 100 ps. In b,c, the system is perturbed with an energy of 814 and 261meV, respectively. Moreover, the D/J ratio has been chosen to be 0.4 and $T = 1$ mK. The red colour indicates an excitation where the atomic magnetic moment deviates from the ground-state orientation that is represented by the moments pointing almost along the z axis. Blue-light colour represents atomic moments oriented almost along the z axis in a ground-state configuration.

the rest and can be decoupled by projecting (2.34) onto a 2×2 subspace $h'_{\mathbf{k}} = Ph_{\mathbf{k}}P$, therefore

$$h'_{\mathbf{k}} = \begin{pmatrix} E_{-1} & c(\tilde{k}_x + i\tilde{k}_y) \\ c(\tilde{k}_x - i\tilde{k}_y) & E_1 \end{pmatrix} = u_0\sigma_0 + \sum_{i=x,y,z} u_i\sigma_i, \tag{2.35}$$

where σ_0 is a 2×2 unit matrix, σ is a set of Pauli matrices, and $u_0 = (\alpha + \Delta)/2$. The determinant of the matrix

$$\begin{pmatrix} u_x \\ u_y \\ u_z \end{pmatrix} = \begin{pmatrix} c & 0 & 0 \\ 0 & -c & 0 \\ 0 & 0 & -3/2 \end{pmatrix} \begin{pmatrix} \tilde{k}_x \\ \tilde{k}_y \\ \Delta \end{pmatrix}, \tag{2.36}$$

is known to determine the change of the Chern numbers across the point $M = (k_x, k_y, \Delta) = (k_{0x}, k_{0y}, 0)$

$$\Delta\mathscr{C}(M) = \mathscr{C}(M+0) - \mathscr{C}(M-0) = \mathrm{sgn}\left(\det||u_{ij}||\right) = 1. \tag{2.37}$$

In a kagome ferromagnet (described by a Hamiltonian, as given in equation (2.26) with $J_2 = 0$, see Paper II), the DM interaction is not forbidden by the symmetry of the lattice because the middle point between two sites is not an inversion centre. Consequently, in the presence of significantly large DM interactions, the magnon dispersion curves of a kagome magnet present similarities with the energy band spectra of topological insulators. In fact, in such a system the magnon dispersion relation is gapped in the bulk but allows traveling gapless edge states that are topologically protected against any variation of the material parameters unless the band gap in the bulk collapses. Even though our studied sample is one atomic-layer thick system, we denote

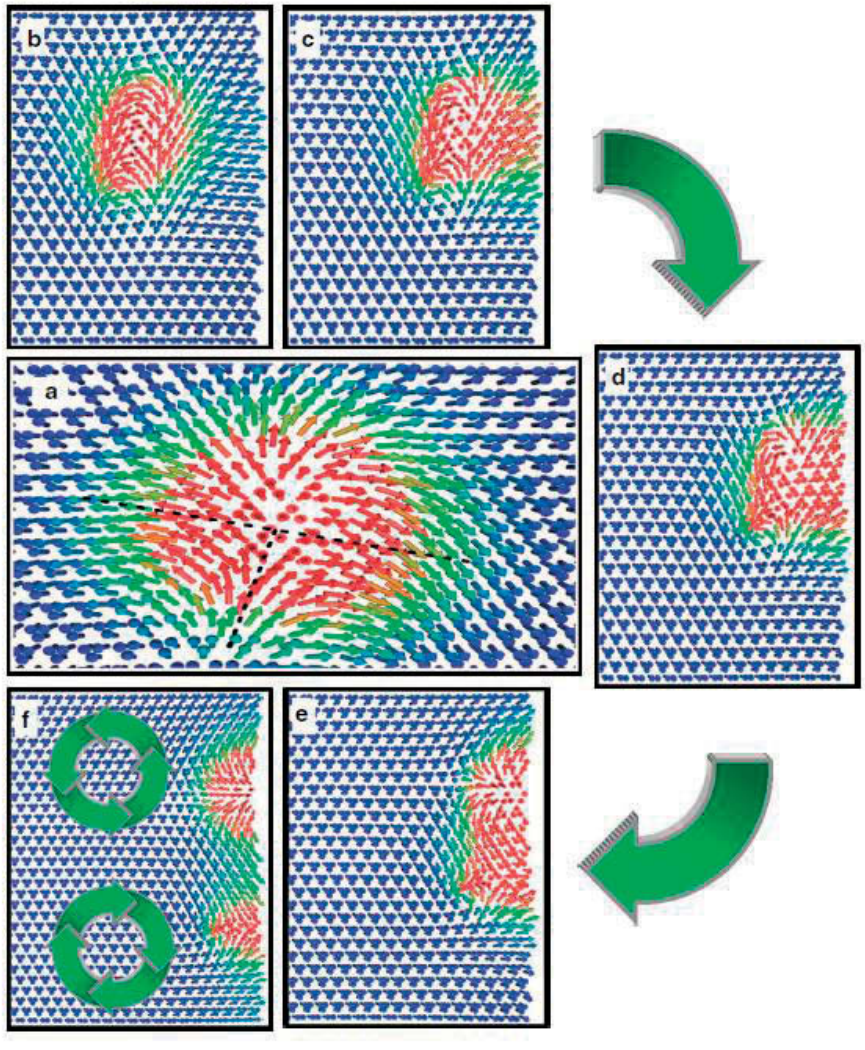

Figure 2.5. (a) Illustration of a skyrmion-antiskyrmion (SA) pair before the collision with the edge of the kagome stripe. Dashed lines are a guide to the eye for recognizing the antiskyrmion magnetic texture, while the other half of the magnetic excitation resembles a magnetic texture like in the Belavin-Polyakov monopole. (b–f) Several frames showing the coupled SA pair colliding with the edge of the stripe and the resulting SA decoupling because of the chiral edge states.

hereafter bulk states by the states that exist well inside the sample and consequently, by abuse of language bulk skyrmions, refers also to the skyrmions that exist inside the 2D sample. We consider here magnetic excitations of a 2D kagome lattice, for example, as given by a [111] surface of the pyrochlore lattice at a temperature of 1 mK, unless stated otherwise. We assume a very low temperature in the majority of our simulations because the results described here are easier to observe at that temperature, and most likely also in experiments, because the perturbations from thermal fluctuations are smaller. Very low temperature conditions make the analysis easier; however, we have also analyzed the conditions to stabilize skyrmions at room temperature in the penultimate subsection of Paper II. We start by analyzing bulk and edge states of this system, and to this end we show in Fig. 2.4a the magnon dispersion, as revealed from the dynamical structure factor. Note that the results in Fig. 2.4a are obtained using open boundary conditions for a large sample composed of 50-400 unit cells. The intense colored curves represent bulk magnons, which are seen to be grouped in three branches, with noticeable gaps in-between. Most noteworthy is that in between the gaps one can find four twisted edge states that form a continuous state. These states cannot be perturbed, so that a gap opens because they represent edge modes that are topologically protected. In fact, the presence of a DM interaction with a fixed handedness acts as an effective magnetic field in the system. This makes the magnon spectrum of the kagome lattice looks similar to the energy band structure of topological insulators. Here we are focused on the generation and manipulation of topological excitations as well as their collisions. In order to analyze the edge and bulk modes in real space, we show the real-space Berry curvature, averaged over a time interval of 100 ps, in Fig. 2.4b,c. The results of Fig. 2.4b,c were obtained after exciting the first two rows of atoms with an external magnetic field on the left side of the sample, and then the time evolution of the system was monitored. The excitation was carried out first with an energy of 261 meV and second with an energy of 814 meV. The first excitation represents magnon energies that are allowed in the bulk, whereas the second excitation represents an energy for which bulk states are forbidden, since this energy lies in the magnon gap. Fig. 2.4c (261 meV case) displays spin waves that propagate over the whole sample, corresponding to the expected bulk modes of the 261-meV excitation, whereas Fig. 2.4b (814 meV case) shows magnon excitations that only propagate along the edges, that is, representing edge modes. The data in Fig. 2.4a–c demonstrate that magnetic excitations of a kagome lattice have just as rich physics, in terms of non-trivial topology, as the electronic structure of topological insulators. The advantage with investigations of magnetic excitations is that it is possible to keep track of the real-space information of the magnetic excitation as a function of time, for example, as given by the information in Fig. 2.4b,c.

In general, a skyrmion that moves towards an edge becomes annihilated. However, for the kagome magnet the annihilation of the skyrmion does not

occur once it reaches the edge, since the existence of chiral magnonic edge states gives rise to profound changes in the excitations of the kagome lattice, as we have seen in Fig. 2.4. Thus, once the skyrmion-antiskyrmion (SA) pair reaches the edge, the chirality forces them to be separated as two distinct entities. The meron and antimeron emanating from the collision of the SA pair at the edge of the kagome lattice have drastically different speeds, since the distance travelled by the antimeron is shorter than the one of the meron during the same period of time. A magnification of the SA pair discussed in Fig. 2.5. For further discussions about the connection between speed and the strength of interaction parameters of the Hamiltonian. Notice that because of the chosen magnetic orientation of the spins studied here, the meron has counterclockwise chirality contrary to the antimeron, which has clockwise chirality. In Fig. 2.5a we show the coupled SA pair, just before it reaches the edge. Note that the dashed line shows the magnetic texture for a half-antiskyrmion. Hence, this illustrates how the SA pair is coupled before it reaches the edge. Figure 2.5b-f shows the time evolution of this SA pair over a time interval of 90 ps, just before (Fig. 2.5b) and just after (Fig. 2.5c–f) it reaches the edge. Note that once the coupled SA pair reaches the edge, it becomes unstable, due to non-trivial topology, and breaks up into a separated meron and antimeron (Fig. 2.5e,f), and then they travel along the edge in a decoupled manner with opposite directions. The results of Fig. 2.5 demonstrate that it is possible to create SA pairs in a kagome lattice and that they are stable over a substantial period of time. It is also clear that SA pairs can travel with supersonic velocities of $\sim$ 1,300 m/s. However, the linear momentum of such SA pairs is unfortunately difficult to control or design by the initial conditions of their generation. A way to overcome this problem is to make use of the topological properties of the edge states of the kagome magnet and to place the local excitation at the edge of the sample. This was elaborated on in Paper II in the list of publications of this thesis.

3. On the possibility of magnetic engineering

3.1 Magnetoplasmonics: When magnetism meets plasmonics

Plasmonics is on of the cutting edges of the modern physics bringing nanotechnology into optics. Fundamentally, plasma oscillations in solids are collective oscillations of electron gas density controlled by electron-electron interaction; in the simplest case, the oscillation dispersion is defined by the electron concentration in the conduction band, the permittivity of the medium (where the electrons are embedded), and their effective mass. However, in a more general situation, e.g., interband plasmons, the plasmon dispersion is determined by the underlying band structure. And its damping is mainly attributed to both single-particle mechanisms of carrier scattering off impurities and Landau damping. Microscopically Landau damping is responsible for plasmon decay to an electron and a hole, while on macroscopic scale this decay is equivalent to the inverse Cherenkov effect (when an electron is accelerated by the field of a plasma wave) [109].

The term plasmonics has been coined to emphasize the connection to the study of plasmons in low-dimensional systems, while frequency and damping of two- and three-dimensional plasmons is defined by the geometry of the sample under consideration and the permittivity of the surrounding space (as Coulomb force lines of interacting electrons also pass through the surrounding medium [121, 191, 35]). The latter results in supersensitive plasmon sensors [231] being developed. Plasmon excitation is widely used in surface spectroscopy [4, 3], and local plasmon excitation is employed for a giant enhancement of Raman light scattering [122] and of different nonlinear optical processes [5]. The feasibility of realizing time-resolved surface plasmon optics has also been discussed, and the first successful steps in this direction have been reported [148, 145]. The excitation of local plasmons on the tip of a scanning probe microscope by an incident electromagnetic wave may be employed for producing under the tip a subwavelength domain with a strongly enhanced field; this, in turn, was used for local spectroscopy and nanolithography with an ultrahigh spatial resolution which far exceeded the Rayleigh limit [144]. Another possible application of plasmons and plasmon polaritons is ultrafast information transfer (for instance, between the elements on a chip), faster than with electron current pulses. Lastly, an interesting possibility consists in the development of quantum plasmonics for quantum informatics, etc.

All these promising applications are significantly restricted by the damping of plasmons – their finite mean free path. This can be overcome with the help

of active plasmonics which operates with spasers, plasmon analogs of lasers [24, 171, 140]. In particular, it will be possible by using a spaser in the form of the tip of a scanning probe microscope and measuring the loss-induced dips in its generation spectrum to realize supersensitive spectroscopy with an ultrahigh spatial resolution [147], which represents, in a sense, a spaser analog of selective near-field laser spectroscopy. This method may also be utilized for the supersensitive spaser spectroscopy of surfaces.

Another possibility of technological use is magnetoplasmonics. The magnetooptical effects are among the most important effects in optics thanks to the possibility to modulate both polarization and intensity of electromagnetic field in the frequency range $10 - 100$ GHz. The effects of this type are the most prominent in ferromagnet materials, which however being opaque in near infra-red region are characterized by quite dramatic optical losses. Nevertheless, the bismuth-based iron garnets [237] are known to possess a lower value of the absorption coefficient, so that for example a thin film with width of 10 μm made of $Bi_2DyFe_5O_{12}$ does not change the intensity of transmitted light dramatically, but rotate the polarization plane by $\pi/4$. The magneto-optical materials play an important role in modern technology, and can be produced artificially with miniaturization, e.g., the optical properties can now be modified not only by changing the chemical structure but also by means of geometry variation, provided the typical size is to be comparable to the wave-length. When this size is much smaller compared to the wave-length of radiation it can be thought as quasi-uniform, such a material is now known as a metamaterial [220]. The peculiarity of the structure in question is that it can be approximated by some effective medium with well-defined permittivity ε and permeability μ, which are of course different from those of uniform medium. Playing with geometric size and shape of a unit block of metamaterial, various resonance peaks in frequency spectra of ε and μ might be obtained. In a certain frequency range both permittivity and permeability are to be negative, so that the refraction index is negative. Furthermore, arrangement of unit elements relative to each other is of quite big importance as well – it was established the most interesting is periodic (crystal-like) structure, thus justifying the name photon crystal.

Hence the appearance of the resonances is mainly due to geometry but not the electronic structure. Interaction of incident electromagnetic light with eigenmodes of such metamaterals can lead to generation of waveguide modes in insulating materials, while in hybrid metal-insulator multilayers a purely surface (surface plasmon-polariton) electromagnetic wave can be probed. The last example is of great interest for engineering applications as it leads to high degree of electromagnetic energy localization right along the interface separating metal and insulator (plasmon crystals).

The optical properties of a macroscopic medium are basically determined by the tensors $\hat{\varepsilon}$ and $\hat{\mu}$. In most of the cases especially in the visible and near infra-red region $\mu_{ij} \approx \delta_{ij}$. Apparently, in magnetically-ordered media the

permittivity tensor $\hat{\varepsilon}(\mathbf{m})$ is determined by the magnetization (ferromagnet) or sub-lattice magnetization (anti-ferromagnet). For the sake of brevity, we provide a quantitative picture for ferromagnet crystals only, thus the permittivity can be written as [237]

$$\varepsilon_{ij} = \varepsilon_{ij}^{(0)} - ie_{ijk}g_k + \kappa_{ijkl}m_k m_l, \tag{3.1}$$

where $g_i = \lambda_{ij}m_j$ defines the gyration vector, e_{ijk} is totally antisymmetric pseudo-tensor, while $\varepsilon_{ij}^{(0)}$, λ_{ij}, and κ_{ijkl} are purely determined by crystallographic symmetry. In isotropic medium the gyration vector is proportional to magnetization $\mathbf{g} \sim \mathbf{m}$. Magneto-optical Faraday effect consists in optical rotation when a linearly-polarized electromagnetic wave propagates along the magnetization direction $\mathbf{m}$ by some angle θ [132].

There are also inverse magnetooptical effects when the optical field changes magnetization of the system through which it propagates [168, 166]. The gyrotropic media with non-zero $\mathbf{g}$ gains a finite magnetization when an elliptically polarized wave travels through a material. It was recently observed by ultrafast magnetization manipulation in ferromagnet materials with femtosecond laser pulse [116, 117, 211, 85]. The formation of external magnetic field in gyrotropic systems can be derived from simple thermodynamic considerations: An isotropic magnetically-ordered medium acquires an extra energy [132, 168, 166, 214]

$$\Delta E_M \sim \mathbf{g} \cdot \left(\mathbf{E}^* \times \mathbf{E}\right) \tag{3.2}$$

due to electromagnetic irradiation, so that an effective magnetic field present in the system $\mathbf{H}_{\text{eff}} = -\partial \Delta E_M / \partial \mathbf{m} \sim \mathbf{E}^* \times \mathbf{E}$, thus requiring the use of elliptically-polarized field to induce magnetization.

The idea to utilize nanostructuring for resonant enhancement of magneto-optical effects was first applied in one-dimensional photonic crystals. Photonic crystals are known to be a spatially periodic material with a period comparable to the wavelength of the optical radiation. Multiple interference of electromagnetic waves diffracted in each unit cell of the crystal leads to the formation of the frequency bands for which it is impossible to spread radiation over photonic crystals, i.e. the photonic band gap. At these frequencies, the light undergoes a perfect reflection from the crystal surface, while at other frequencies the light passes through the photonic crystal.

The possibility of external influence on the optical properties of photonic crystals [129, 43, 154] extends the range of applications in integrated optics. One option for this is the use of photonic crystals made of magnetic materials. This raises the opportunity of controlling the optical properties of the photonic crystal by an external magnetic field [130, 229, 30, 69, 93]. The last two options are of particular interest because they not only can achieve substantial restructuring, but also lead to new interesting effects in magneto-optics, such as a giant circular and linear birefringence or mode conversion.

One-dimensional magnetophotonic crystals consisting of anisotropic dielectric layers and the ferromagnet are theoretically studied in [69]. In such a structure, the effect of strong spectral nonreciprocity, having a high practical value, was detected, e.g. the crystal may be opaque to the wave propagating from right to left, and at the same time, allow this wavelength to pass in the reverse direction. Along with one-dimensional magnetophotonic crystals their two- and three-dimensional counterparts were also considered [173, 123, 20, 110, 111, 55]. In most cases, an experimental realization of these structures are colloidal solutions of ordered particles of spherical or cylindrical shape. Dramatic enhancement of magneto-optical effects in such crystals have been observed.

Magneto-optical effects can also be enhanced by the excitation of eigenwaves of a structure, particularly in the metal-dielectric structures by exciting surface plasmon-polaritons (SPP). The most interesting regime of surface plasmon-polariton generation can be implemented on a metal-insulator heterostructure consisting of perforated metal layer and homogeneous ferromagnetic dielectric film deposited on a non-magnetic substrate.

From the first site, the nanostructured film of a ferromagnetic metal on the substrate is the most suitable system for amplification of magneto-optical effects, since the specific Faraday rotation in such films is $\sim 10^{5\circ}/cm^{-1}$. However, for typical ferromagnetic metals such as Fe, Ni, Co and their alloys within optical frequency range optical losses are quite large, and the plasmon propagation does not exceed a few micrometers. At the same time, for the periodicity of the structure to be of a significant impact on their optical properties, it is necessary that the length of the propagation of the SPP to be significantly larger than the period of the structure (about 10 micrometers and more). Consequently, all optical phenomena caused by the SPP, in such metals are strongly suppressed.

If the magnetic material in a plasmonic heterostructure is replaced by weakly absorbing ferromagnetic insulator ($\alpha \sim 100$ cm^{-1} at $\lambda = 800$ nm), one can significantly reduce the optical losses. Furthermore, it avoids the use of ferromagnetic metal. Thus, it becomes possible to use instead of the ferromagnet, noble metals which optical losses are substantially lower. Since the optical losses in both insulating and metallic layers are relatively small, the propagation of SPP increased several times compared with the structures containing ferromagnetic metals. An example is the system [bismuth-substituted iron garnet] / [silver] $\ell = 7$ μm at $\lambda = 900$ nm. In addition, small optical losses in the magnetic dielectric layer are capable of driving in it waveguide modes, which, along with the plasmon modes can also have a significant influence on the magneto-optical properties of the material. Thus, the heterostructure type [ferromagnetic insulator] / [precious metal] has great potential for plasmonics and magneto-optics.

Periodic system of holes or slits in the considered heterostructure permits to manipulate the energy spectrum of SPP and other electromagnetic modes

excited in this system. The period of the structure must be comparable with the wavelength of the modes. Therefore, by analogy with the photonic crystal, the system can be called plasmon crystal.

3.2 Spin polarization: Optically induced phenomena

Another method to get over the difficulty pointed out in the previous section involves the search for and use of novel systems with a weak plasmon damping like doped graphene. Fundamentally, the genuine interest in graphene – a one-atom thick layer of carbon atoms, which is stable even without a substrate (see [78, 160, 42, 108, 47, 128, 146, 1]) – and in recently found (three-dimensional) topological insulators (see [86, 172]) is due to the fact that there is a two-dimensional electron gas with a zero effective mass and a zero gap between the conduction and valence bands in these entirely different materials. The two-dimensional electron gas in question is described by the Dirac equation with a zero mass (similar to neutrinos), thus making a possibility to bridge ultrarelativistic physics of elementary particles and quark matter with condensed matter. This leads to a number of interesting effects, e.g. the absence of backward reflection from potential barriers at normal incidence (Klein tunnelling), weak anti-localization, and the half-integer quantum Hall effect (which happens even at room temperature) [108].

In low-dimensional structures like quantum wells, qauntum dots, graphene the motion of charge carriers is restricted to one- or more directions and gives rise to quasiparticle spectrum redistribution owing to size-quantization effects. The latter strongly affects optical and kinetic properties in such systems and leads to a variety of new phenomena to be observed [75, 58]. The key ingredient of spintronics consists in detailed investigations of interaction between spin-degree of freedom and a polarized external field, e.g. optical orientation of spins [230] happens due to angular momentum transferring from a photon of external field to the electron sub-system of a low-dimensional structure. This can be mainly attributed to spin-orbit coupling: In semiconductor nanostructures a value of such coupling is determined from symmetric and geometric considerations. In narrow-band semiconductors spin-momentum locking is rather rigid, whereas in graphene the influence of spin-orbit coupling can be neglected which means that the interaction with light is defined by orbital degree of freedom of electrons and holes exclusively.

A considerable distinction from ultrarelativistic particle physics can be observed: In the Dirac equation for graphene, instead of the speed of light a quantity 300 times lower appears, while this equation holds only in the lab frame (this turns out to be an artifact of the Galilean-invariant Schrödinger equation which can be reduced after straightforward algebra to the effective Dirac equation describing quasiparticles in graphene). One should also keep in mind that these are the so called envelopes which obey the Dirac equation

in an external field. These envelopes describe the slow modulation (due to slowly varying external fields) of Bloch functions which oscillate with a lattice period (in this case the adiabatic approximation is used, which leads for ordinary crystals to the Schrödinger equation with an effective mass).

The linear dispersion of quasiparticles in graphene [227, 198] can be derived from the Schrödinger equation, taking account of the symmetry and the existence of two sublattices in monolayer graphite, within an approximation accounting for the closest neighbor interaction. But this linear spectrum (valid up to an energy of the order of 1 eV), i.e. the presence of Dirac-effective electrons, is associated, as may be shown, with the symmetry of graphene, and this property is protected from the presence of impurities (and some other perturbations by symmetry with respect to time reversal). The role of spin can be attributed to pseudospin which emerges due to the fact that the hexagonal lattice in graphene may be represented in the form of two equivalent triangular lattices displaced relative to each other. The presence of two more components in the Dirac equation for graphene is associated with the existence of two independent valleys in the Brillouin zone (since the existence of two sites in the elementary cell of graphene results in two sites in the elementary cell of the reciprocal lattice).

An important property of graphene is the possibility to easily control the density of electrons or holes by means of control electrodes or chemical doping, which opens up an opportunity to graphene-based plasmonics [153, 125, 25, 127]. In particular, it is possible to produce plasmon waveguides and plasmon switches using the specially profiled coatings and control electrodes. Critically important additional virtues of graphene for plasmonics are a weak damping, a long mean free path of plasmons in it, and the capability of working in the terahertz frequency range. The weak damping opens the way for the development of a graphene-based quantum plasmonics or single-plasmonics. It will be of interest to control plasmons by applying external magnetic field [25]. The specific character of the graphene band structure results in nontrivial features of its dielectric response: Singularity in the low-frequency range (however weaker than for normal metals), unusual optical properties [67], and a weak damping of quasiparticles. These properties demonstrate an ability to create graphene-based photonic crystals with a photonic gap in the far-infrared spectral region [26].

As noted above, Dirac electrons exist not only in graphene, but also on the surfaces of recently discovered new materials – three-dimensional topological insulators [86, 172]. Up to now different realizations of two- and three-dimensional topological insulators have been studied. The new paradigm is that topological insulators are not associated with the emergence of spontaneous symmetry breaking in a crystal and, in turn, with its attendant order parameter (as in the case, for example, of magnetics, ferroelectrics, etc.), but with the emergence of a topological invariant in Hilbert space, which is determined by the properties of the Bloch states occupied by electrons. In this

sense, there is an analogy between the properties of topological insulators and the quantum Hall effect in which none of the states in the plateau region inside the system is conductive, but there are zero-gap chiral states (a unidirectional current determined by the direction of the magnetic field) at the system boundaries protected against the scattering off impurities by the presence of a topological invariant. This picture is especially simple in sufficiently strong magnetic fields, where the drift approximation applies to electrons and the topological invariant has a simple meaning: It characterizes the connectivity of drift electron trajectories [15]. In three-dimensional (so called strong) topological insulators, there is a gap in the spectrum of bulk states, as in ordinary insulators, but on the surface they have, thanks to the existence of the topological invariant, zero-gap surface electron states with zero effective mass of electrons and holes (similar to graphene), which are described by the Dirac equation with a zero mass.

These states are known to be topologically protected: Nonmagnetic impurities cannot form a gap and localize these states because of the presence of a topological invariant. One of the most important properties of the Dirac equation with a zero mass is a strict connection between the directions of electron momentum and spin (or pseudospin for graphene). Thanks to strong spin-orbit coupling, electrons on the surface of a topological insulator possess a rigid correlation between the spin and momentum directions: Their spin is perpendicular to the momentum, and this property was experimentally revealed by angle- and spin-resolved photoelectron spectroscopy. A similar strict connection between electron momentum and pseudospin (and not spin) is true for graphene owing to the mathematical equivalence of the Dirac equations with a zero mass for both systems, which this connection follows from.

The plasmon dispersion law can be found by linearizing the equations of motion for Dirac electrons, which corresponds to a random phase approximation. The validity of the random phase approximation is defined by the dimensionless quantum parameter equal to the ratio between the characteristic energy of Coulomb interaction and the quantum kinetic energy. For Dirac electrons with a linear dispersion, this ratio is independent of the electron concentration and equal to the effective fine-structure constant in which the speed of light is replaced by the electron velocity from the underlying Dirac equation for a topological insulator/graphene, and the charge squared is divided by the permittivity of the surrounding medium. This permittivity is rather large for topological insulators, and the random phase approximation, therefore, makes sense. Thus, a plasma wave in a topological insulator is always associated with a spin wave owing to spin-momentum locking (if the electron momentum, which defines the plasmon momentum, is oriented along a certain direction the plasmon momentum is fixed, because of the strict momentum-spin connection for Dirac electrons, a certain spin polarization emerges as well).

Interesting effects occur when a magnetic impurity layer or a film of magnetic material is deposited onto the surface of a topological insulator. The

external exchange interaction (noninvariant with respect to time reversal) of this layer with Dirac electrons induces a gap in the spectrum of the Dirac electrons, and the topological insulator becomes a quantum magnetoelectric: An external electric field induces (apart from the ordinary electric polarization of the volume) a magnetic moment, while a magnetic field induces an electric dipole moment. This gives rise, notably, to appearing quantized nondiagonal Hall conductivity, and therefore to the quantum Faraday and Hall effect – quantized rotations of the polarization plane of transmitted or reflected electromagnetic waves (in the absence of an external magnetic field). The chiral properties of the system give rise to chiral properties of the excitons inside the topological insulator gap (dependence of the energy on the sign of angular momentum projection). That is why these chiral excitons make a resonance contribution to the nondiagonal conductivity of the system, which may greatly enhance the Faraday effect in comparison with its quantized magnitude (defined only by the fine-structure constant) (see Refs [66, 175]).

The Coulomb field of the electrons located above the surface of a topological insulator with two-dimensional chiral electrons induces a magnetic polarization which is equivalent, owing to the symmetry of the problem, to the presence of image magnetic monopoles (similarly to image charges). For a sufficiently dense two-dimensional electron gas, the emerging total external magnetic field of all the image monopoles may be considered to be uniform and proportional to the surface density of the external electrons and the magnetic monopole charge. This field can manifest itself in the Hall effect for the external electrons and a change in the plasmon dispersion.

When irradiated with an external field the system goes to a non-equilibrium state due to absorption and emission of energy quanta, spin and charge currents appear as a result. These processes are more prominently manifested in optical and kinetic response. Quasiparticle dispersion in the vicinity of two Dirac cones in graphene can be linearised [42], so that

$$\varepsilon_{\mathbf{k}} = \pm v_F |\mathbf{k}|, \tag{3.3}$$

where $v_F \approx c/300$ is quasiparticle effective velocity and $\mathbf{k}$ is a quasimomentum measured from $\mathbf{K}$ (or $\mathbf{K}'$) points of corresponding Brillouin zone. The signs $\pm$ in the formula are attributed to conduction and valence bands respectively. The linear dependence of the spectrum (3.3) suggests an analogy with two-dimensional electron gas with extremely huge spin-orbit splitting. In theory, two operators of pseudo-spin, consistent with usual spintronics notations, are defined around $\mathbf{k} = 0$.

Electron transport and optical properties of graphene in the linear regime [47, 67, 165] are well-studied and are not of interest, contrary to phenomena happening in the non-linear regime which help to establish the symmetry of a system, identify the band structure, as well as to measure relaxation parameters peculiar to spin, charge and energy [97, 75, 77, 68, 98]. Photoconduc-

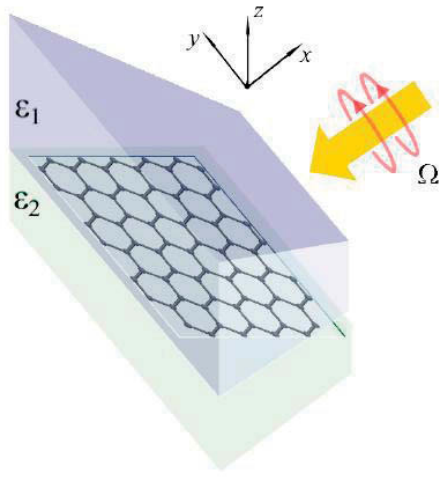

Figure 3.1. A monolayer graphene, placed in the $x-y$ plane and surrounded by two semi-infinite dielectric media with permittivities ε_1 and ε_2, is irradiated with circularly polarized light (yellow arrow).

tivity, high harmonic generation, optical rectification, electron photon-drag are among the effects well studied for parabolic-band semiconductors and are now established in graphene. However, in the absence of spin-orbit coupling the direct spin polarization with circularly-polarized electromagnetic field is impossible in graphene, but the orbital dynamics of electrons and holes are strongly modified leading to a number of peculiarities in photo-electric coefficients.

To provide a phenomenological picture of new effects generated in clean suspended graphene [76, 106, 81] we put a system to an external electromagnetic field

$$\mathbf{E}(\mathbf{r},t) = \mathbf{E}(\mathbf{q},\omega)e^{-i\omega t+i\mathbf{qr}} + \mathbf{E}^*(\mathbf{q},\omega)e^{i\omega t-i\mathbf{qr}} \tag{3.4}$$

with a complex amplitude $\mathbf{E}(\mathbf{q},\omega)$ of the frequency ω and a wave-vector $\mathbf{q}$. The current density in powers of the field amplitude reads

$$\begin{aligned} j_\lambda(\mathbf{r},t) = \left[\sigma^{(1)}_{\lambda\nu}E_\nu(\mathbf{q},\omega)e^{-i\omega t+i\mathbf{qr}} + c.c.\right] + \sigma^{(2)}_{\lambda\nu\eta}E_\nu(\mathbf{q},\omega)E^*_\eta(\mathbf{q},\omega) \\ + \left[\tilde{\sigma}^{(2)}_{\lambda\nu\eta}E_\nu(\mathbf{q},\omega)E_\eta(\mathbf{q},\omega)e^{-2i\omega t+2i\mathbf{qr}} + c.c.\right], \end{aligned} \tag{3.5}$$

where subscripts correspond to Cartesian coordinates. In the formula (3.5) terms up to quadratic are taken into account only: The first term is responsible for linear electron transport, the second one generates the d.c. current, while the last one leads to the second harmonic generation. Being extremely sensitive to underlying crystalline symmetry the second-order response is non-zero

provided point-group symmetry does not contain spatial inversion and the conductivities $\sigma^{(2)}_{\lambda\nu\eta}$ and $\tilde{\sigma}^{(2)}_{\lambda\nu\eta}$ to be odd functions of $\mathbf{k}$. Thus, in the system with lack of inversion the lowest contribution is given by

$$\sigma^{(2)}_{\lambda\nu\eta}(\mathbf{q},\omega) = \sigma^{(2)}_{\lambda\nu\eta}(0,\omega) + \Phi_{\lambda\mu\nu\eta} q_\mu \tag{3.6}$$

and $\sigma^{(2)}_{\lambda\nu\eta}(0,\omega)$ is non-zero. The point-group symmetry of an infinite monolayer of clean suspended graphene is D_{6h} which comprises spatial inversion, thus only the processes with momentum-transfer are allowed, i.e. $\sigma^{(2)}(0,\omega) = \tilde{\sigma}^{(2)}(0,\omega) = 0$. The tensor $\Phi_{\lambda\mu\nu\eta}$ can be split into symmetric and antisymmetric terms relative to ν and η permutation

$$j_\lambda = T^S_{\lambda\mu\nu\eta} q_\mu \frac{E_\nu E^*_\eta + E^*_\nu E_\eta}{2} + i T^A_{\lambda\mu\nu} q_\mu \left(\mathbf{E}\times\mathbf{E}^*\right)_\nu . \tag{3.7}$$

Symmetric with respect to ν, η permutation, the fourth-rank tensor $T^S_{\lambda\mu\nu\eta}$ is responsible for the linear electron-photon drag which is non-sensitive to the sign of light circular polarization; while the third-rank pseudo-tensor $T^A_{\lambda\mu\eta}$ provides the contribution to circular electron drag, sensitive to it.

It is worth to note that the current can flow only on the graphene plane (let say $x-y$ plane): In D_{6h} $\lambda = x,y$ is characterized by four independent components $T_1 = T^S_{xxxx} + T^S_{xxyy}$, $T_2 = T^S_{xxxx} - T^S_{xxyy} = 2T^S_{xyxy}$, $T_3 = 2T^S_{xzxz}$, and $T_4 = T^S_{xxzz}$, thus

$$\begin{aligned} j_x = T_1 \frac{|E_x|^2 + |E_y|^2}{2} q_x + T_2 \left(\frac{|E_x|^2 - |E_y|^2}{2} q_x + \frac{E_x E^*_y + E^*_x E_y}{2} q_y \right) \\ + T_3 \frac{E_x E^*_z + E^*_x E_z}{2} |E|^2 q_z + T_4 q_x |E_z|^2 \end{aligned} \tag{3.8}$$

and

$$\begin{aligned} j_y = T_1 \frac{|E_x|^2 + |E_y|^2}{2} q_y + T_2 \left(\frac{|E_y|^2 - |E_x|^2}{2} q_y + \frac{E_x E^*_y + E^*_x E_y}{2} q_x \right) \\ + T_3 \frac{E_y E^*_z + E^*_y E_z}{2} q_z + T_4 q_y |E_z|^2 . \end{aligned} \tag{3.9}$$

A quick look at the formulas (3.8) and (3.9) shows that a drag current is present in the system at oblique incident of light, while the circular drag effect permitted by D_{6h} determined by antisymmetric $T^A_{\lambda\mu\eta}$

$$j_x = i\tilde{T}_1 q_y \left(\mathbf{E}^*\times\mathbf{E}\right)_z - i\tilde{T}_2 q_z \left(\mathbf{E}^*\times\mathbf{E}\right)_y \tag{3.10}$$

and

$$j_y = -i\tilde{T}_1 q_x \left(\mathbf{E}^* \times \mathbf{E}\right)_z + i\tilde{T}_2 q_z \left(\mathbf{E}^* \times \mathbf{E}\right)_x \tag{3.11}$$

with $\tilde{T}_1 = T^A_{xyz}$ and $\tilde{T}_2 = T^A_{yzx}$. The photocurrent appears in the direction perpendicular to the incident plane. The formulas (3.8), (3.9), (3.10), and (3.11) can be drastically simpified taking account the fact that the coefficients T_3, T_4, and $\tilde{T}_2$ are negligibly small when the band structure is formed by π – orbital electrons (in this case the z – component of a field is absent), so these terms might be dropped out. Therefore,

$$j_x = T_1 \frac{|E_x|^2 + |E_y|^2}{2} q_x + T_2 \frac{|E_x|^2 - |E_y|^2}{2} q_x, \tag{3.12}$$

$$j_y = T_2 \frac{E_x E_y^* + E_x^* E_y}{2} q_x - i\tilde{T}_1 q_x \left(\mathbf{E}^* \times \mathbf{E}\right)_z \left(|E_x|^2 + |E_y|^2\right). \tag{3.13}$$

The other non-linear effects can be addressed in the same fashion.

The presence of a circularly polarized field strongly affects transport of quasiparticles propagating in graphene. Moreover, a time-periodic field gives rise to a dynamical gap opening, while the resulting photocurrent can flow without any applied bias voltage. Taking account of non-linear phenomena dramatically enhances the number of processes which could be observed. The recently discovered photovoltaic Hall effect is among them. Being illuminated by intense circularly polarized light the wave function of charge carriers in graphene picks up a geometric phase due to a non-adiabatic evolution of $\mathbf{k}$ – points in the Brillouin zone. In fact, when the trajectory of a $\mathbf{k}$ – point encircles the Dirac cone, a gap opens up in the Floquet quasienergy spectrum at zero-momentum. In this case the geometric phase coincides with so called Aharonov–Anandan phase. The formation of a gap can be formally associated with topological effects and experimentally detected via Hall-type conductivity (which can be linked to quantum anomalies from high-energy physics). The wave function of any quantum system subjected to an external periodic field acquires a non-trivial topological phase. Typically such systems are characterized by a set of quasienergies, whereas any topological phase originates from a certain gauge symmetry, making the standard analysis based on symmetry considerations inapplicable. Therefore, a systematic study of a quantum problem including combination of both non-linearity and time-periodic potential seems illusive. However, certain information can be extracted from a perturbative expansion. For the probing field with frequency ω we can evaluate the dynamical conductivity of graphene irradiated with circularly polarized light, using the Kubo formula:

$$\sigma_{ab}(\omega, T) = \frac{i}{\omega} \int dt e^{i\omega t} \Pi^R_{ab}(T + t/2, T - t/2). \tag{3.14}$$

In the following we analyze both longitudinal and transverse (Hall) components. The retarded current-current correlation function which appears in the formula (3.14) is given by

$$\Pi^R_{ab}(t_1,t_2) = -ig_s g_v \theta(t_1-t_2)\sum_{\mathbf{k}} \left\langle \left[\hat{j}_a(t_1),\hat{j}_b(t_2)\right]\right\rangle, \tag{3.15}$$

the current operator is determined by $\hat{j}_a = ev_F\hat{\sigma}_a$. It is worthy to note that in (3.14) we have defined $T=(t_1+t_2)/2$ and Fourier transformed with respect to $t=t_1-t_2$. The momentum summation in (3.15) can be done within the so called generalized Kadanoff–Baym ansatz (Paper IV) which assumes the direct relation between the lesser Green function and occupation fraction, i.e.

$$G^<_{\mathbf{k}}(t_1,t_2) = i\sum_{\alpha,\beta=\pm}\rho_{\mathbf{k}\alpha\beta}|\Phi_{\mathbf{k}\alpha}(t_1)\rangle\langle\Phi_{\mathbf{k}\beta}(t_2)|, \tag{3.16}$$

the subscripts α and β denote the band indices, whereas $\rho_{\mathbf{k}\alpha\beta}$ is the non-equilibrium density matrix, which is in fact different from its steady-state counterpart as long as the system is driven out-of-equilibrium and in general needs to be determined from a kinetic equation. However, in order to simplify the analysis we assume the density matrix to be diagonal, while its non-zero elements coincide with the Fermi distribution and use the form $\rho_{\mathbf{k}\alpha\beta} = \theta(E_F-\varepsilon_{\mathbf{k}\alpha})\delta_{\alpha\beta}$ (the system is supposed to be doped up to $E_F>0$). By doing so we obtain a closed set of equations, while the information related to quasiparticle dynamics in graphene is encoded in Eq. (3.14). Furthermore, this information is redundant to some degree: Indeed, unless we are interested in accurate time-resolved measurements we can average this expression over T, and derive

$$\hat{\sigma}(\omega) = \sum_l \begin{pmatrix} \sigma_0^{(l)}(\omega) & \sigma_H^{(l)}(\omega) \\ -\sigma_H^{(l)}(\omega) & \sigma_0^{(l)}(\omega)\end{pmatrix}, \tag{3.17}$$

where the summation index l counts the number of photons participating in the process. To be specific and without loss of generality we present calculations for one-photon processes, i.e. we restrict ourselves to $l=-1;0;1$. However, experimental results can be fit easily with our formula as long as the used approximations hold. One should also keep in mind that the results obtained for pristine samples are more accurate in the high-frequency region, otherwise electron transport in graphene is strongly affected by subtleties of scattering processes which are beyond the scope of our work. It is worth noticing that in the absence of photons the conductivity tensor is diagonal and its real part coincides with the well known result $\mathrm{Re}\sigma_0(\omega) = e^2/(4\hbar)\theta(\hbar\omega-2E_F)$, whereas non-linear processes associated with photon emission/absorption give rise to a photovoltaic Hall effect with non-zero off-diagonal part. Analytically, the longitudinal conductivity $\sigma_0(\omega) = \sum_{l=-1,0,1}\sigma_H^{(l)}(\omega)$ can be written

$$\sigma_0(\omega) = \frac{F(\omega)}{8} + \frac{D\Omega^2}{\omega}\left(\frac{F(\omega-\Omega)}{\omega-\Omega} + \frac{F(\omega+\Omega)}{\omega+\Omega}\right), \tag{3.18}$$

whereas the expression for the Hall term, $\sigma_H(\omega) = \sum_{l=\pm 1} \sigma_H^{(l)}(\omega)$, is

$$\sigma_H(\omega) = i\frac{D\Omega^2}{\omega}\left(\frac{F(\omega-\Omega)}{\omega-\Omega} - \frac{F(\omega+\Omega)}{\omega+\Omega}\right). \tag{3.19}$$

Here $D = \left(ev_F E_0/(\hbar\Omega^2)\right)^2$, and in the expressions above we have used the function

$$F(z) = \frac{2e^2}{\hbar}\left(\theta\left(\hbar|z| - 2E_F\right) + \frac{i}{\pi}\log\left|\frac{\hbar z - 2E_F}{\hbar z + 2E_F}\right|\right). \tag{3.20}$$

Interestingly, the combination of logarithmic singularity as well as step-like behavior at $z = 2E_F$, i.e. the energy of interband transition, in Eq. (3.20) is typical to materials with linear dispersion. However, this singularity is smoothed either with increasing temperature (we performed our calculations at $T = 0$) or taking into account momentum relaxation.

Considerable interest to graphene-based optoelectronics and plasmonics is mainly caused by the linear dispersion of charge carriers. In fact, it is well-known that in a two-dimensional electron gas, with parabolic dispersion, placed at the interface between two dielectric media only the TM – polarized mode, known as the surface plasmon polariton, can propagate. However, general arguments predict the existence of a TE – mode in materials with linear spectrum, like graphene. In the tiny region near the Dirac point the imaginary part of the conductivity is negative and an almost undamped mode exists for $1.67E_F \leq \hbar\omega \leq 2E_F$. Interestingly, the spectrum corresponding to the TM – mode can be derived purely from microscopic analysis making allowance for retardation effects, while a proper description of the TE – wave requires solution of Maxwell equations. As a result, dispersion of the TE – mode approximately coincides with that for light in media. Moreover, in the previous section we demonstrated that the conductivity tensor (3.17) is characterized by both longitudinal (3.18) and transverse (3.19) components. This fact can lead to a number of unexpected phenomena, like hybrid surface waves in graphene, by mixing the TE – and TM – modes together. To demonstrate this, we assume a monolayer of graphene placed in the $x-y$ plane (Fig. 3.1) which is surrounded by two dielectric media (e.g., graphene placed on a substrate with a dielectric medium on top) with permittivity ε_1 ($z > 0$) and ε_2 ($z < 0$) (see Fig. 3.1). The appearance of the off-diagonal conductivity (3.19) gives, as we shall see below, rise to TE – and TM – mode coupling similar to that in the presence of magnetic field. To proceed we solve Maxwell equations with corresponding boundary conditions on the interface $(\mathbf{E}_+ - \mathbf{E}_-) \times \mathbf{z} = 0$ and $(\mathbf{H}_+ - \mathbf{H}_-) \times \mathbf{z} = 4\pi\hat{\sigma}\mathbf{E}_\parallel/c$. The substitution $\mathbf{E}_\pm, \mathbf{H}_\pm = \tilde{\mathbf{E}}_\pm, \tilde{\mathbf{H}}_\pm e^{-i\omega t + i\beta x \mp \lambda z}$

results in $\lambda_{\pm}^2 = \beta^2 - \varepsilon_{\pm} k_0^2$ with $k_0 = \omega/c$. It is important to emphasize that the complex parameter β can be viewed as a wave-vector for modes propagating towards the $x-$ direction and that are independent (uniform) of y. A set of Maxwell equations enables two self-consistent solutions, namely: the TE – mode with non-zero H_x, E_y, and H_z,

$$\tilde{E}_{\pm}^{\mathrm{TE}} = (0,1,0), \quad \tilde{H}_{\pm}^{\mathrm{TE}} = (\mp i\lambda_{\pm}, 0, \beta)/k_0 \tag{3.21}$$

as well as the TM – mode with E_x, H_y, and E_z components

$$\tilde{E}_{\pm}^{\mathrm{TM}} = (\pm i\lambda_{\pm}, 0, -\beta)/(\varepsilon_{\pm} k_0), \quad \tilde{H}_{\pm}^{\mathrm{TM}} = (0,1,0). \tag{3.22}$$

Keeping (3.21) and (3.22) in mind we can construct the general solution to a set of Maxwell equations as a superposition of TE – and TM – modes

$$\tilde{E}_{\pm} = A_{\pm}\tilde{E}_{\pm}^{\mathrm{TE}} + B_{\pm}\tilde{E}_{\pm}^{\mathrm{TM}}, \quad \tilde{H}_{\pm} = A_{\pm}\tilde{H}_{\pm}^{\mathrm{TE}} + B_{\pm}\tilde{H}_{\pm}^{\mathrm{TM}}, \tag{3.23}$$

where the coefficients $A_{\pm}$ and $B_{\pm}$ showing the relative weight of modes of different polarization are to be determined by matching the correspondent boundary conditions at the interface $z = 0$. Thus, the dispersion relation is defined by

$$\left(\frac{i\sigma_0}{c} - \frac{\varepsilon_+ k_0}{4\pi\lambda_+} - \frac{\varepsilon_- k_0}{4\pi\lambda_-}\right)\left(\frac{i\sigma_0}{c} + \frac{\lambda_+}{4\pi k_0} + \frac{\lambda_-}{4\pi k_0}\right) = \frac{\sigma_H^2}{c^2}. \tag{3.24}$$

We note that whenever $\sigma_H = 0$ the expression (3.24) becomes decoupled and is nothing but a superposition of two waves propagating independently of each other. In fact, if a circularly polarized field is not present in the system, the conductivity tensor is diagonal $\sigma_0 = F(\omega)/8$ compared to (3.18) and the dispersion (3.24) is split into a TM – wave (the first multiplier) and a TE – wave (the second multiplier). On the other hand, a non-zero Hall conductivity causes a coupling, resulting in hybrid surface waves. Interestingly, contrary to the case of a metal, the graphene-based setup shown in Fig. 3.1, permits to manipulate hybrid surface wave polarization by changing chemical doping as well as by adjusting external circularly polarized field parameters. This opens new perspectives to create graphene-based elements in the rapidly developing area of metamaterials. Further considerations of the discussion presented here can be found in Paper IV of the list of publications for this thesis.

3.3 Topological matter: Non-magnetic gap opening

Observation of the spin Hall effect in a class of semiconductors with strong spin-orbit coupling [104, 27, 124, 91] has revived an interest to topological phases in condensed matter. A term topological insulator has been coined to

describe a system which behaves like an insulator in the bulk but conducts at the surface. The conduction is due to the presence of extended edge states which possess a remarkable property of topological protection. It is predicted that the electrons traveling along the surface are protected against the back-scattering and preserve their quantum phase coherence over a long distance despite the presence of impurities, interactions, and external fields. Superconductor analogs of topological insulators give rise to exotic edge modes which are composed of a "real-valued" fermion field known as Majorana fermion. Some aspects of these modes are experimentally confirmed [156]. This achievement greatly increases the chances of quantum computation being realized in the solid state. Topological phases have been explored in other physical systems such as photonic crystals, cold atomic gases, strongly-correlated electron systems and liquid helium [176, 224, 28]. Much of excitement about topological insulators is related to the nature of surface conduction which is provided by unidirectional quantum states. The phenomenon which is called topological protection makes it harder to destroy the quantum phase coherence of conducting electrons propagating at the surface.

The modern theory of phase transitions originates in the Landau's suggestion that the transition from one state of matter to another must correspond to a spontaneous symmetry breaking. This idea gives rise to the phenomenological theory of phase transitions which is formulated in terms of the order parameter. The quantum Hall effect (QHE), discovered more than 30 years ago, has posed some awkward questions regarding the original Landau approach. Indeed, the QHE might be treated as a phase since the macroscopic observables such as the quantized Hall conductivity are not affected by smooth variations of material parameters. Still the transitions between different Hall plateaus are not related to violation of any underlying symmetry. The puzzle has been successfully resolved with the introduction of topological order. The quasiclassical dynamics of the wave packet propagating in periodic dissipative media turned out to be instrumental for the theoretical understanding of the order. In an attempt to explain the anomalous Hall effect in a ferromagnet as an intrinsic property of the band structure, Karplus and Luttinger [107] pointed out that the position operator, $\hat{x}$, in a periodic lattice fails to commute with itself. As a consequence the standard quasiclassical expression for the group velocity acquires an anomalous term, which is proportional to what is now called the Berry curvature. In modern interpretation the Berry curvature being integrated over a Brillouin zone gives a topological invariant, the Chern number. The system possessing a non-zero topological invariant may be called topological matter. The relation between topological invariants and the scattering matrix was recently established [6]. The boundary between topological phases with different Chern numbers (or other topological invariants) must support the edge modes. These are exactly the edge modes, which are present e.g. on the surface of a two-dimensional topological insulator. The modes are topologically protected against any variations of the material parameters

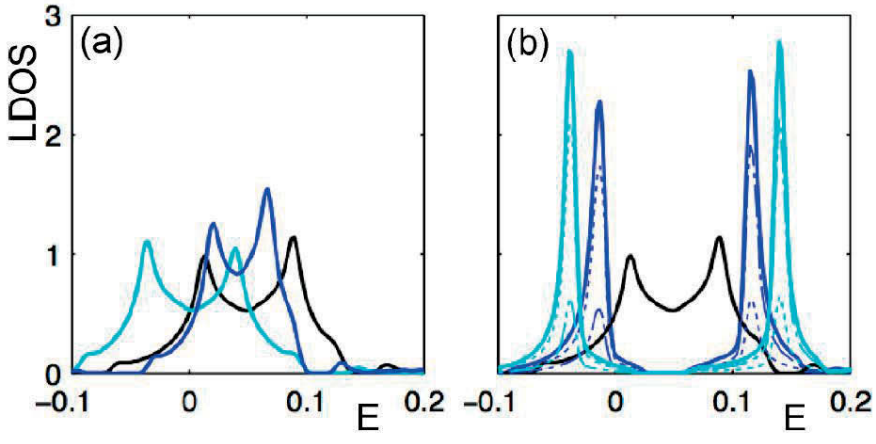

Figure 3.2. Low-energy LDOS (states/energy/area) averaged over in-plane nearest-neighbour sites to a TI surface potential impurity. (a) Non-interacting system with a vacancy and supercell size $n = 10$ (black), $n = 14$ (blue), and a $V = 65t$ impurity and size $n = 10$ (cyan). (b) System with a vacancy and size $n = 10$ for no interactions $U = 0$ (black), $U = 2t$ (blue), and $U = 2.4t$ (cyan), where $U_c = 1.8t$. For the spin-polarized systems the spin-up LDOS (dotted line) and spin-down LDOS (dashed-dotted line) are plotted. The linearly dispersing TI surface state LDOS ~ 0.01 for $E = \pm 0.5$ and is not visible.

unless the band gap in the bulk of the material is collapsed. Based on the general theory outlined above one can search for the presence of edge modes in magnonic crystals. To perform the task we shall identify time-reversal and inversion symmetric band structure characterized by the touching bands which split as soon as the time-reversal symmetry is broken. To compute the band structure the well-established plane-wave method is typically used. Depending on the periodicity one can distinguish one-, two-, and three-dimensional magnonic crystals. The simplest example of the one-dimensional magnonic crystal is the sandwich-like structure consisting of periodically placed magnets. The spectrum of such a crystal is gaped in the direction perpendicular to the layers.

Moving back to topological insulators we show that, in the presence of even weak electron-electron interactions, nonmagnetic impurities can generate a magnetic state locally around the impurities (within mean-field paradigm). More specifically, the critical interaction strength to reach a spin-polarized state is dependent on the impurity strength and concentration, following a Stoner-like criterion and approaching zero for dilute concentrations of strong impurities. Moreover, we find that the magnetic state induces an energy gap, which is directly proportional to the maximum value of the magnetization, but reduced with decreasing impurity concentration. Thus, nonmagnetic impurities can, in the presence of even weak electron-electron interactions, sponta-

neously generate a finite mass in the Dirac surface state of a TI. Nonmagnetic impurities on the surface of a TI have been shown to induce localized impurity resonances, with the impurity resonance energy scaling as $E_{\text{res}} \sim 1/V$. Thus a vacancy, where V approaches infinity, gives a resonance at the Dirac point, as shown in Fig. 3.2a for the noninteracting case. Finite impurity concentrations lead to a double-peak resonance, which narrows with decreasing concentration (compare black and blue). It also shifts the resonance slightly past the original Dirac point, since potential impurities induce a small residual overall doping into the system. A resonance peak firmly located at the Dirac point for finite supercells thus requires a large, but finite, V (cyan). The large DOS around the Fermi level close to a strong potential impurity fundamentally changes the sensitivity to interaction effects. In Fig. 3.2b we show how the resonance peak changes between the noninteracting case (black) and $U > U_c$ (blue, cyan). The resonance peak splits into two spin-polarized peaks with an energy gap developing in between. The peak splitting increases with interaction strength and the spin polarization is large but not complete. The resulting magnetization is strongly localized around the impurity. We find that the magnetization is essentially zero beyond the fourth in-plane neighbors and a surface effect, dying out within six atomic layers (one lateral unit cell). The magnetization is antiferromagnetically aligned between [111] planes but ferromagnetic in each plane, apart from the surface plane where it oscillates with the distance to the impurity. The critical interaction strength U_c for finite magnetization depends on both impurity strength and concentration, as we will discuss below, but is always significantly reduced from the clean limit for strong impurities, e.g., in Fig. 3.2b, $U_c = 1.8t$ compared to $U_c \geq 5t$ without impurities.

In order to determine when a finite magnetization is induced by nonmagnetic surface impurities, we plot U_c as a function of impurity strength for a fixed impurity concentration in Fig. 3.3a. Even though Lieb's theorem does not guarantee $U_c = 0$ for vacancies, we still find that a particular large and finite impurity strength gives essentially $U_c = 0$, and thus finite magnetization even for infinitesimally weakly interacting TIs. This result can be explained by studying the impurity resonance peak positions in Fig. 3.2a. Strong impurities push the resonance peak towards the Fermi level and thus U_c goes down sharply as the resonance state starts to generate a large DOS around the Fermi level. However, a finite concentration of strong impurities also induces a finite residual doping in the system. This leads to the impurity resonance eventually moving past the Fermi level, which reduces the DOS at the Fermi level, and thus U_c increases again when approaching the unitary scattering limit. With decreasing impurity concentration the residual doping decreases and the dip in U_c is found for increasing impurity strengths, such that in the limit of an isolated vacancy $U_c \approx 0$. To corroborate this picture we also plot the energy of the central dip in the double-peak resonance structure (blue). Clearly, having the resonance peak exactly positioned at the Fermi level, i.e., the dip at $E = 0$, is extremely well correlated with a vanishing U_c. In Fig. 3.3b

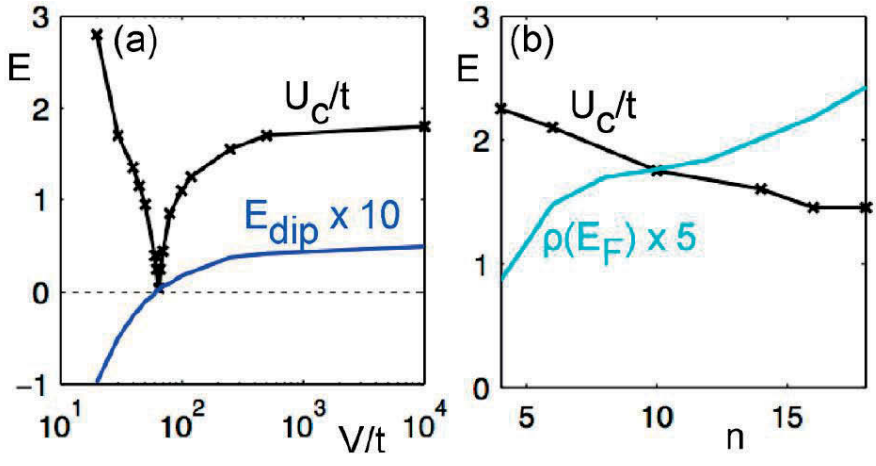

Figure 3.3. Critical interaction strength U_c/t (black, crosses) as a function of impurity strength V/t for supercell size $n = 10$ (a) and as a function of supercell size n for a vacancy (b). In (a) the energy of the dip (scaled by a factor of 10) in the double-peak resonance is also plotted (blue) along with zero energy (dotted line). In (b) the DOS at the Fermi level $\rho(E_F)$ averaged over in-plane nearest-neighbour sites to the impurity (scaled by a factor of 5) is also plotted (cyan).

we investigate more closely the concentration dependence of U_c for vacancies. Decreasing concentration leads to both narrower resonance peaks and smaller residual doping. This results in a higher DOS at the Fermi level for vacancies (cyan) and we see how this transfers into U_c steadily decreasing with the supercell size n. This inverse correlation between DOS at the Fermi level and U_c is a very characteristic feature of Stoner magnetism. The Stoner criterion for a bulk ferromagnetic state reads $U_c\rho(E_F)/2 = 1$, where $\rho(E_F)/2$ is the bulk DOS at the Fermi level E_F for one spin species in the paramagnetic state. However, in nonhomogenous systems with impurities, impurity-induced Stoner magnetism has been shown to not be sensitive to the precise DOS at E_F, but to the whole impurity band if it is narrow enough.We clearly see such an effect in Fig. 3.3a,where U_c is primarily determined by the center of the resonance peak, i.e., the dip between the two peaks. We find an approximately constant relation between U_c and $\rho(E_F)$ for a range of different impurity concentrations, but the critical interaction strength is noticeably reduced compared to the bulk Stoner criterion.

The energy gap E_g could, in principle, depend on the supercell size n, the interaction strength U, and the impurity strength V. Above we have shown that V determines the DOS at the Fermi level, which in turn sets U_c through an impurity-induced Stoner mechanism, and thus we replace the dependence on V with U_c. In Fig. 3.4a we then plot the energy gap E_g (cyan) as a function of U for fixed n and two different U_c. We also plot the maximum magnetization

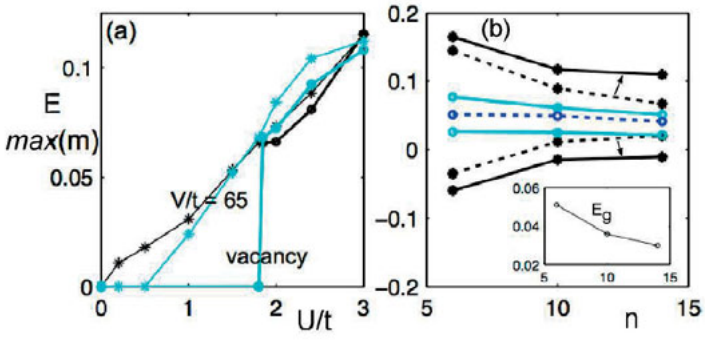

Figure 3.4. (a) Energy gap (cyan) and maximum site magnetization (black) tracking each other essentially perfectly as a function of interaction strength U/t for a supercell with $n = 10$ and a vacancy (thick lines, circles) and a $V/t = 65$ impurity (thin lines, stars). (The similarity in y values is a coincidence.) (b) Energies for the two impurity-induced resonance peaks (black, stars) and the in-between dip (blue, circles) for a vacancy in a non-interacting system (dotted lines) and for the corresponding spin-polarized system when $U/U_c = 1.14$ (solid lines) with energy gap edges (cyan, circles) as a function of system size n. Small arrows mark the shift of the peak energies appearing at finite spin polarization. The inset shows the extracted energy gap (difference between cyan lines).

$\max(m)$ (black), which we find to be a function of only $(U/U_c - 1)$. For both a vacancy, where $U_c = 1.8t$, and for a $V = 65t$ impurity, where $U_c \approx 0$, the energy gap tracks the maximum magnetization extremely well over the whole range of interaction strengths. The maximum magnetization value is found on the nearest-neighbor sites to the impurity (second surface layer), but instead using the average magnetization gives a similarly strong linear dependence between the energy gap and magnetization. We thus conclude that the functional dependencies of the energy gap can be reduced to $E_g = C(n)\max(m)$, with C being a function only of the impurity concentration. For any finite impurity concentration we find that the energy gap is a global property of the system, i.e., it does not vary with distance from the impurity. Thus the energy gap decreases when the impurity concentration is decreasing, since the same maximum magnetization needs to sustain an energy gap over a larger area. This is verified in the inset in Fig. 3.4b, where we plot the energy gap as a function of the concentration for fixed magnetizations and find that $C(n)$ clearly decreases for increasing n. In Fig. 3.4b we show more details on how the resonance peak structure evolves with impurity concentration for a noninteracting system (dashed) and for a fixed $U/U_c > 1$ (solid). The energy gap (cyan) develops around the initial dip (blue) in the double-peak resonance. In order to accommodate the finite energy gap for $U/U_c > 1$ the two resonance peaks (black) are pushed out to larger energies.With decreasing impurity concentration both the overall energy gap and the peak-peak distance decrease.

We can now also draw qualitative conclusions in the limit of very low impurity concentrations. The overall residual doping is then diminished and thus only vacancies produce impurity-induced resonance peaks close to zero energy. Such resonance peaks are very sharp so U_c approaches zero for isolated vacancies and even extremely weakly interacting TIs will have a finite magnetization. However, even though $\max(m)$ only depends on U/U_c and can therefore be large even for very weakly interacting TIs, the size of the induced energy gap will be severely limited by the small function $C(n)$. We thus do not expect any sizable energy gap in the limit of very low impurity concentrations. Further aspects of this problem, are elaborated upon in Paper III in the list of publications of this thesis.

To complement the above supercell calculations using a Hubbard-U interaction, we also study the effect of long-range Coulomb interactions in a continuum model while treating the impurities within the coherent potential approximation (CPA) [137]. The kinetic part is here described by a 2D gapless Dirac term, whereas the electron-electron interaction strength is characterized by the dimensionless coupling $g = e^2/(\varepsilon_0 v_F)$, where e is the charge of the electron and ε_0 the dielectric constant of the system. We further here assume that the impurities are randomly distributed over the lattice sites, with the on-site potential taking values V and 0 with probabilities c and $(1-c)$, respectively, which allows for a binary alloy analogy with the impurity concentration directly linked to c. For a strongly scattering medium with low impurity concentration the effect of the impurities can be incorporated in a self-consistent manner using CPA, which is based on a single-site approximation in a multiple scattering description. It takes into account terms that are linear in c but disregards scattering off impurity clusters.

Using the self-energy, which is assumed to be translationally invariant after configurational averaging, as well as spin independent and site diagonal, the single particle Green's function of the disordered (but noninteracting) system can be written as $G^{\pm}_{CPA}(\varepsilon,\mathbf{k}) = \left(\varepsilon - \sigma_{CPA}(\varepsilon) - \varepsilon^{\pm}_{\mathbf{k}}\right)^{-1}$, where $\varepsilon = \pm v_F k$ is the bare dispersion relation and $\sigma_{CPA}(\varepsilon)$ is determined by self-consistently:

$$\sigma_{CPA}(\varepsilon) = \frac{cu}{1 - u g_0(\varepsilon - \sigma_{CPA}(\varepsilon))}, \tag{3.25}$$

where u is the impurity strength. For small concentrations of vacancies ($\mathrm{Im}\sigma \ll v_F k_c$ with a cutoff k_c for integral regularization) with the bare Green's function [196]

$$g_0(\varepsilon) = \frac{1}{4\pi v_F^2}\left[2\varepsilon \log\left(\frac{|\varepsilon|}{v_F k_c}\right) - i\pi|\varepsilon|\right]. \tag{3.26}$$

we obtain a finite concentration of charge carriers in the vicinity of $\varepsilon = 0$. Calculating the change in energy (similar to [164])

$$E = \sum_{\mathbf{k}\sigma} \varepsilon_{\mathbf{k}\sigma} f(\varepsilon_{\mathbf{k}\sigma}) - \frac{\pi g}{2S} \sum_{\mathbf{kp}} \sum_{\sigma_1\sigma_2} \frac{1 + \sigma_1\sigma_2 \cos(\varphi_{\mathbf{k}} - \varphi_{\mathbf{p}})}{|\mathbf{k} - \mathbf{p}|} f(\varepsilon_{\mathbf{k}\sigma_1}) f(\varepsilon_{\mathbf{p}\sigma_2}) \tag{3.27}$$

relative to the paramagnetic state we find ferromagnetism when $g_c \approx 3.7$, to be compared to $g_c \approx 5$ in the absence of disorder (here S is area and the distribution function $f(\varepsilon_{\mathbf{k}\sigma})$ can be found by integrating out frequency in $\mathrm{Im}G_{CPA}(\varepsilon, \mathbf{k})$). Thus, also a continuum model with long-range Coulomb interactions facilitates a finite magnetization for noticeably weaker electron-electron interactions in the presence of impurities treated within the CPA. Note that this is in spite of the CPA averaging over impurity configurations, thus not explicitly relying on localized impurity-induced resonance states.

4. Conclusions and outlooks

In the last chapter we briefly summarize the results emphasized in the thesis, outline the directions where some of our findings can be applied, and provide a brief outlook for current trends in technological development.

- We have studied the formation of extended van Hove singularities in the triangular lattice. We have found from both the renormalization group and strong-coupling numerical analysis that the phenomenon is driven by many-body interactions: The delicate interplay of many-particle scattering and nesting gives rise to band flattening near saddle points, while the associated high intensity in the spectral function may find interesting applications in tunneling experiments and spintronics. The phenomenon can be interpreted as a precursor to a strongly correlated many-body ground state. Its study in the controlled environment of cold atom experiments may fundamentally improve our understanding of correlated systems.We have shown the effect to be robust when tuning interaction, temperature, and chemical potential. In particular, its signature in the occupation function is found to persist to relatively high temperatures, making the phenomenon detectable in experiments with ultracold atoms in optical lattices.

- We have discovered the formation of the topologically protected magnon edge states in the kagome lattice and shown that the kagome lattice supports skyrmion-antiskyrmion pairs, meron and antimeron excitations even at room temperature. The latter has been detected for a wide range of parameters describing the magnetic excitations, in particular, for the DM coupling and the Heisenberg exchange interaction. The results clearly demonstrate that the interlayer exchange interaction does not affect the stability of the skyrmionic excitations. We have established the possibility to control the movement of skyrmionic excitations and that such excitations are long-lived. We have also observed that these particle-like excitations can move on well-defined straight lines and even be made to turn around corners. This opens a way to use such excitations in different emerging technologies, e.g., in data storage or magnetic bits manipulation. We have also investigated meron-meron and meron-antimeron collisions. The former are found to undergo elastic collisions, whereas the latter are more complex. Thus, the annihilation of a meron-antimeron after collision is followed by the creation of a new meron, a process which occurs as a highly non-local phenomenon.

- We have investigated the formation of quasienergy spectra in monolayer graphene irradiated with circularly polarized light. The system evolving under time-periodic Hamiltonian gains a non-adiabatic topological phase and acquires Hall-type conductivity as a result. We have worked out the conductivity tensor in one-photon approximation and show that it leads to the formation of hybrid surface waves propagating in graphene sandwiched between two dielectrics. The dispersion relation derived for such waves shows that they incorporate the effects associated with interband particle-hole transitions. The results can be applied in experimental studies of hybrid surface waves in graphene, that could help realizing and implementation of graphene-based plasmonics.

- We have shown that strong nonmagnetic impurities on the surface of a strong topological insulator can induce a finite magnetization and an energy gap in the presence of even weak electron-electron interactions. Strong impurities and also vacancies give rise to localized resonance peaks around the Dirac point. The resulting increased low-energy DOS leads to a strongly reduced critical interaction strength to reach a magnetic surface state. Thus, even very weakly interacting topological insulators will have a finite magnetization emerging around strong nonmagnetic impurities. The finite magnetization gives rise to a global energy gap which is linearly dependent on the maximum value of the magnetization, but decreases with reduced impurity concentration.

The main results of this thesis can be put into context of trends in modern solid state physics, mesoscopic physics and nanotechnology. Nowadays, nanotechnology is a collection of methods and techniques, allowing to manipulate matter and information on nanoscale (100 nm and less, e.g., nanowires, nanoelectronics, nanopowder), rather than a completed technological platform. The main tool for investigating processes on submolecular level is an atomic force microscope (it permits to measure interatomic distance and address each atom individually), while plasma synthesis, molecular deposition, and lithography are among the methods used for nanostructure fabrication. In the meanwhile, mesoscopic physics (basically what this thesis is about), which is able to accurately explain a bunch of phenomena at microscopic level where quantum coherence is an important entity, is also in the basis of modern nanotechnology, therefore the trend on technologization of mesoscopic effects will continue (for instance, quantum dots or quantum wells from theoretical viewpoint). The term “mesoscopics” has been introduced in physics by W. van Kempen and M. Ya. Azbel from paleontology and is used to refer to relatively small systems, where however the number of particles is too large to apply the equations of quantum mechanics directly, but still too small to use statistics (since fluctuations characterizing the system are of the order of corresponding mean

values). Thus, at the moment two disentangled concepts, namely atomic force microscopy, which enables to address atoms and molecules directly and in general originates from optics and metrology, and mesoscopic physics, which enables material synthesis and realization of quantum transistor and is mainly rooted in quantum field theory, are a pillar of modern nanotechnology. This self-contradiction can potentially lead to either splitting of nanotechnology into two independent areas or setting of a new universal technology allowing matter manipulation on atomic scale. In fact, atomic force microscopy, widely used in modern technology, has helped to achieve extremely high on-chip integration, but the principle direction is likely to be related to the ability to create a densely packed and ordered arrays of quantum dots – nanotransistors. Such a technology will speed up the emergence of nanosensors, and in combination with spintronics will lead to femto-technology replacing thus the nanoparadigm. Principally new results can be reached by including the effects of purely quantum-mechanical nature into nanotechnological considerations, e.g. quantum paradoxes (one can think of recently achieved quantum cryptography or quantum teleportation). Therefore, subsequent technologization of the concept of entangled states is highly desirable, which undoubtedly leads to the invention of a quantum computer with extremely high performance, making the progress in energetics and propulsion engineering unavoidable.

Nanotechnology along with biotechnology is currently considered as the only large-scale project from natural science that can have a considerable economic impact. However, one can point our three different scenarios associated with social transformation due to technological progress. The first, or inertial, scenario basically assumes the subsequent development of information technology (IT) and progress in bio- and nanotech based on state-of-art IT infrastructure. The second option, or natural scenario, suggests to focus on biotech development. While the last one, the breakthrough scenario, merely relies on nanotech and requires institutionalization of nanotechnology and emergence of new universal tools capable to address the matter on atomic scale independent of its physical nature. The inertial scenario in its turn can be divided into two sub-scenarios: IT development in the context of up-to-date trends, relying on the use of existing computers and network infrastructure, and total robotization, which requires building of infrastructure compatible with robot-androids. In the latter case currently exploited IT services will have to pale into insignificance. However, from our perspective, the nanotechnological scenario seems more reasonable to speculate about. Nanotechnological revolution, if any, will mainly be determined by the progress in material fabrication and characterization and is expected to revive space exploration on new technological grounds and allow man-made ecosystems. This is in contrast to biotech scenario, which is believed to govern human development and human's environment. In the paradigm of nanotechnology we ideally can produce any material for a particular application. Social transformations under nanotech revolution are known to be extremely dramatic: A capability to synthesize any substance with de-

sired properties dictates new standards of manufacturing and potentially leads to new regionalization and the emergence of closed autonomous nanotechnological clusters. An important ingredient of nanotechnological paradigm is the ability to systematically utilize quantum effects in a macroscopic world. Thus, the main direction has to be the subsequent implementation of quantum effects in materials and machines. Consequently, the natural definition of nanotechnology can be granted in the following way: A set of methods and technology which transfer the quantum effects to a macroscopic level. To conclude, we are at the crossroads at the particular moment when we have to make a choice in favor of one of the futures, though the logic of the dynamical scenario allows variability and excludes strict determinism. In case of success, nanotech revolution will bring new possibilities for the exploration of deep space and world oceans, give an impulse for medicine, energetics, and engineering, and perhaps will be referred to as the transition to the "quantum world" (or, "man-created inanimate world").

In this thesis we have treated strongly correlated systems from different perspectives, however we believe that such a multidisciplinary consideration will facilitate practical implementation of the concepts proposed above. In fact, we simply list a few possible options: Computer modeling of the physical properties of complex compounds is an essential element of technological design of advanced materials for applications in modern industry. The number of possible variants of multicomponent systems, in general, is so great that a blind search for materials with the desired properties can be prohibitively expensive and time consuming. The ability to quickly and relatively cheap try a potential compound by computer simulation is the only way to solve this problem. Currently, the most common methods are based on the paradigm of density functional theory (DFT). These methods work well for wide-band materials where the kinetic energy of the electrons exceeds the Coulomb interaction. Based on this approximation one can obtain not only complete information on the spectral properties of materials, defined by electron transitions, but also on the magnetic properties, the elastic constants, and phonon spectra describing the vibrations of the crystal lattice. Nevertheless, the most challenging at the moment are the narrow-band materials in which the direct account of the Coulomb interaction fluctuations is necessary for the correct description of their physical properties, and DFT methods are not sufficient. These materials are interesting because they may be on a way towards electronic, magnetic or structural transition, which results in anomalous response to external field, making, thus, this class of materials promising for prospective application. The developed in the last years methods like DFT+U (Hubbard U correction) and DFT+DMFT allow to describe the properties of many new narrow-gap materials, though these methods are far from being panacea and have to be modified. In that sense, combination with dual fermion approach could be indispensable for band-structure computation. The second example comes from IT sector: Nowadays the flagships of IT industry are focusing on the cre-

ation of a new generation of computing systems in which information will be transferred by light pulses instead of electrical signals as it takes place now. Basically, to convert the space-time optical signals diffractive structures with resonant properties are used. Under resonance we mean anomalous change of reflection and transmission coefficients occurring when the eigenmodes of the diffractive structure are excited. Thus produced resonant structures, e.g., diffraction gratings, nanoresonators, and multilayer coatings, can be applied to differentiation and integration of incoming optical signals, to the optical resolution of differential equations as well as to the problem of the phase-amplitude modulation of optical radiation, setting the platform for all-optical data processing. In the meanwhile, direct application of topological insulators has to rely on the existence of topologically protected surface states. Incorporation of impurities allow to control the spin magnetization, as well as achieve Hall quantization at zero field, which is highly desirable for quantum metrology.

5. Svensk sammanfattning

Stora framsteg inom informationsteknologi är ofta nära länkat med gårdagens science fiction. Vid granskning av ett par populära websidor dedikerade åt framtidens datoranvändning demonstrerar I-Net-samfundet tydligt att de redan har lagt grunden till en nano-slang. Vi kan till exempel finna att en nanodator är antingen en högpresterande kvantmekanisk dator i storleksordningen nano; eller en dator gjord av datorlogiska element av molekylär storlek; eller att nanorobot-kontrollen måste vara nano. Problemet med terminologin är inte vad skaparna av ny hårdvara är bekymrade över. Förändring av fysikaliska egenskaper hos logiska enheter vid reducering av storleken på dess arbetselement, montering och integration av dessa enheter, möjligheten till deterministisk kontroll av dess funktion, förlorad information och termodynamik hos nanoenheter, den fysikaliska begränsningen av att representera och bearbeta data är några av de kritiska frågorna som noggrant måste utredas. Nanoelektronik, nanodatorer, nanorobotar och molekylära mekaniska maskiner kommer inte enbart att förändra IT mot ett mer avancerat ämnesbaserat område, det kommer också att ställa många besvärliga frågor av humanistisk natur. I jämförelse med till dags dato spekulationer om kloning av djur med hjälp av stamceller eller användandet av dem i medicin kommer kanske etiska frågeställningar om nano-vetenskap inte att verka så förfärliga. Med övergången till nanovärlden kommer det att vara möjligt att reducera den minimalt tillåtna storleken på en dator till subcellulär nivå. Lagringstätheten av artificiella system överskrider redan den mänskliga arvsmassan. Sätt att presentera information i system skapade av människan har nästan redan nått den fysikaliska begränsningen satt av de fundamentala naturlagarna. Det är tydligt att nanodatorer kommer att utvecklas samtidigt i ett par olika riktningar beroende av bearbetning av information – med kvantlogik som bas, klassisk logik, neurologik och också några andra mer svårdefinierade – genetisk, molekylärt biologiskt och molekylärt mekaniskt.

För tillfället så är den mest avancerade hårdvaran baserad på elektroniska nanotransistorer, inkluderande singel-elektron transistorer och spinnpolariserade, eller spinntroniska transistorer. Den kvantmekaniska begränsningen satt av Paulis uteslutningsprincip och Heisenbergs osäkerhetsprincip har redan nåtts. Dessutom, begränsningen av värmeavgivning definierad av Landauers princip när en bit av information går förlorad i irreversibla datorberäkningar är också nådd. Fastän applikationer av singel-elektron transistorer fortfarande ligger långt in i framtiden så arbetas det på att designa diverse arkitektoniska

nanodatorer. Emellertid så är de fysikaliska kriterierna som i allmänhet bestämmer de beräkningsmässiga möjligheterna onekligen avgörande. För att illustrera detta så betraktar vi artificiellt odlade kvantprickar. Dessa är halvledande öar inbäddade i en dielektrisk matris vilka karaktäriseras av att de har ett kvantifierbart antal elektroner. Kvantnummer avser antalet elektroner inom fysiken och detta tros inte fluktuera. Coulombkraften mellan elektronerna är signifikativ och om till exempel en kvantprick är ockuperad av en elektron så hindrar repulsionen en andra elektron från att befinna sig i samma kvantprick. Detta fenomen kallas för kvantblockad. Kvantblockad är hjärtat av singelelektrontransistorer. Kanske är en kvantprick det enklaste exemplet på ett korrelerat elektronsystem. I allmänhet så ses korrelationen som en växelverkan mellan olika komponenter i ett komplext system. Emellertid så föreligger det en paradox som kommer av det faktum att man med modern fysik idag kan skriva ekvationer för att beskriva nästan vilket system som helst, dock klarar man inte alltid av att lösa dessa ekvationer. Man kan bara finna en lösning då systemet består av en uppsättning av partiklar som inte interagerar med varandra och kan hanteras separat eller bara svagt interagerar. I det sistnämnda fallet så säger vi att vi kan utveckla en teori som har en liten parameter. Små parametrar är väldigt viktiga för existensen av vår värld som helhet. Till exempel så är ljuset i vår värld svagt kopplat med materia där individuella atomer och elektromagnetiska vågor inte talar med varandra. Numeriskt så beror detta på att det finns en motsvarande liten parameter känd som finstrukturkonstanten (approximativt 1/137). I de flesta fall är fysik baserat på konceptet om små parametrar som kan väljas på ett eller annat sätt. Att därför driva hårdvaruprestandan till dess gräns kan potentiellt belysa problemet med högtemperatursupraledare, där elektronkorrelationen inte bara är stark, utan där råder också icke-lokalitet i rummet. Densiteten hos transistorer i integrerade nanokretsar är för närvarande extremt hög, likväl i det långa loppet är energifrågor under de tillstånden väldigt viktiga för nanodatorteknologin. Där finns en fundamental begränsning av densitet på logiska element som inte är associerat med atomstrukturen på materian, det är istället en fråga om termodynamik och den datorberäknande processen i sig själv. Dess härkomst är uttryckt av Landuers princip, vilken säger att en bit av förlorad information leder till en frigivning av värmeenergi motsvarande $k_B T \log 2$, där k_B är Boltzmans konstant och T är processorns temperatur. Ingenjörer söker för närvarande efter lösningar på problemet med överhettning genom att till exempel implementera reversibla datorberäkningar vilket är möjligt för datorprocesser baserade på vetenskapen om kvantinformation. Där finns några andra fysikaliska mekanismer som tillåter optimering av termodynamiken hos en klassisk datorer. Härledda under antagandet att en temperatur T kan användas för att karaktärisera en datorberäkning kan Landauers princip i omgivningen av en datorberäkning karaktäriseras av en temperatur T och att vi med Landauers princip kan relaxera systemet i system med två eller fler temperaturer (dessa system är kända för att inte vara i termodynamisk jämvikt). Ett välkänt paradigmatiskts exempel

är urladdning av en fluorescerande lampa där atommolekylära delsystem är karaktäriserade av rumstemperatur (300 K), i jämförelse med 30-50 gånger högre temperatur (10000 K) för fria elektroner. Därmed föreslår det sistnämnda att datorberäkningar bör genomföras i superkylda delsystem med mycket låg temperatur och att information bör skrivas innan informationen är påverkad av förlusten från att systemet går mot termisk jämvikt. Konsekvent implementering av detta tillvägagångssätt leder oss till idén om en optimal kombination mellan kvantmekaniska och klassiska beräkningar. Till exempel kan man använda växelverkan mellan kalla kvantstrålar av ljuspartiklar med arrayer av varmare tunga partiklar. Sådana datorer existerar redan, till exempel en optisk dator där ljusstrålar med låg entropi kan passera igenom ett system utan praktiskt taget någon termisk förlust. Enligt Landauer så frigörs värme bara vid strålningsdetektorer när resultatet skrivs ut. Detta är den huvudsakliga fördelen med fiberoptiska kommunikationssystem. Därmed utför optiska datorer de kallaste beräkningarna. Emellertid kan en liknande typ av process också implementeras i elektroniska datorer. Datorberäkningsprocessen kan utföras i ett termodynamiskt icke-jämviktsläge eftersom massan av en elektron är mycket mindre än den för en atom. Man kan skapa nanostrukturer för datorberäkningar med buntar av superkylda elektroner som fortplantar sig i en matris med tunga atomer. Transistorer där elektroner kan passera genom en fungerande kanal nästan helt utan att utsättas för några termiska kollisioner med atomer existerar redan (ballistiska transistorer). Nästa steg blir att utforma en ballistisk transistor med kalla elektroner.

Vi kan sammanfattningsvis säga att en av de mest pressande utmaningarna med modern elektronik är att skapa mycket snabba enheter med minimala termiska förluster. Att vända på elektroners spinn (eller rättare sagt deras riktning) möjliggör ändring av ett materials magnetiska eller elektroniska tillstånd. Än viktigare är att spinn kan ändras väldigt enkelt genom att applicera ett externt magnetfält, ett elektriskt fält eller att mekaniskt töja materialet. Idén att använda spinns frihetsgrader ledde till uppkomsten av två nya grenar inom elektroniken – spinntronik och forskning på magnoner (studier av spinnvågor, det vill säga magnetiska fluktuationer som propagerar i tiden med en våglängd i storleksordningen en tiondel av ljus med samma frekvens). Spinntronik är praktiskt taget en gren i fasta tillståndets elektronik där fysikaliskt relevant information är presenterad inte enbart med laddning utan också med partiklarnas spinn, som kan ses som deras egna mekaniska moment. Spinn kan visualiseras som en rotation av en partikel runt sin egna axel, emellertid, trots tydligheten i presentationen och den självklara meningen med termen så kan inte klassisk fysik förklara uppkomsten av spinn. En följdriktig förklaring ges enbart av relativistisk kvantmekanik. Varje elementarpartikel är karaktäriserad av ett spinnkvanttal som bara kan anta positiva heltal (0, 1, 2,...) eller halvtal (1/2, 3/2, 5/2,...). Till exempel har en foton spinn 1 och en elektron spinn 1/2. Förutom det mekaniska spinnmomentet så kan en del partiklar också ha ett magnetisk moment. En foton har noll magnetiskt moment medan en elektrons

magnetiska moment är skilt från noll. Om vi betraktar laddningsöverföringen uppkomna av partiklars rörelse hamnar vi i konceptet om konventionell elektrisk ström. Om vi betraktar spinntransport får vi spinnström (mekanisk och magnetisk). Under normala förhållanden så är tillstånd med olika spinnprojektioner lika populerade så att spinnströmmen är noll. I framtiden tros man kunna hitta batterier utan kemiska reaktioner som konverterar elektrisk energi till magnetisk och vice versa, magnetoresistiva minnen med noll energiförbrukning med nästan evinnerliga resurser och optiska enheter på nanoskala. Nyckeln till denna typ av innovation är att kontrollera spinnet hos partiklar i funktionella material. Inom spinntronikforskningen så utforskas för tillfället den magnetiska och den magnetooptiska växelverkan i halvledarstrukturer, dynamik och spinnkoherensegenskaper i kondenserad materia och kvantmagnetiska fenomen i nanostrukturer. Tillsammans med tidigare kända magneter har nya funktionella material för spinntronikapplikationer dykt upp, till exempel substanser som på en och samma gång kan vara magnetiska, halvledande och optiskt aktiva.

6. Acknowledgements

I would like to finish with perhaps the most readable part of the thesis, the Acknowledgments. Foremost, I want to express my sincere gratitude to my advisor Prof. Olle Eriksson for his continuous support, patience, immense knowledge, and good sense of humor. His guidance helped me a lot in all the time of research and invaluable suggestions made this work successful. To work with you has been a real pleasure to me. Furthermore, I have been privileged to get to know and to collaborate with many other great people who became friends over the last several years. I learned a lot from you how to attack the new problems and develop methods to solve them. Prof. Mikhail Katsnelson and Prof. Alexander Lichtenstein have been a pleasure to work with. Your expertise in theoretical questions had a great influence on me.

I have greatly enjoyed the opportunity to work with Hartmut Hafermann, your example of an independent researcher was a valuable source of motivation. I am also grateful to my co-author Daniel, thank you for your fun and encouraging discussions while my stay in Hamburg. I am thankful to Annica, my work has greatly benefited from your suggestions and encouragement. Your technical skills and attention to detail is astonishing.

I would like to express my sincere thanks to Manuel, Jonathan, Corina, and Anders for generously sharing their time and knowledge in our cooperative work. I thank my fellow office-mates in Uppsala (in chronological order): Oscar, thank you for all the advice, ideas, and support during my first year. Manuel and Corina, I am grateful to you for creating nice and friendly atmosphere over the last two years.

In my daily work I have been surrounded by a friendly and vivacious group. Thank you, Robert, for motivating me to be better than I am. You were one of the first friendly faces to greet me when I began this doctoral program. When I became too serious, your humor and friendly sarcasm allowed me to laugh and lightened my perspective. My gratitude is also extended to Yaroslav. Thank you for your humor, Sudip, you are always friendly and cheerful about everything. Anyway, I am indebted to many people for making the last few years an unforgettable experience. I thank all the present members of the group: Kristofer, Kostas, Johann, Erna, Igor, Myskal, Leyla, Nina, Anna, Jonas, Mattias, Krisztina, Moyses, Iulia, Anton, Vancho, Ralph, Inka, Pablo, Jan, Attila.

I would like to thank Anton N. for stimulating discussions and for sharing memories about our common Alma Mater “Fizteh” with me.

The last but not least, I am deeply and forever indebted to my family for their support and encouragement throughout my entire life.

References

[1] D. S. L. Abergel, V. Apalkov, J. Berashevich, K. Ziegler, and Tapash Chakraborty. Properties of graphene: A theoretical perspective. *Advances in Physics*, 59(4):261–482, 2010.

[2] A. A. Abrikosov, L. P. Gorkov, and I. E. Dzyaloshinskii. *Quantum field theoretical methods in statistical physics*. Pergamon, Oxford, 1965.

[3] Agranovich. *Excitations in Organic Solids*. Oxford University Press, Oxford, 2009.

[4] V. M. Agranovich and D. L. Mills, editors. *Surface Polaritons: Electromagnetic Waves at Surfaces and Interfaces*. North-Holland, Amsterdam, 1982.

[5] A. V. Aiboushev, A. A. Astafiev, Yu. E. Lozovik, S. P. Merkulova, V. A. Nadtochenko, O. M. Sarkisov, and M. Willander. Enhanced luminescence and two-photon absorption of silver nano-clusters. *Physica Status Solidi (C)*, 6(S1):S162–S166, 2009.

[6] A. R. Akhmerov, J. P. Dahlhaus, F. Hassler, M. Wimmer, and C. W. J. Beenakker. Quantized conductance at the Majorana phase transition in a disordered superconducting wire. *Phys. Rev. Lett.*, 106:057001, Jan 2011.

[7] J. Altmann, W. Brenig, and A.P. Kampf. Anisotropic scattering rates and antiferromagnetic precursor effects in the $t-t'-U$ Hubbard model. *The European Physical Journal B - Condensed Matter and Complex Systems*, 18(3):429–433, 2000.

[8] M. Ya. Amusia, A. Z. Msezane, and V. R. Shaginyan. Two types of the effective mass divergence and the Grüneisen ratio in heavy-fermion metals. *Physics Letters A*, 320(5–6):459–464, 2004.

[9] M. Ya. Amusia, K. G. Popov, V.R. Shaginyan, and V. A. Stephanovich. *Theory of Heavy-Fermion Compounds*. Springer, 2015.

[10] M. Ya. Amusia and V. R. Shaginyan. Quasiparticle picture of high-temperature superconductors in the frame of a Fermi liquid with the fermion condensate. *Phys. Rev. B*, 63:224507, May 2001.

[11] P. W. Anderson. Localized magnetic states in metals. *Phys. Rev.*, 124:41–53, Oct 1961.

[12] Philip W. Anderson. Sources of quantum protection in high-T_c superconductivity. *Science*, 288(5465):480–482, 2000.

[13] A. F. Andreev. Thermal conductivity of the intermediate state of superconductors. *Journal of Experimental and Theoretical Physics*, 19(5):1228–1231, 1964. Russian original – ZhETF, Vol. 46, No. 5, p. 1823, November 1964.

[14] S. N. Andrianov and S. A. Moiseev. Magnon qubit and quantum computing on magnon Bose-Einstein condensates. *Phys. Rev. A*, 90:042303, Oct 2014.

[15] S. M. Apenko and Yu. E. Lozovik. Quantization of the Hall conductivity of a two-dimensional electron gas in a strong magnetic field. *Journal of Experimental and Theoretical Physics*, 62(2):328–336, 1985.
[16] A. G. Aronov and G. E. Pikus. Spin injection into semiconductors. *Sov. Phys. Semicond.*, 10:698, 1976. Russian original – Fiz. Tekh. Poluprovodn., Vol. 10, p. 1177, 1976.
[17] S. A. Artamonov, Yu. G. Pogorelov, and V. R. Shaginyan. Ground state instability in systems of strongly interacting fermions. *JETP Letters*, 68(12):893–899, 1998.
[18] M. N. Baibich, J. M. Broto, A. Fert, F. Nguyen Van Dau, F. Petroff, P. Etienne, G. Creuzet, A. Friederich, and J. Chazelas. Giant magnetoresistance of (001)Fe/(001)Cr magnetic superlattices. *Phys. Rev. Lett.*, 61:2472–2475, Nov 1988.
[19] S. E. Barnes and S. Maekawa. Generalization of Faraday's law to include nonconservative spin forces. *Phys. Rev. Lett.*, 98:246601, Jun 2007.
[20] A. V. Baryshev, T. Kodama, K. Nishimura, H. Uchida, and M. Inoue. Three-dimensional magnetophotonic crystals based on artificial opals. *Journal of Applied Physics*, 95(11):7336–7338, 2004.
[21] G. Baym and C. Pethick. *Landau Fermi-Liquid Theory*. Wiley, 1991.
[22] V. I. Belyavskii and Yu. V. Kopaev. Superconductivity of repulsive particles. *Physics-Uspekhi*, 49(5):441–467, 2006.
[23] L. Berger. Emission of spin waves by a magnetic multilayer traversed by a current. *Phys. Rev. B*, 54:9353–9358, Oct 1996.
[24] David J. Bergman and Mark I. Stockman. Surface plasmon amplification by stimulated emission of radiation: Quantum generation of coherent surface plasmons in nanosystems. *Phys. Rev. Lett.*, 90:027402, Jan 2003.
[25] Oleg L. Berman, Godfrey Gumbs, and Yurii E. Lozovik. Magnetoplasmons in layered graphene structures. *Phys. Rev. B*, 78:085401, Aug 2008.
[26] Oleg L. Berman, Roman Ya. Kezerashvili, and Yurii E. Lozovik. Can we move photons? *Physics Letters A*, 374(35):3681–3684, 2010.
[27] B. Andrei Bernevig, Taylor L. Hughes, and Shou-Cheng Zhang. Quantum spin Hall effect and topological phase transition in HgTe quantum wells. *Science*, 314(5806):1757–1761, 2006.
[28] W. Beugeling, J. Everts, and C. Morais Smith. Topological phase transitions driven by next-nearest-neighbor hopping in two-dimensional lattices. *Phys. Rev. B*, 86:195129, Nov 2012.
[29] N. E. Bickers. Review of techniques in the large-N expansion for dilute magnetic alloys. *Rev. Mod. Phys.*, 59:845–939, Oct 1987.
[30] E. L. Bizdoaca, M. Spasova, M. Farle, M. Hilgendorff, and F. Caruso. Magnetically directed self-assembly of submicron spheres with a Fe_3O_4 nanoparticle shell. *Journal of Magnetism and Magnetic Materials*, 240(1–3):44–46, 2002. 4th International Symposium on Metallic Multilayers.
[31] A. N. Bogdanov and D. A. Yablonski. Thermodynamically stable "vortices" in magnetically ordered crystals. The mixed state of magnets. *Journal of Experimental and Theoretical Physics*, 68(1):101–103, 1989.
[32] I. G. Bostrem, Jun-ichiro Kishine, and A. S. Ovchinnikov. Theory of spin current in chiral helimagnets. *Phys. Rev. B*, 78:064425, Aug 2008.

[33] I. G. Bostrem, Jun-ichiro Kishine, and A. S. Ovchinnikov. Transport spin current driven by the moving kink crystal in a chiral helimagnet. *Phys. Rev. B*, 77:132405, Apr 2008.

[34] V. Bouchiat, D. Vion, P. Joyez, D. Esteve, and M. H. Devoret. Quantum coherence with a single Cooper pair. *Physica Scripta*, 1998(T76):165, 1998.

[35] S. I. Bozhevolnyi, editor. *Plasmonic Nanoguides and Circuits*. Pan Stanford Publishing, Singapore, 2009.

[36] Arne Brataas, Andrew D. Kent, and Hideo Ohno. Current-induced torques in magnetic materials. *Nat Mater*, 11(5):372–381, 05 2012.

[37] Ralf Bulla, Theo A. Costi, and Thomas Pruschke. Numerical renormalization group method for quantum impurity systems. *Rev. Mod. Phys.*, 80:395–450, Apr 2008.

[38] A. B. Butenko, A. A. Leonov, A. N. Bogdanov, and U. K. Rößler. Theory of vortex states in magnetic nanodisks with induced Dzyaloshinskii-Moriya interactions. *Phys. Rev. B*, 80:134410, Oct 2009.

[39] A. B. Butenko, A. A. Leonov, A. N. Bogdanov, and U. K. Rößler. Influence of the Dzyaloshinskii-Moriya interaction on vortex states in magnetic nanodisks. *Journal of Physics: Conference Series*, 200(4):042012, 2010.

[40] M. Büttiker. Zero-current persistent potential drop across small-capacitance Josephson junctions. *Phys. Rev. B*, 36:3548–3555, Sep 1987.

[41] Yu. A. Bychkov, L. P. Gorkov, and I. E. Dzyaloshinskii. Possibility of superconductivity type phenomena in a one-dimensional system. *Journal of Experimental and Theoretical Physics*, 23(3):489–501, 1966. Russian original – ZhETF, Vol. 50, No. 3, p. 738, September 1966.

[42] A. H. Castro Neto, F. Guinea, N. M. R. Peres, K. S. Novoselov, and A. K. Geim. The electronic properties of graphene. *Rev. Mod. Phys.*, 81:109–162, Jan 2009.

[43] E. Centeno and D. Felbacq. Light propagation control by finite-size effects in photonic crystals. *Physics Letters A*, 269(2–3):165–169, 2000.

[44] R. Coldea, D. A. Tennant, K. Habicht, P. Smeibidl, C. Wolters, and Z. Tylczynski. Direct measurement of the spin hamiltonian and observation of condensation of magnons in the 2d frustrated quantum magnet Cs_2CuCl_4. *Phys. Rev. Lett.*, 88:137203, Mar 2002.

[45] Piers Coleman and Andrew J. Schofield. Quantum criticality. *Nature*, 433(7023):226–229, 01 2005.

[46] J. Custers, P. Gegenwart, H. Wilhelm, K. Neumaier, Y. Tokiwa, O. Trovarelli, C. Geibel, F. Steglich, C. Pépin, and P. Coleman. The break-up of heavy electrons at a quantum critical point. *Nature*, 424(6948):524–527, 07 2003.

[47] S. Das Sarma, Shaffique Adam, E. H. Hwang, and Enrico Rossi. Electronic transport in two-dimensional graphene. *Rev. Mod. Phys.*, 83:407–470, May 2011.

[48] M. de Llano and J. P. Vary. Generalized Fermi sea for plane-wave Hartree-Fock theory: One dimensional model calculation. *Phys. Rev. C*, 19:1083–1088, Mar 1979.

[49] J. J. Deisz, D. W. Hess, and J. W. Serene. Incipient antiferromagnetism and low-energy excitations in the half-filled two-dimensional Hubbard model. *Phys. Rev. Lett.*, 76:1312–1315, Feb 1996.

[50] V. E. Demidov, O. Dzyapko, S. O. Demokritov, G. A. Melkov, and A. N. Slavin. Thermalization of a parametrically driven magnon gas leading to Bose-Einstein condensation. *Phys. Rev. Lett.*, 99:037205, Jul 2007.

[51] V. E. Demidov, O. Dzyapko, S. O. Demokritov, G. A. Melkov, and A. N. Slavin. Observation of spontaneous coherence in Bose-Einstein condensate of magnons. *Phys. Rev. Lett.*, 100:047205, Jan 2008.

[52] S. O. Demokritov, V. E. Demidov, O. Dzyapko, G. A. Melkov, A. A. Serga, B. Hillebrands, and A. N. Slavin. Bose-Einstein condensation of quasi-equilibrium magnons at room temperature under pumping. *Nature*, 443(7110):430–433, 09 2006.

[53] H. Dery, W. Hui, B. Ciftcioglu, M. Huang, S. Yang, R. Kawakami, S. Jing, I. Krivorotov, I. Zutic, and L. J. Sham. Nanospintronics based on magnetologic gates. *IEEE Transactions on Electron Devices*, 59(1):259–262, 2011.

[54] Guy Deutscher. Andreev-Saint James reflections: A probe of cuprate superconductors. *Rev. Mod. Phys.*, 77:109–135, Mar 2005.

[55] V. A. Dmitriev. 2d magnetic photonic crystals with square lattice-group theoretical standpoint. *Progress In Electromagnetics Research*, 58:71–100, 2006.

[56] Raimundo R. dos Santos. Enhanced pairing in the repulsive Hubbard model with next-nearest-neighbor hopping. *Phys. Rev. B*, 39:7259–7262, Apr 1989.

[57] R. A. Duine, A. S. Núñez, Jairo Sinova, and A. H. MacDonald. Functional Keldysh theory of spin torques. *Phys. Rev. B*, 75:214420, Jun 2007.

[58] M. I. Dyakonov, editor. *Spin physics in semiconductors*. Springer-Verlag, Berlin, Heidelberg, 2008.

[59] M. I. Dyakonov and V. I. Perel. Current-induced spin orientation of electrons in semiconductors. *Physics Letters A*, 35(6):459–460, 1971.

[60] I. E. Dzyaloshinskii. Theory of helicoidal structures in antiferromagnets. I. Nonmetals. *Journal of Experimental and Theoretical Physics*, 19(4):960–971, 1964. Russian original – ZhETF, Vol. 46, No. 4, p. 1420, October 1964.

[61] I. E. Dzyaloshinskii. Superconducting transitions due to van Hove singularities in the electron spectrum. *Journal of Experimental and Theoretical Physics*, 66(4):848–854, 1987. Russian original – ZhETF, Vol. 93, No. 4, p. 1487, September 1987.

[62] I. E. Dzyaloshinskii and E. I Kats. Theory of the antiferromagnetism of chromium. *Journal of Experimental and Theoretical Physics*, 35(3):584–590, 1972. Russian original – ZhETF, Vol. 62, No. 3, p. 1104, September 1972.

[63] I. E. Dzyaloshinskii and V. M. Yakovenko. Weak-coupling theory for La_2CuO_4. *Journal of Experimental and Theoretical Physics*, 67(4):844–849, 1988. Russian original – ZhETF, Vol. 94, No. 4, p. 344, April 1988.

[64] Igor Dzyaloshinskii. Extended van Hove singularity and related non-Fermi liquids. *J. Phys. I France*, 6(1):119–135, 1996.

[65] O. Dzyapko, V. E. Demidov, S. O. Demokritov, G. A. Melkov, and A. N. Slavin. Direct observation of Bose-Einstein condensation in a parametrically driven gas of magnons. *New Journal of Physics*, 9(3):64, 2007.

[66] D. K. Efimkin and Yu. E. Lozovik. Resonant manifestations of chiral excitons in Faraday and Kerr effects in a topological insulator film. *Phys. Rev. B*, 87:245416, Jun 2013.

[67] L. A. Falkovsky. Optical properties of graphene and IV - VI semiconductors. *Physics-Uspekhi*, 51(9):887–897, 2008.
[68] Manfred Fiebig, Victor V. Pavlov, and Roman V. Pisarev. Second-harmonic generation as a tool for studying electronic and magnetic structures of crystals: Review. *J. Opt. Soc. Am. B*, 22(1):96–118, Jan 2005.
[69] A. Figotin and I. Vitebsky. Nonreciprocal magnetic photonic crystals. *Phys. Rev. E*, 63:066609, May 2001.
[70] Marcus Fleck, Andrzej M. Oleś, and Lars Hedin. Magnetic phases near the van Hove singularity in *s*- and *d*-band Hubbard models. *Phys. Rev. B*, 56:3159–3166, Aug 1997.
[71] A. A. Fraerman, B. A. Gribkov, S. A. Gusev, A. Yu. Klimov, V. L. Mironov, D. S. Nikitushkin, V. V. Rogov, S. N. Vdovichev, B. Hjorvarsson, and H. Zabel. Magnetic force microscopy of helical states in multilayer nanomagnets. *Journal of Applied Physics*, 103(7), 2008.
[72] A. A. Fraerman and O. G. Udalov. Diode effect in a medium with helical magnetic structure. *Phys. Rev. B*, 77:094401, Mar 2008.
[73] A. A. Fraerman and O. G. Udalov. Photogalvanic effect in ferromagnets with a noncoplanar magnetization distribution. *JETP Letters*, 87(3):159–163, 2008.
[74] Nobuo Furukawa, T. M. Rice, and Manfred Salmhofer. Truncation of a two-dimensional Fermi surface due to quasiparticle gap formation at the saddle points. *Phys. Rev. Lett.*, 81:3195–3198, Oct 1998.
[75] S. Ganichev and W. Prettl. *Intense terahertz excitation of semiconductors*. Oxford Science Publications, 2006.
[76] S. D. Ganichev, J. Karch, P. Olbrich, M. Schmalzbauer, C. Zoth, C. Brinsteiner, U. Wurstbauer, M. M. Glazov, S. A. Tarasenko, D. Weiss, J. Eroms, R. Yakimova, S. Lara-Avila, S. Kubatkin, and E. L. Ivchenko. Photon helicity driven currents in graphene. In *Infrared Millimeter and Terahertz Waves (IRMMW-THz), 2010 35th International Conference on*, pages 1–1, Sept 2010.
[77] S. D. Ganichev and W. Prettl. Spin photocurrents in quantum wells. *Journal of Physics: Condensed Matter*, 15(20):R935, 2003.
[78] Andre K. Geim. Nobel lecture: Random walk to graphene. *Rev. Mod. Phys.*, 83:851–862, Aug 2011.
[79] Antoine Georges, Gabriel Kotliar, Werner Krauth, and Marcelo J. Rozenberg. Dynamical mean-field theory of strongly correlated fermion systems and the limit of infinite dimensions. *Rev. Mod. Phys.*, 68:13–125, Jan 1996.
[80] Roy J. Glauber. Coherent and incoherent states of the radiation field. *Phys. Rev.*, 131:2766–2788, Sep 1963.
[81] M. M. Glazov. Second harmonic generation in graphene. *JETP Letters*, 93(7):408–413, 2011.
[82] J. Grollier, V. Cros, A. Hamzic, J. M. George, H. Jaffrès, A. Fert, G. Faini, J. Ben Youssef, and H. Legall. Spin-polarized current induced switching in Co/Cu/Co pillars. *Applied Physics Letters*, 78(23):3663–3665, 2001.
[83] H. Hafermann. *Numerical approaches to spatial correlations in strongly interacting fermion systems*. Cuvillier Verlag, Göttingen, 2009.
[84] Christoph J. Halboth and Walter Metzner. Renormalization-group analysis of the two-dimensional Hubbard model. *Phys. Rev. B*, 61:7364–7377, Mar 2000.
[85] Fredrik Hansteen, Alexey Kimel, Andrei Kirilyuk, and Theo Rasing.

Nonthermal ultrafast optical control of the magnetization in garnet films. *Phys. Rev. B*, 73:014421, Jan 2006.

[86] M. Z. Hasan and C. L. Kane. Topological insulators. *Rev. Mod. Phys.*, 82:3045–3067, Nov 2010.

[87] R. Hlubina, S. Sorella, and F. Guinea. Ferromagnetism in the two dimensional $t-t'$ Hubbard model at the van Hove density. *Phys. Rev. Lett.*, 78:1343–1346, Feb 1997.

[88] Richard Hlubina. Phase diagram of the weak-coupling two-dimensional $t-t'$ Hubbard model at low and intermediate electron density. *Phys. Rev. B*, 59:9600–9605, Apr 1999.

[89] C. Honerkamp, M. Salmhofer, N. Furukawa, and T. M. Rice. Breakdown of the Landau-Fermi liquid in two dimensions due to umklapp scattering. *Phys. Rev. B*, 63:035109, Jan 2001.

[90] Carsten Honerkamp and Manfred Salmhofer. Magnetic and superconducting instabilities of the Hubbard model at the van Hove filling. *Phys. Rev. Lett.*, 87:187004, Oct 2001.

[91] D. Hsieh, D. Qian, L. Wray, Y. Xia, Y. S. Hor, R. J. Cava, and M. Z. Hasan. A topological Dirac insulator in a quantum spin Hall phase. *Nature*, 452(7190):970–974, 04 2008.

[92] J. Hubbard. Electron correlations in narrow energy bands. *Proceedings of the Royal Society of London A: Mathematical, Physical and Engineering Sciences*, 276(1365):238–257, 1963.

[93] Mitsuteru Inoue, Ken'ichi Arai, Toshitaka Fujii, and Masanori Abe. Magneto-optical properties of one-dimensional photonic crystals composed of magnetic and dielectric layers. *Journal of Applied Physics*, 83(11):6768–6770, 1998.

[94] V. Yu. Irkhin and Yu. P. Irkhin. *Electronic structure, correlation effects and properties of d- and f-metals and their compounds*. Cambridge International Science Publishing, 2007.

[95] V. Yu. Irkhin, A. A. Katanin, and M. I. Katsnelson. Robustness of the van Hove scenario for high-T_c superconductors. *Phys. Rev. Lett.*, 89:076401, Jul 2002.

[96] V. Yu. Irkhin, M. I. Katsnelson, and A. V. Trefilov. Anomalies caused in the lattice properties of band magnetic materials by features of the electronic structure. *JETP Letters*, 56(6):315–319, 1992.

[97] E. L. Ivchenko. *Optical spectroscopy of semiconductor nanostructures*. Alpha Science, Harrow UK, 2005.

[98] E. L. Ivchenko and S. D. Ganichev. Spin-photogalvanics. In M. I. Dyakonov, editor, *Spin physics in semiconductors*. Springer, 2008.

[99] M. Jaime, V. F. Correa, N. Harrison, C. D. Batista, N. Kawashima, Y. Kazuma, G. A. Jorge, R. Stern, I. Heinmaa, S. A. Zvyagin, Y. Sasago, and K. Uchinokura. Magnetic-field-induced condensation of triplons in han purple pigment $BaCuSi_2O_6$. *Phys. Rev. Lett.*, 93:087203, Aug 2004.

[100] Mark Johnson. Bipolar spin switch. *Science*, 260(5106):320–323, 1993.

[101] Mark Johnson and R. H. Silsbee. Thermodynamic analysis of interfacial transport and of the thermomagnetoelectric system. *Phys. Rev. B*, 35:4959–4972, Apr 1987.

[102] M. Jullière. Tunneling between ferromagnetic films. *Physics Letters A*,

54(3):225–226, 1975.
[103] A. Kampf and J. R. Schrieffer. Pseudogaps and the spin-bag approach to high-T_c superconductivity. *Phys. Rev. B*, 41:6399–6408, Apr 1990.
[104] C. L. Kane and E. J. Mele. Quantum spin Hall effect in graphene. *Phys. Rev. Lett.*, 95:226801, Nov 2005.
[105] E. A. Karashtin, O. G. Udalov, and A. A. Fraerman. Optical activity in media with noncoplanar magnetization distribution. *Journal of Experimental and Theoretical Physics*, 109(6):973–978, 2009.
[106] J. Karch, P. Olbrich, M. Schmalzbauer, C. Zoth, C. Brinsteiner, M. Fehrenbacher, U. Wurstbauer, M. M. Glazov, S. A. Tarasenko, E. L. Ivchenko, D. Weiss, J. Eroms, R. Yakimova, S. Lara-Avila, S. Kubatkin, and S. D. Ganichev. Dynamic Hall effect driven by circularly polarized light in a graphene layer. *Phys. Rev. Lett.*, 105:227402, Nov 2010.
[107] Robert Karplus and J. M. Luttinger. Hall effect in ferromagnetics. *Phys. Rev.*, 95:1154–1160, Sep 1954.
[108] M. I. Katsnelson. *Graphene: Carbon in Two Dimensions*. Cambridge University Press, Cambridge, 2012.
[109] L. V. Keldysh, D. A. Kirzhnitz, and A. A. Maradudin, editors. *The Dielectric Function of Condensed Systems*. North-Holland, Amsterdam, 1989.
[110] A. B. Khanikaev, A. B. Baryshev, P. B. Lim, H. Uchida, M. Inoue, A. G. Zhdanov, A. A. Fedyanin, A. I. Maydykovskiy, and O. A. Aktsipetrov. Nonlinear Verdet law in magnetophotonic crystals: Interrelation between Faraday and Borrmann effects. *Phys. Rev. B*, 78:193102, Nov 2008.
[111] A. B. Khanikaev, A. V. Baryshev, M. Inoue, A. B. Granovsky, and A. P. Vinogradov. Two-dimensional magnetophotonic crystal: Exactly solvable model. *Phys. Rev. B*, 72:035123, Jul 2005.
[112] V. A. Khodel and V. R. Shaginyan. Superfluidity in system with fermion condensate. *JETP Letters*, 51(9):553–555, 1990.
[113] V. A. Khodel, V. R. Shaginyan, and V. V. Khodel. New approach in the microscopic Fermi systems theory. *Physics Reports*, 249(1–2):1 – 134, 1994.
[114] D. V. Khveshchenko, R. Hlubina, and T. M. Rice. Non-Fermi-liquid behavior in two dimensions due to long-ranged current-current interactions. *Phys. Rev. B*, 48:10766–10776, Oct 1993.
[115] Naoki Kikugawa, Christoph Bergemann, Andrew Peter Mackenzie, and Yoshiteru Maeno. Band-selective modification of the magnetic fluctuations in Sr_2RuO_4: A study of substitution effects. *Phys. Rev. B*, 70:134520, Oct 2004.
[116] A. V. Kimel, A. Kirilyuk, P. A. Usachev, R. V. Pisarev, A. M. Balbashov, and Th. Rasing. Ultrafast non-thermal control of magnetization by instantaneous photomagnetic pulses. *Nature*, 435(7042):655–657, 06 2005.
[117] Andrei Kirilyuk, Alexey V. Kimel, and Theo Rasing. Ultrafast optical manipulation of magnetic order. *Rev. Mod. Phys.*, 82:2731–2784, Sep 2010.
[118] S. I. Kiselev, J. C. Sankey, I. N. Krivorotov, N. C. Emley, R. J. Schoelkopf, R. A. Buhrman, and D. C. Ralph. Microwave oscillations of a nanomagnet driven by a spin-polarized current. *Nature*, 425(6956):380–383, 09 2003.
[119] Jun-ichiro Kishine, I. G. Bostrem, A. S. Ovchinnikov, and Vl. E. Sinitsyn. Coherent sliding dynamics and spin motive force driven by crossed magnetic fields in a chiral helimagnet. *Phys. Rev. B*, 86:214426, Dec 2012.

[120] Jun-ichiro Kishine, A. S. Ovchinnikov, and I. V. Proskurin. Sliding conductivity of a magnetic kink crystal in a chiral helimagnet. *Phys. Rev. B*, 82:064407, Aug 2010.
[121] V. V. Klimov. *Nanoplasmonics*. Pan Stanford Publishing, Singapore, 2013.
[122] K. Kneipp, M. Moskovits, and H. Kneipp, editors. *Surface-Enhanced Raman Scattering: Physics and Applications*. Springer, Berlin, 2006.
[123] C. Koerdt, G. L. J. A. Rikken, and E. P. Petrov. Faraday effect of photonic crystals. *Applied Physics Letters*, 82(10):1538–1540, 2003.
[124] Markus König, Steffen Wiedmann, Christoph Brüne, Andreas Roth, Hartmut Buhmann, Laurens W. Molenkamp, Xiao-Liang Qi, and Shou-Cheng Zhang. Quantum spin Hall insulator state in HgTe quantum wells. *Science*, 318(5851):766–770, 2007.
[125] Frank H. L. Koppens, Darrick E. Chang, and F. Javier Garcia de Abajo. Graphene plasmonics: A platform for strong light-matter interactions. *Nano Letters*, 11(8):3370–3377, 2011.
[126] M. P. Kostylev, A. A. Serga, T. Schneider, B. Leven, and B. Hillebrands. Spin-wave logical gates. *Applied Physics Letters*, 87(15), 2005.
[127] O. V. Kotov and Yu. E. Lozovik. Cavity plasmon polaritons in monolayer graphene. *Physics Letters A*, 375(26):2573–2576, 2011.
[128] Valeri N. Kotov, Bruno Uchoa, Vitor M. Pereira, F. Guinea, and A. H. Castro Neto. Electron-electron interactions in graphene: Current status and perspectives. *Rev. Mod. Phys.*, 84:1067–1125, Jul 2012.
[129] Vladimir Kuzmiak and Alexei A. Maradudin. Localized defect modes in a two-dimensional triangular photonic crystal. *Phys. Rev. B*, 57:15242–15250, Jun 1998.
[130] D. Lacoste, F. Donatini, S. Neveu, J. A. Serughetti, and B. A. Van Tiggelen. Photonic Hall effect in ferrofluids: Theory and experiments. *Phys. Rev. E*, 62:3934–3943, Sep 2000.
[131] L. D. Landau. Theory of Fermi-liquids. *Journal of Experimental and Theoretical Physics*, 3:920, 1957. Russian original – ZhETF, Vol. 30, p. 1058, 1956.
[132] L. D. Landau, L. P. Pitaevskii, and E. M. Lifshitz. *Electrodynamics of Continuous Media.Volume 8 (Course of Theoretical Physics)*. Butterworth-Heinemann, 2 edition, 1984.
[133] L. D. Landau, L. P. Pitaevskii, and E. M. Lifshitz. *Statistical Physics, Part 1. Volume 5 (Course of Theoretical Physics)*. Butterworth-Heinemann, 2 edition, 1984.
[134] L. D. Landau, L. P. Pitaevskii, and E. M. Lifshitz. *Statistical Physics, Part 2: Theory of the Condensed State. Volume 9 (Course of Theoretical Physics)*. Butterworth-Heinemann, 2 edition, 1984.
[135] R. B. Laughlin and David Pines. The theory of everything. *Proceedings of the National Academy of Sciences*, 97(1):28–31, 2000.
[136] D. Lidsky, J. Shiraishi, Y. Hatsugai, and M. Kohmoto. Simple exactly solvable models of non-Fermi-liquids. *Phys. Rev. B*, 57:1340–1343, Jan 1998.
[137] I. M. Lifshitz, S. A. Gredeskul, and L. A. Pastur. *Introduction to the theory of disordered systems*. John Wiley, New York, 1988.
[138] H. Q. Lin and J. E. Hirsch. Two-dimensional Hubbard model with nearest- and

next-nearest-neighbor hopping. *Phys. Rev. B*, 35:3359–3368, Mar 1987.
[139] Ivan Lisenkov, Vasyl Tyberkevych, Andrei Slavin, Pavel Bondarenko, Boris A. Ivanov, Elena Bankowski, Thomas Meitzler, and Sergey Nikitov. Spin-wave edge modes in finite arrays of dipolarly coupled magnetic nanopillars. *Phys. Rev. B*, 90:104417, Sep 2014.
[140] A. A. Lisyansky, I. A. Nechepurenko, A. V. Dorofeenko, A. P. Vinogradov, and A. A. Pukhov. Channel spaser: Coherent excitation of one-dimensional plasmons from quantum dots located along a linear channel. *Phys. Rev. B*, 84:153409, Oct 2011.
[141] E. Y. Loh, J. E. Gubernatis, R. T. Scalettar, S. R. White, D. J. Scalapino, and R. L. Sugar. Sign problem in the numerical simulation of many-electron systems. *Phys. Rev. B*, 41:9301–9307, May 1990.
[142] Hilbert v. Löhneysen, Achim Rosch, Matthias Vojta, and Peter Wölfle. Fermi-liquid instabilities at magnetic quantum phase transitions. *Rev. Mod. Phys.*, 79:1015–1075, Aug 2007.
[143] Daniel Loss, Paul Goldbart, and A. V. Balatsky. Berry's phase and persistent charge and spin currents in textured mesoscopic rings. *Phys. Rev. Lett.*, 65:1655–1658, Sep 1990.
[144] Yu. E. Lozovik and S. P. Merkulova. The outlook for nanolocal femtosecond spectroscopy and nanolithography. *Physics-Uspekhi*, 42(3):284–285, 1999.
[145] Yu. E. Lozovik, S. P. Merkulova, M. M. Nazarov, A. P. Shkurinov, and P. Masselin. Time resolved nonlinear surface plasmon optics. *JETP Letters*, 75(9):551–554, 2002.
[146] Yu. E. Lozovik, S. P. Merkulova, and A. A. Sokolik. Collective electron phenomena in graphene. *Physics-Uspekhi*, 51(7):727–744, 2008.
[147] Yu. E. Lozovik, I. A. Nechepurenko, A. V. Dorofeenko, A. A. Pukhov, and E. S. Andrianov. Spaser spectroscopy with subwavelength spatial resolution. arXiv:1208.3389.
[148] Yu.E. Lozovik, S.P. Merkulova, M. M. Nazarov, and Shkurinov A. P. From two-beam surface plasmon interaction to femtosecond surface optics and spectroscopy. *Physics Letters A*, 276(1–4):127–132, 2000.
[149] Yoshiteru Maeno, T. Maurice Rice, and Manfred Sigrist. The intriguing superconductivity of strontium ruthenate. *Physics Today*, 54(1):42–47, 2001.
[150] G. Mahan. *Many-Particle Physics*. Springer Science, 2000.
[151] I. I. Mazin and David J. Singh. Ferromagnetic spin fluctuation induced superconductivity in Sr_2RuO_4. *Phys. Rev. Lett.*, 79:733–736, Jul 1997.
[152] Nicholas Metropolis, Arianna W. Rosenbluth, Marshall N. Rosenbluth, Augusta H. Teller, and Edward Teller. Equation of state calculations by fast computing machines. *The Journal of Chemical Physics*, 21(6):1087–1092, 1953.
[153] S. A. Mikhailov and K. Ziegler. New electromagnetic mode in graphene. *Phys. Rev. Lett.*, 99:016803, Jul 2007.
[154] C. Monat, C. Seassal, X. Letartre, P. Regreny, P. Rojo-Romeo, P. Viktorovitch, M. Le Vassor d'Yerville, D. Cassagne, J. P. Albert, E. Jalaguier, S. Pocas, and B. Aspar. InP based photonic crystal microlasers on silicon wafer. *Physica E: Low-dimensional Systems and Nanostructures*, 17(0):475–476, 2003. Proceedings of the International Conference on Superlattices, Nano-structures

and Nano-devices (ICSNN) 2002.
[155] S. Moukouri, S. Allen, F. Lemay, B. Kyung, D. Poulin, Y. M. Vilk, and A.-M. S. Tremblay. Many-body theory versus simulations for the pseudogap in the Hubbard model. *Phys. Rev. B*, 61:7887–7892, Mar 2000.
[156] V. Mourik, K. Zuo, S. M. Frolov, S. R. Plissard, E. P. A. M. Bakkers, and L. P. Kouwenhoven. Signatures of Majorana fermions in hybrid superconductor-semiconductor nanowire devices. *Science*, 336(6084):1003–1007, 2012.
[157] K. P. Mukhamatchin and A. A. Fraerman. Noncollinear states in a chain of single-domain magnetic particles. *JETP Letters*, 93(12):716–719, 2011.
[158] Shuichi Murakami, Naoto Nagaosa, and Manfred Sigrist. $SO(5)$ model of p-wave superconductivity and ferromagnetism. *Phys. Rev. Lett.*, 82:2939–2942, Apr 1999.
[159] T. Nikuni, M. Oshikawa, A. Oosawa, and H. Tanaka. Bose-Einstein condensation of dilute magnons in $TlCuCl_3$. *Phys. Rev. Lett.*, 84:5868–5871, Jun 2000.
[160] K. S. Novoselov. Nobel lecture: Graphene: Materials in the flatland. *Rev. Mod. Phys.*, 83:837–849, Aug 2011.
[161] Philippe Nozières. Properties of Fermi liquids with a finite range interaction. *J. Phys. I France*, 2(4):443–458, 1992.
[162] W. K. Park, L. H. Greene, J. L. Sarrao, and J. D. Thompson. Andreev reflection at the normal-metal/heavy-fermion superconductor $CeCoIn_5$ interface. *Phys. Rev. B*, 72:052509, Aug 2005.
[163] S. Paschen, T. Lühmann, S. Wirth, P. Gegenwart, O. Trovarelli, C. Geibel, F. Steglich, P. Coleman, and Q. Si. Hall-effect evolution across a heavy-fermion quantum critical point. *Nature*, 432(7019):881–885, 12 2004.
[164] N. Peres, F. Guinea, and A. Castro Neto. Coulomb interactions and ferromagnetism in pure and doped graphene. *Phys. Rev. B*, 72:174406, Nov 2005.
[165] N. M. R. Peres. The transport properties of graphene: An introduction. *Rev. Mod. Phys.*, 82:2673–2700, Sep 2010.
[166] P. S. Pershan. Nonlinear optical properties of solids: Energy considerations. *Phys. Rev.*, 130:919–929, May 1963.
[167] D. Pines and P. Nozières. *The theory of quantum liquids, Vol. 1 Normal Fermi liquids*. Benjamin, New York, 1966.
[168] L. P. Pitaevskii. Electric forces in a transparent dispersive medium. *Journal of Experimental and Theoretical Physics*, 12(5):1008–1012, 1961. Russian original – ZhETF, Vol. 39, No. 5, p. 1450, May 1961.
[169] Yu. G. Pogorelov and V. R. Shaginyan. Transition from non-Fermi liquid behavior to Landau-Fermi-liquid behavior induced by magnetic fields. *JETP Letters*, 76(8):614–618, 2002.
[170] I. Ya. Pomeranchuk. On the stability of a Fermi-liquid. *Journal of Experimental and Theoretical Physics*, 8:361, 1959. Russian original – ZhETF, Vol. 35, p. 524, 1958.
[171] I. E. Protsenko, A. V. Uskov, O. A. Zaimidoroga, V. N. Samoilov, and E. P. O'Reilly. Dipole nanolaser. *Phys. Rev. A*, 71:063812, Jun 2005.
[172] Xiao-Liang Qi and Shou-Cheng Zhang. Topological insulators and

superconductors. *Rev. Mod. Phys.*, 83:1057–1110, Oct 2011.
[173] Yabing Qi, Lingyun Zhang, and Weijia Wen. Anisotropy properties of magnetic colloidal materials. *Journal of Physics D: Applied Physics*, 36(1):L10, 2003.
[174] T. Radu, H. Wilhelm, V. Yushankhai, D. Kovrizhin, R. Coldea, Z. Tylczynski, T. Lühmann, and F. Steglich. Bose-Einstein condensation of magnons in Cs_2CuCl_4. *Phys. Rev. Lett.*, 95:127202, Sep 2005.
[175] S. Raghu, Suk Bum Chung, Xiao-Liang Qi, and Shou-Cheng Zhang. Collective modes of a helical liquid. *Phys. Rev. Lett.*, 104:116401, Mar 2010.
[176] S. Raghu and F. D. M. Haldane. Analogs of quantum-Hall-effect edge states in photonic crystals. *Phys. Rev. A*, 78:033834, Sep 2008.
[177] E. I. Rashba. Theory of electrical spin injection: Tunnel contacts as a solution of the conductivity mismatch problem. *Phys. Rev. B*, 62:R16267–R16270, Dec 2000.
[178] S. M. Rezende and N. Zagury. Coherent magnon states. *Physics Letters A*, 29(1):47–48, 1969.
[179] Ulrich K. Rößler, Andrei A. Leonov, and Alexei N. Bogdanov. Chiral skyrmionic matter in non-centrosymmetric magnets. *Journal of Physics: Conference Series*, 303(1):012105, 2011.
[180] A. N. Rubtsov, M. I. Katsnelson, and A. I. Lichtenstein. Dual fermion approach to nonlocal correlations in the Hubbard model. *Phys. Rev. B*, 77:033101, Jan 2008.
[181] Ch. Rüegg, N. Cavadini, A. Furrer, H. U. Güdel, K. Krämer, H. Mutka, A. Wildes, K. Habicht, and P. Vorderwisch. Bose-Einstein condensation of the triplet states in the magnetic insulator $TlCuCl_3$. *Nature*, 423(6935):62–65, 05 2003.
[182] S. Sachdev. *Quantum Phase Transitions*. Cambridge University Press, 2001.
[183] Ulrich Schollwöck. The density-matrix renormalization group in the age of matrix product states. *Annals of Physics*, 326(1):96–192, 2011. January 2011 Special Issue.
[184] T. Senthil and Matthew P. A. Fisher. Z_2 gauge theory of electron fractionalization in strongly correlated systems. *Phys. Rev. B*, 62:7850–7881, Sep 2000.
[185] T. Senthil, Subir Sachdev, and Matthias Vojta. Quantum phase transitions out of the heavy Fermi-liquid. *Physica B: Condensed Matter*, 359–361(0):9–16, 2005. Proceedings of the International Conference on Strongly Correlated Electron Systems.
[186] T. Senthil, Ashvin Vishwanath, Leon Balents, Subir Sachdev, and Matthew P. A. Fisher. Deconfined quantum critical points. *Science*, 303(5663):1490–1494, 2004.
[187] V. R. Shaginyan. Dissymmetrical tunnelling in heavy fermion metals. *JETP Letters*, 81(5):283–286, 2005.
[188] V. R. Shaginyan, M. Ya. Amusia, and K. G. Popov. Universal behavior of strongly correlated Fermi systems. *Physics-Uspekhi*, 50(6):563–593, 2007.
[189] V. R. Shaginyan, J. G. Han, and J. Lee. Fermion condensation quantum phase transition versus conventional quantum phase transitions. *Physics Letters A*, 329(1–2):108–115, 2004.

[190] V. R. Shaginyan and K. G. Popov. Asymmetric tunneling, Andreev reflection and dynamic conductance spectra in strongly correlated metals. *Physics Letters A*, 361(4–5):406–412, 2007.
[191] V. M. Shalaev and S. Kawata, editors. *Nanophotonics with Surface Plasmons*. Elsevier, Amsterdam, 2007.
[192] R. Shankar. Renormalization-group approach to interacting fermions. *Rev. Mod. Phys.*, 66:129–192, Jan 1994.
[193] Ryuichi Shindou, Ryo Matsumoto, Shuichi Murakami, and Jun-ichiro Ohe. Topological chiral magnonic edge mode in a magnonic crystal. *Phys. Rev. B*, 87:174427, May 2013.
[194] Ryuichi Shindou, Jun-ichiro Ohe, Ryo Matsumoto, Shuichi Murakami, and Eiji Saitoh. Chiral spin-wave edge modes in dipolar magnetic thin films. *Phys. Rev. B*, 87:174402, May 2013.
[195] Y. Sidis, M. Braden, P. Bourges, B. Hennion, S. NishiZaki, Y. Maeno, and Y. Mori. Evidence for incommensurate spin fluctuations in Sr_2RuO_4. *Phys. Rev. Lett.*, 83:3320–3323, Oct 1999.
[196] Yu. V. Skrypnyk and V. M. Loktev. Impurity effects in a two-dimensional system with the Dirac spectrum. *Phys. Rev. B*, 73:241402, Jun 2006.
[197] J. C. Slonczewski. Current-driven excitation of magnetic multilayers. *Journal of Magnetism and Magnetic Materials*, 159(1–2):L1–L7, 1996.
[198] J. C. Slonczewski and P. R. Weiss. Band structure of graphite. *Phys. Rev.*, 109:272–279, Jan 1958.
[199] David Snoke. Condensed-matter physics: Coherent questions. *Nature*, 443(7110):403–404, 09 2006.
[200] S. O. S.O. Demokritov, B. Hillebrands, and A. N. Slavin. Brillouin light scattering studies of confined spin waves: Linear and nonlinear confinement. *Physics Reports*, 348(6):441–489, 2001.
[201] J. Sólyom. The Fermi gas model of one-dimensional conductors. *Advances in Physics*, 28(2):201–303, 1979.
[202] G. R. Stewart. Non-Fermi-liquid behavior in d- and f-electron metals. *Rev. Mod. Phys.*, 78:743–753, Jul 2006.
[203] M. D. Stiles and A. Zangwill. Anatomy of spin-transfer torque. *Phys. Rev. B*, 66:014407, Jun 2002.
[204] S. M. Stishov and A. E. Petrova. Itinerant helimagnet MnSi. *Physics-Uspekhi*, 54(11):1117, 2011.
[205] Henk T. C. Stoof, Dennis B. M. Dickerscheid, and Koos Gubbels. *Ultracold Quantum Fields*. Springer, 1 edition, 2009.
[206] M. Tanaka and S. Sugahara. MOS-based spin devices for reconfigurable logic. *IEEE Transactions on Electron Devices*, 54(5):961–976, 2007.
[207] Hal Tasaki. Ferromagnetism in the Hubbard models with degenerate single-electron ground states. *Phys. Rev. Lett.*, 69:1608–1611, Sep 1992.
[208] Gen Tatara and Hiroshi Kohno. Permanent current from noncommutative spin algebra. *Phys. Rev. B*, 67:113316, Mar 2003.
[209] Yaroslav Tserkovnyak, Arne Brataas, Gerrit E. W. Bauer, and Bertrand I. Halperin. Nonlocal magnetization dynamics in ferromagnetic heterostructures. *Rev. Mod. Phys.*, 77:1375–1421, Dec 2005.
[210] M. Tsoi, A. G. M. Jansen, J. Bass, W.-C. Chiang, M. Seck, V. Tsoi, and

P. Wyder. Excitation of a magnetic multilayer by an electric current. *Phys. Rev. Lett.*, 80:4281–4284, May 1998.
[211] K. Vahaplar, A. M. Kalashnikova, A. V. Kimel, D. Hinzke, U. Nowak, R. Chantrell, A. Tsukamoto, A. Itoh, A. Kirilyuk, and Th. Rasing. Ultrafast path for optical magnetization reversal via a strongly nonequilibrium state. *Phys. Rev. Lett.*, 103:117201, Sep 2009.
[212] S. O. Valenzuela and M. Tinkham. Direct electronic measurement of the spin Hall effect. *Nature*, 442(7099):176–179, 07 2006.
[213] T. Valet and A. Fert. Theory of the perpendicular magnetoresistance in magnetic multilayers. *Phys. Rev. B*, 48:7099–7113, Sep 1993.
[214] J. P. van der Ziel, P. S. Pershan, and L. D. Malmstrom. Optically-induced magnetization resulting from the inverse Faraday effect. *Phys. Rev. Lett.*, 15:190–193, Aug 1965.
[215] P. C. van Son, H. van Kempen, and P. Wyder. Boundary resistance of the ferromagnetic-nonferromagnetic metal interface. *Phys. Rev. Lett.*, 58:2271–2273, May 1987.
[216] H. R. J. van Tyull. Spin transfer in helical magnets. Master's thesis, Utrecht University, the Netherlands, 2009.
[217] C.M. Varma, Z. Nussinov, and Wim van Saarloos. Singular or non-Fermi liquids. *Physics Reports*, 361(5–6):267–417, 2002.
[218] S. N. Vdovichev, B. A. Gribkov, S. A. Gusev, A. Yu. Klimov, V. L. Mironov, I. M. Nefedov, V. V. Rogov, A. A. Fraerman, and I. A. Shereshevskii. Magnetoresistance and noncollinear structures of multilayer ferromagnetic nanoparticles. *JETP Letters*, 94(5):386–389, 2011.
[219] M. Vekić and S. R. White. Pseudogap formation in the half-filled Hubbard model. *Phys. Rev. B*, 47:1160–1163, Jan 1993.
[220] V. G. Veselago. The electrodynamics of substances with simultaneously negative values of ε and μ. *Physics-Uspekhi*, 10(4):509–514, 1968.
[221] Y. M. Vilk and A.-M. S. Tremblay. Non-perturbative many-body approach to the Hubbard model and single-particle pseudogap. *J. Phys. I France*, 7(11):1309–1368, 1997.
[222] Matthias Vojta. Quantum phase transitions. *Reports on Progress in Physics*, 66(12):2069, 2003.
[223] G. E. Volovik. A new class of normal Fermi liquids. *JETP Letters*, 53(4):222–225, 1991.
[224] G. E. Volovik, editor. *The Universe in a Helium Droplet*. Clarendon Press, Oxford, 2003.
[225] G. E. Volovik. Topology of momentum space and quantum phase transitions. *Acta Physica Slovaca*, 56(2):49–56, 2006.
[226] G. E. Volovik. Quantum phase transitions from topology in momentum space. In William G. Unruh and Ralf Schützhold, editors, *Quantum Analogues: From Phase Transitions to Black Holes and Cosmology*, volume 718 of *Lecture Notes in Physics*, pages 31–73. Springer Berlin Heidelberg, 2007.
[227] P. R. Wallace. The band theory of graphite. *Phys. Rev.*, 71:622–634, May 1947.
[228] Zheng Wang, Yidong Chong, J. D. Joannopoulos, and Marin Soljačić. Observation of unidirectional backscattering-immune topological

electromagnetic states. *Nature*, 461(7265):772–775, 10 2009.
[229] X. Xu, G. Friedman, K. D. Humfeld, S. A. Majetich, and S. A. Asher. Superparamagnetic photonic crystals. *Advanced Materials*, 13(22):1681–1684, 2001.
[230] Zakharchenya. Optical orientation. In F. Meier and B. P. Zakharchenya, editors, *Optical Orientation*. North Holland, Amsterdam, 1984.
[231] Sergiy J. Zalyubovskiy, Maria Bogdanova, Alexei Deinega, Yurii Lozovik, Andrew D. Pris, Kwang Hyup An, W. Paige Hall, and Radislav A. Potyrailo. Theoretical limit of localized surface plasmon resonance sensitivity to local refractive index change and its comparison to conventional surface plasmon resonance sensor. *J. Opt. Soc. Am. A*, 29(6):994–1002, Jun 2012.
[232] D. Zanchi and H. J. Schulz. Superconducting instabilities of the non-half-filled Hubbard model in two dimensions. *Phys. Rev. B*, 54:9509–9519, Oct 1996.
[233] Lifa Zhang, Jie Ren, Jian-Sheng Wang, and Baowen Li. Topological magnon insulator in insulating ferromagnet. *Phys. Rev. B*, 87:144101, Apr 2013.
[234] Shou-Cheng Zhang. A unified theory based on $SO(5)$ symmetry of superconductivity and antiferromagnetism. *Science*, 275(5303):1089–1096, 1997.
[235] J. Zinn-Justin. *Quantum Field Theory and Critical Phenomena*. Clarendon Press, 2002.
[236] M. V. Zverev and M. Baldo. The multi-connected momentum distribution and fermion condensation. *Journal of Physics: Condensed Matter*, 11(9):2059, 1999.
[237] A. K. Zvezdin and V. A. Kotov. *Modern Magnetooptics and Magnetooptical Materials, Condensed Matter Physics.* Taylor and Francis Group, New York, 1997.
[238] A. K. Zvezdin, K. A. Zvezdin, and A. V. Khvalkovskii. The generalized Landau-Lifshitz equation and spin transfer processes in magnetic nanostructures. *Physics-Uspekhi*, 51(4):412–417, 2008.

Acta Universitatis Upsaliensis

Digital Comprehensive Summaries of Uppsala Dissertations from the Faculty of Science and Technology 1214

Editor: The Dean of the Faculty of Science and Technology

A doctoral dissertation from the Faculty of Science and Technology, Uppsala University, is usually a summary of a number of papers. A few copies of the complete dissertation are kept at major Swedish research libraries, while the summary alone is distributed internationally through the series Digital Comprehensive Summaries of Uppsala Dissertations from the Faculty of Science and Technology. (Prior to January, 2005, the series was published under the title "Comprehensive Summaries of Uppsala Dissertations from the Faculty of Science and Technology".)

Distribution: publications.uu.se
urn:nbn:se:uu:diva-238177

ACTA
UNIVERSITATIS
UPSALIENSIS
UPPSALA
2015